Scuola Normale Superiore

Classe di Scienze

Corso di Perfezionamento in Chimica

Ph.D. Thesis

Chemical Generation of Volatile Species in Analytical Chemistry

Enea Pagliano

Supervisor

Dr. Alessandro D'Ulivo

Reviewers

Prof. Nelson Belzile

Prof. Joerg Feldmann

Table of Contents

Introduction

In Analytical Chemistry the use of derivatization reactions is widespread and extremely useful. The reasons to perform a derivatization are several and usually are related to the instrumental set-up available, e.g. in gas chromatography a derivatization is successful when increases the volatility of the analyte, decreasing its polarity [1]. In general a derivatization should entail better chromatographic separation and increase the detection power.

This thesis relies on the study of derivatization reactions able to convert a non-volatile analyte – usually an ion in aqueous solution – in a volatile derivative. This approach, called *chemical vapor generation*, gives the possibility to separate the analyte from its matrix under the form of a gas, limiting interference problem, contamination, and increasing the limits of detection [2]. Historically the first analytical application of chemical vapor generation dates back to 1836 when James Marsh [3] published *"Account of a method of separating small quantities of arsenic from substances with which it may be mixed"*. Marsh test, used since the 19th century in forensic science to detect arsenic poisoning, entails the conversion of As_2O_3 to the volatile AsH_3 by reduction with zinc in acidic media. In a similar fashion, a wide set of strategies to perform vapor generation have been explored in the 20th century, *i.e.*, hydride generation, alkylation, halide generation, generation of metal-carbonyls, and cold vapor generation [4–5]. This arsenal of reactions represents an important tool for analytical chemists, allowing widespread applications for the determination and speciation of metals, metalloids, and organometallic compounds.

The focus of this thesis is the study of fundamental aspects and new analytical applications of chemical vapor generation. In the first part (Part 1) of this PhD thesis are presented new analytical applications of triethyloxonium derivatization in analytical chemistry. The second (Part 2) deals with a series of fundamental

(theoretical) studies upon the generation of volatile arsanes by aqueous phase reaction of simple inorganic and methylated arsenic species with $NaBH_4$.

Part 1 - Chemical vapor generation with trialkyloxonium salts: *state-of-the-art*

The use of $Et_3O^+[BF_4]^-$ as analytical reagent was first implemented during my graduation program [6] and published in 2009 [7] in *Analytical Chemistry*. Triethyloxonium derivatization allows the determination of iodide, bromide, chloride, nitrite, nitrate, cyanide, thiocyanate, and sulfide by headspace GC/MS [7]. This methodology is a valid opponent to the classical ion chromatography, because it assures better analytical performance (resolution, sensitivity, and specificity) for the determination of anions that can be converted in stable ethyl-derivatives.

This first paper has inspired further developments, in particular in 2010 has been published an application of the triethyloxonium method for the determination of iodine in a iodine-starch matrix [8], and in 2011 for the quantitation of iodine in intact granular starches [9].

Despite few applications of Meewein's salt in analytical chemistry, these reagents are known since 1937 [10] and have been used extensively in organic chemistry for performing difficult alkylation [11].

In the present thesis is intended to explore the application of the triethyloxonium to the derivatization of nitrite, nitrate and fluoride.

Part 2 – Mechanism of generation of volatile hydrides: *state-of-the-art*

The second part of the thesis deals with the mechanisms of hydride generation. Chemical generation of volatile hydrides by reduction of aqueous samples with tetrahydridoborate [2] and other borane complexes like amine boranes [12] is a powerful approach which is typically coupled with atomic spectroscopy and mass

spectrometry. Hydride generation is employed for the determination and speciation of trace and ultratrace of Ge, Sn, Pb, As, Sb, Bi, Se, Te, Hg, Cd and also some noble and transition metals. Along the last 40 years [13–14] a huge amount of literature has been published on this topic, however, only limited efforts have been dedicated to clarify the mechanistic aspects which rule the derivatization itself. Thus, analytical chemical vapor generation is still dominated by erroneous concepts which, during the year, have been consolidated in the analytical community. An example of such misconception is the hypothesis of the "nascent hydrogen" which was proposed by Robbins and Caruso in 1979 [15] to explain the mechanism of hydrogen transfer from the borano complex to the element forming the hydride. This hypothesis postulated the formation of atomic hydrogen as a result of the acidic hydrolysis of $[BH_4]^-$ according to the following reaction:

$$[BH_4]^- + H^+ + 3H_2O \rightarrow H_3BO_3 + 8H$$

The resulting atomic hydrogen is then able to reduce the analyte (E^{m+}) to the volatile hydride:

$$E^{m+} + (m+n)\ H \rightarrow EH_n + mH^+$$

This hypothesis, already criticized by Laborda in 2002 [16], was definitely dismissed after D'Ulivo's results which greatly contribute to the understanding of this system [17–21]. Indeed the mechanism of hydride generation operated by reduction with borane complexes was proved to be a concerted transfer of hydrogen from the borane complex to the analyte.

The key processes of chemical hydride generation can be summarized in 4 major points [22–23]:

1. Mechanism of hydrolysis of $[BH_4]^-$ in aqueous media.
2. Mechanism of generation of volatile hydrides and other volatile species in aqueous media.
3. Mechanism of liquid phase interferences arising from foreign chemical species.
4. Mechanisms of action of additives.

In this thesis the attention has been focused on the effects which can generate a perturbation on the ideal "analytical" mechanism of generation of the volatile hydride.

In particular the concentration of the analyte and the presence of trace amount of noble metals – Au(III), Pt(II), Pd(II), and Rh(III) – are responsible for the formation of unwanted by-products (which mainly arise by competing condensation reactions) and for a strong perturbation in the mechanism of hydrogen transfer from $[BH_4]^-$ to the analytical substrate.

Most of the scientific contributions of this thesis are published on scientific journals and the relevant papers are included in the Annex. Therefore, in this manuscript, I avoided to report technical details on the experiments performed, with the aim to give more strength to the critical discussion of the results obtained.

Acknowledgments. Scuola Normale Superiore is greatly acknowledged to have invested on this Ph.D. project in 2010. The first part of my experimental work has been done at Consiglio Nazionale delle Ricerche in Pisa and I thank my supervisor Alessandro D'Ulivo and Massimo Onor for the support they have given to me. Since April 2011 I had the opportunity to continue my work at National Research Council Canada in Ottawa. Beyond the shadow of doubt I can say that this has been the most significant scientific experience for me so far. Working with Juris Meija Zoltán Mester, and Ralph Sturgeon has been a unique opportunity for my professional growth. Since my first days at NRC my ideas and my work have been appreciated; for a scientist at the beginning of his carrier this is invaluable. The reviewers of this thesis, Nelson Belzile and Joerg Feldmann, are also greatly acknowledged for the careful revision. Finally, I would like to thank all my friends I have met along my Ph.D.: you guys made these three years really unforgivable!

Algonquin park – Canada

Scientific contributions

International projects

1. I partook in the International Inter-laboratory Comparison Exercise CCQM-P135 organized under the auspices of the International Committee of Weights and Measures (BIPM/CIPM) during the months of May and June 2012. This pilot study was focused on the determination of anionic impurities in pure sodium chloride (NaCl) which is intended to be used as a standard in elemental analysis. This challenging determination was performed using the triethyloxonium derivatization method, developed during this PhD and discussed in the first chapter of the thesis. The challenge of this exercise was the determination of traces of anions (bromide and nitrate) in a highly concentrated sodium chloride matrix. The triethyloxonium method produced results in excellent agreement with the other laboratories taking part to the exercise.

2. I partook in the certification of MOOS-3 Seawater Certified Reference Material for Nutrient. The content of nitrite and nitrate in this seawater sample (collected at latitude 47.062833 °N, longitude 59.982333 °W, off the northern tip of Cape Breton Island, NS, Canada) was determined by using triethyloxonium derivatization as described in the first chapter of this thesis. This certified reference material is primarily intended for use in the calibration of procedures and the development of methods for the analysis of nutrients in seawater.

Publications on ISI journals

I. **Pagliano, E. (ca)**; Onor, M.; Pitzalis, E.; Mester, Z.; Sturgeon, R. E.; D'Ulivo, A. Quantification of nitrite and nitrate in seawater by triethyloxonium tetrafluoroborate derivatization – Headspace SPME GC–MS. *Talanta* **2011**, *85*, 2511–2516

II. **Pagliano, E.**; Onor, M.; Meija, J.; Mester, Z.; Sturgeon, R. E.; D'Ulivo, A. Mechanism of hydrogen transfer in arsane generation by aqueous tetrahydridoborate: interference effects of Au^{III} and other noble metals. *Spectrochim. Acta Part B* **2011**, *66*, 740–747

III. D'Ulivo, A.; Meija, J.; Mester, Z.; **Pagliano, E.**; Sturgeon R. E. Condensation cascades and methylgroup transfer reactions during the formation of arsane, methyl- and dimethylarsane by aqueous borohydride and (methyl) arsenates. *Anal. Bioanal. Chem* **2012**, *402*, 921–933

IV. **Pagliano, E. (ca)**; Meija, J.; Sturgeon R. E.; Mester, Z.; D'Ulivo, A. Negative chemical ionization GC/MS determination of nitrite and nitrate in seawater using exact matching double spike isotope dilution and derivatization with triethyloxonium tetrafluoroborate. *Anal. Chem.* **2012**, *84*, 2592–2596

V. **Pagliano, E. (ca)**; D'Ulivo, A.; Mester, Z.; Sturgeon, R. E.; Meija, J. The binomial distribution of hydrogen and deuterium in arsanes, diarsanes, and triarsanes generated from As(III)/$[BH_nD_{4-n}]^-$ and the effect of trace amounts of Rh(III) ions. *J. Am. Soc. Mass Spectrom.* **2012**, *23*, 2178–2186

VI. **Pagliano, E. (ca)**; Meija. J.; Ding, J.; Sturgeon, R. E.; D'Ulivo, A.; Mester, Z. Novel ethyl-derivatization approach for the determination of fluoride by headspace gas chromatography/mass spectrometry. *Anal. Chem.* **2012**, DOI: 10.1021/ac302303r.

VII. **Pagliano, E.**; Mester, Z.; Meija, J. Reduction of measurement uncertainty by experimental design in high-order (double, triple, and quadruple) isotope dilution mass spectrometry: application to GC-MS measurement of bromide. *Anal. Bioanal. Chem.* **2013**, DOI: 10.1007/s00216-013-6724-5.

Lectures

D'Ulivo, A.; **Pagliano, E.**; Onor, M.; Pitzalis, E.; Meija, J.; Mester, Z.; Sturgeon, R. E. Applications and mechanistic aspects of chemical vapor generation: some recent developments. Colloquium Spectroscopicum Internationale XXXVII, Keynote Lecture, Book of Abstract, KL13

Awards

NRC-INMS Peer Award 2011 in recognition of development of isotope dilution methods that open avenues for new Certified Reference Materials

Winner of the Springer's "Standard addition challenge", *Anal. Bioanal. Chem.* **2012**, *403*, 2461–2462

NRC-INMS peer award 2011

Part 1

Ethylation with Et_3O^+ salts in Analytical Chemistry

Triethyloxonium tetrachloroferrate - $Et_3O^+[FeCl_4]^-$
synthesized in this work

Trialkyloxonium salts had been discovered by H. Meerwein in 1937 [10]. Although the applications of these reagents have been explored in organic chemistry over the 20th century [11, 24], their application in analytical chemistry for the determination of inorganic anions is a recent introduction [7]. Reactivity of trialkyloxonium salts in aqueous media can be described as follow:

$X^- + R_3O^+ \rightarrow RX + R_2O$ (derivatization reaction)

$R_3O^+ + H_2O \rightarrow R_2O + ROH + H^+$ (hydrolysis)

where X^- is an anion (such as Br^-, NO_3^- or I^-), whereas R is an alkylic group (such as Me or Et)

These two reactions are competitive and depending on the alkyl group chosen, the time of hydrolysis changes. For example trimethyloxonium hydrolyzes much faster than triethyloxonium, while triphenyloxonium is rather stable in aqueous media and

long times and severe conditions are required for its reaction with nucleophiles [11]. For the analytical applications explored so far, triethyloxonium gives an optimum compromise between the rate of hydrolysis and the alkylation of the analyte. The hydrolysis of triethyloxonium generates an equivalent amount of protons, which means that the sample solution becomes increasingly acidic during the reaction. Under acidic conditions some of the anions generated by weak acids (nitrite, fluoride, cyanide, sulfide, etc) can undergo protonation (HF, HCN, H_2S) and escape from the solution. Furthermore, their anionic forms are more activated toward Et_3O^+ derivatization with respect to the protonated forms. Adjustment of pH could be problematic as the buffer can react with Et_3O^+. Buffering with ammonia is preferred over NaOH, because at pH = 10 the hydrolysis of the reagent is still acceptable slow, while at superior level of alkalinity the hydrolysis of Et_3O^+ becomes too fast.

In this first part two major applications of Et_3O^+ derivatization are reported. In paragraph 1.1 is presented a new method for the simultaneous determination of nitrite and nitrate, while in paragraph 1.2 is discussed a novel methodology for the determination of fluoride. In both case the use of ammonia to buffer the sample at pH = 10 assured an ideal environment for the derivatization.

1.1

Papers attached: Annex I and IV

Determination of nitrite and nitrate by GC/MS

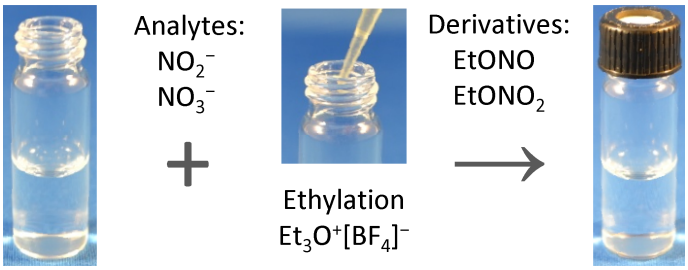

Reproduced in part from *Anal. Chem.* **2012**, *84*, 2592–2596
Copyright 2012 American Chemical Society

Introduction. The determination of nitrite and nitrate in samples of different origin is important in environmental and biological sciences [25]. Moorcroft et al. [25] reviewed strategies for detection of these analytes, discussing advantages and limitations of the various methodologies. Jobgen et al. [26] focused their analysis on the determination of nitrite and nitrate in biological samples using high-pressure liquid chromatography (HPLC), whereas Helmke et al. [27] discussed the application of gas chromatography/mass spectrometry (GC/MS). In general, methods which entail the use of molecular spectroscopy or electrochemical detection have limited sensitivity and selectivity and suffer from matrix effects. Furthermore, there are more methods for the direct detection of nitrite than nitrate, and in many analytical protocols the determination of nitrate is achieved following a critical reduction to nitrite, usually by cadmium [28]. Nitrite and nitrate are nonvolatile anions, and their determination by GC/MS can be achieved by derivatization in order to generate volatile species, for example, nitration of aromatic compounds has been used for this

purpose [27]. This approach, however, does not work for nitrite and requires the use of strongly acidic conditions which may be critical if any nitrite is present because of its possible conversion to nitrate [29–30]. Another GC/MS technique entails alkylation with pentafluorobenzyl bromide (F_5BzBr) to convert nitrite and nitrate to $F_5Bz{-}NO_2$ and $F_5Bz{-}ONO_2$, respectively [31]. The pentafluorobenzyl derivatives are suitable for negative chemical ionization (CI–) GC/MS, but they are not employed for static headspace analysis at room temperature due to their low volatility. Despite the achievement of low detection limits (subfmol, absolute) and the possibility of simultaneous determination of both analytes, this derivatization method employs organic solvents (acetone and toluene) and the subsequent injection of the organic extract which may contain some component of sample matrix and the un-reacted F_5BzBr. Here is reported a new GC/MS method for the simultaneous determination of nitrite and nitrate after triethyloxonium derivatization [32–33].

Discussion and conclusion. Triethyloxonium tetrafluoroborate can convert nitrite and nitrate to their ethyl esters through an O-alkylation on both analytes:

$$NO_2^-(aq) + Et_3O^+(aq) \rightarrow EtONO(g) + Et_2O$$
$$NO_3^-(aq) + Et_3O^+(aq) \rightarrow EtONO_2(g) + Et_2O$$

These derivatives are volatile and can be sampled by direct headspace or by solid phase micro-extraction (SPME) and detected by GC/MS using both electron impact (EI) or chemical ionization (CI). For analytical application CI– shows the best sensitivity, allowing detection limit of $\gamma(NO_2^-)_{DL}$ = 150 ng/L and $\gamma(NO_3^-)_{DL}$ = 600 ng/L. The estimation of the detection limit is based on the signal-to-noise ratio calculated from the standard deviation of the baseline (i.e., detection limit is the concentration which produce a signal-to-noise ratio of 3). These limits of detection are competitive or better respect to the reported limits of detection for routine

methods (using spectrophotometry or electrochemical detection) [25] and are comparable with those reported by Tzikas [31] for the GC/MS determination of nitrite and nitrate after F_5BzBr derivatization ($((NO_2^-)_{DL}$ = 160 ng/L and $\gamma(NO_3^-)_{DL}$ = 2 µg/L).

The CI− mass spectrum of EtONO and $EtONO_2$ are shown in Fig. 1.1. The validation of this method was done measuring these two analytes in a certified seawater (MOOS-2) and obtaining results in excellent agreement with the certified property values of the material.

For the determination of nitrite and nitrate it is important to ensure alkaline conditions during the course of the derivatization. The pretreatment of the sample with aqueous ammonia entails an ideal buffering at pH =10 which prevent the unwanted conversion of nitrite to nitrate, which can occur in acidic media, and stop oxygen scrambling between the analytes and the solvents, those making possible ^{18}O labeling for isotope dilution experiments. In this alkaline environment, significant oxidation of nitrite to nitrate can occur only at high concentrations of nitrite. A standard solution of 100 mg/L of nitrite undergoes a 0.07% conversion to nitrate (no conversion was detected below this mass fraction).

Quantitation entails the use of isotopically enriched standards ($N^{18}O_2^-$ and $^{15}NO_3^-$), which also permits monitoring of potential conversion from nitrite to nitrate during the analysis. The proposed method, based on exact-matching double spike isotope dilution calibration [34–35], is simple, sensitive, analyte specific, and does not require organic solvents. Furthermore, this method achieves a transparent traceability and is promising for application to a wide variety of samples.

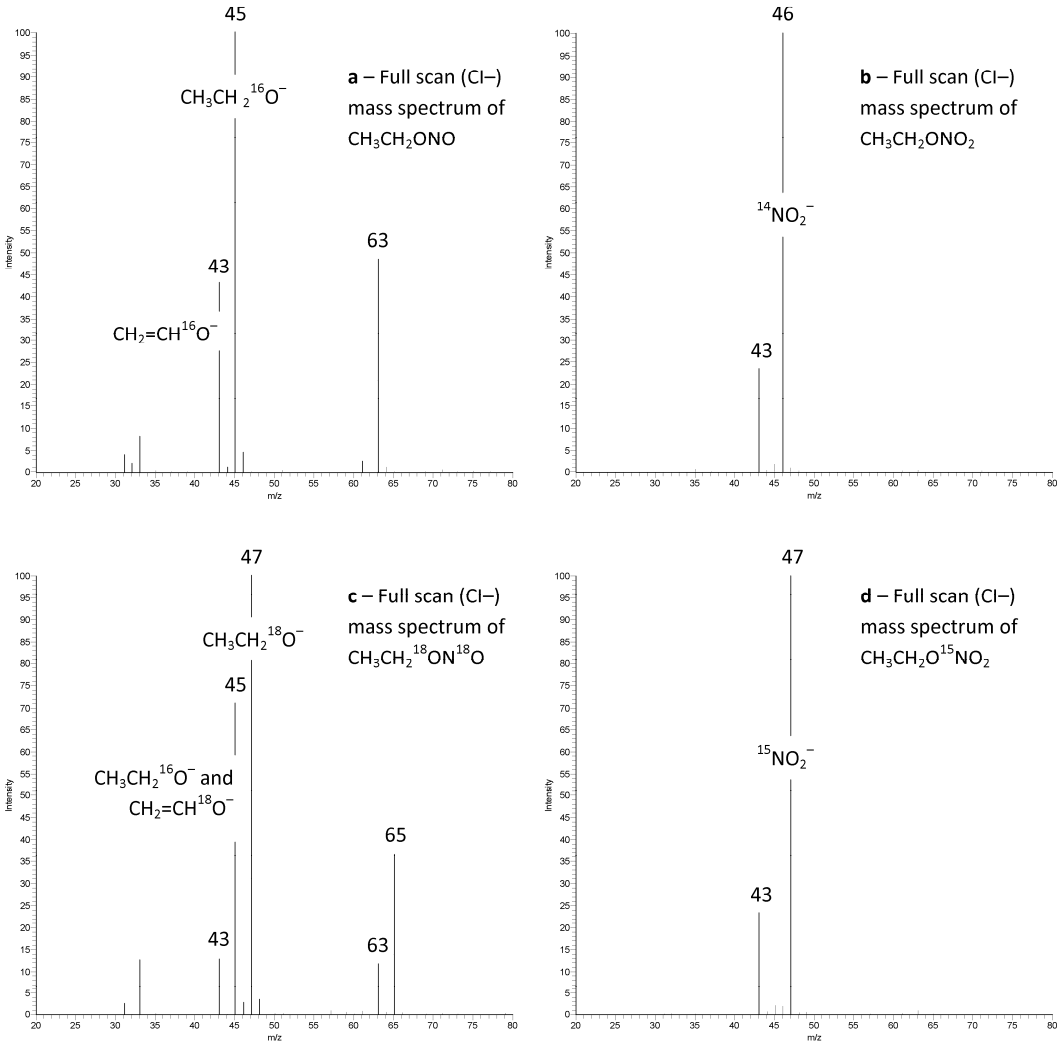

Figure 1.1 CI– mass spectra (a) nitrite ethyl ester: $CH_2{=}CH^{16}O^-$ (*m/z* = 43 Da), $CH_3CH_2{}^{16}O^-$ (*m/z* = 45 Da), and $CH_3CH_2{}^{16}O^-{\cdot}H_2O$ (*m/z* = 63 Da). (b) Nitrate ethyl ester: $CH_2{=}CH_{16}O^-$ (*m/z* = 43 Da), $^{14}NO_2^-$ (*m/z* = 46 Da). (c) (^{18}O)nitrite ethyl ester: $CH_2{=}CH^{16}O^-$ (*m/z* = 43 Da), $CH_3CH_2{}^{16}O^-$ and $CH_2{=}CH^{18}O^-$ (*m/z* = 45 Da), $CH_3CH_2{}^{18}O^-$ (*m/z* = 47 Da), $CH_3CH_2{}^{16}O^-{\cdot}H_2O$ (*m/z* = 63 Da), and $CH_3CH_2{}^{18}O^-{\cdot}H_2O$ (*m/z* = 65 Da). (d) (^{15}N)nitrate ethyl ester: $CH_3CH_2{}^{16}O^-$ (*m/z* = 43 Da) and $^{15}NO_2^-$ (*m/z* = 47 Da).

Analysis of MOOS-2 CRM. Fig. 1.2 shows the CI– GC/MS chromatogram obtained for the analysis of nitrite and nitrate in seawater (MOOS-2 CRM). The chromatographic conditions chosen give and extremely clean chromatography, despite a void of about 10 minutes between the elution of the two analytes. This aspect of the chromatography can be readily improved by choosing a shorter column or modifying the oven program.

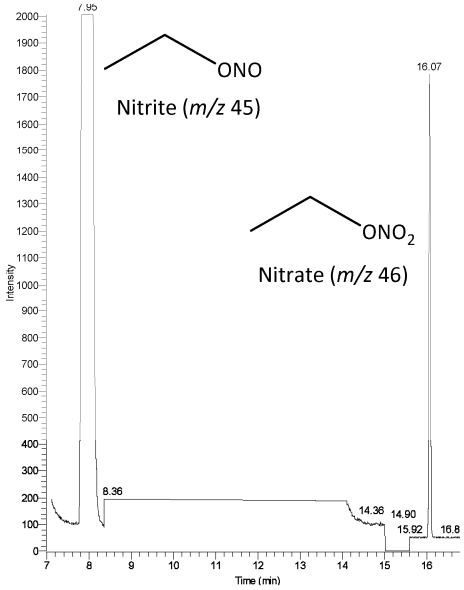

Figure 1.2 CI− GC/MS chromatogram (SIM mode) of MOOS-2 CRM with $c(NO_2^-)$ = 3.4 µM and $c(NO_3^-)$ = 22 µM. Nitrite ion in the form of CH_3CH_2ONO elutes at 7.95 min (m/z = 45 Da); and nitrate ion in the form of $CH_3CH_2ONO_2$ elutes at 16.07 min (m/z = 46 Da).

Results for 14 independent measurements of MOOS-2 are reported in Table 1.1 and achieved by the use of the following equation:

$$c_A = c_A^0 \cdot \frac{R_2 - R_N}{R_2 - R_E} \cdot \frac{R_1 - R_E}{R_1 - R_N}$$

Where c_A is the concentration of the analyte in the sample, c_A^0 is the concentration of the reference analyte (primary standard); R_1 and R_2 are the isotope amount ratios (m/z 45/47 for nitrite and 46/47 for nitrate) arising from the spiked blend of the sample (MOOS-2) and of the spiked blend of the reference, respectively; R_N and R_E are the isotope amount ratios for the sample and the enriched spike, respectively. The isotope patterns of the analyte and the primary standard are identical. Note that there is no need for mass bias correction since all four isotope amount ratios R_1, R_2, R_E, and R_N in the above equation can be substituted with the corresponding measured isotope

ratios r_1, r_2, r_E, and r_N. The above equation is equivalent to that reported in 1994 by Henrion [34]. Formally, the concentration of the analyte is written as a function of the concentration of a primary standard and measured isotope amount ratios. In order to minimize the instrumental measurement biases, both the sample and the reference were spiked with the same amount of enriched analyte in order to obtain matching amount ratios $R_1 = R_2 = 1$.

To realize this, the concentration of the primary standard has to be the same as that of the analyte in the sample. When $R_1 = R_2 = 1$, the equation reduces to $c_A = c_A^0$, which permits significant reduction in the systematic errors arising from the measurements. In addition, prior knowledge of the isotope patterns of the spike and analyte is not necessary. Table 1.1 summarizes results for the measurements on MOOS-2 obtained by exact matching. The concentration of nitrite and nitrate found, $c(NO_2^-) = 3.37 \pm 0.08$ µM and $c(NO_3^-) = 22.0 \pm 0.2$ µM, are in good agreement with the certified property values, $c(NO_2^-) = 3.31 \pm 0.18$ µM and $c(NO_2^-) + c(NO_3^-) = 24.9 \pm 1.0$ µM, and exhibit good precision for both nitrite and nitrate.

Table 1.1 Exact matching isotope dilution determination of nitrite and nitrate in MOOS-2[a].

Nitrite				Nitrate			
r_1	r_2	c^0_A /µM	$c_{A,\ MOOS\text{-}2}$ /µM	r_1	r_2	c^0_A /µM	$c_{A,\ MOOS\text{-}2}$ /µM
0.9356			3.31	1.030			22.1
0.9543			3.48	1.028			22.1
0.9325	0.9371	3.32	3.28	1.035	1.007	21.6	22.3
0.9477			3.42	1.025			22.0
0.9255			3.22	1.022			22.0
1.086			3.48	1.003			21.7
1.073			3.38	1.022			22.1
1.068	1.064	3.32	3.35	1.029	0.9993	21.6	22.3
1.086			3.48	1.017			22.0
1.066			3.34	1.016			22.0
0.9565			3.41	1.021			21.9
0.9415	0.9596	3.43	3.29	1.021	1.027	22.0	21.9
0.9450			3.32	1.025			22.0
0.9606			3.44	1.028			22.0
		Mean	**3.37**			**Mean**	**22.0**
		u	**0.08**			***u***	**0.2**
		u_r	**2.5 %**			u_r	**0.7 %**

[a]Certified property values: $c(NO_2^-)$ = 3.31 ± 0.18 µM and $c(NO_2^-) + c(NO_3^-)$ = 24.9 ± 1.0 µM.

1.2

Paper attached: Annex VI

Determination of fluoride by GC/MS: a novel methodology

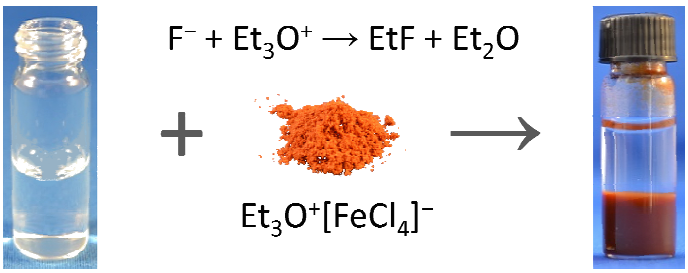

Reproduced from *Anal. Chem.* **2012**, DOI: 10.1021/ac302303r
Copyright 2012 American Chemical Society

Introduction. A large number of municipalities in North America voluntarily supplement their drinking water with fluoride as it prevents tooth decay owing to its cariostatic activity. At high concentration it is toxic and it must be balanced against the potential risk of over-exposure, leading to fluorosis [36–39]. Ensuing debates over the efficacy of fluoridation notwithstanding, accurate monitoring of fluoride is of importance in countries where water fluoridation is practiced. Due to the toxic effects of fluoride at higher concentration, a guideline value of 1.5 mg/L was recommended by the World Health Organization as a level at which dental fluorosis should be minimal. Considering also that levels of fluoride can vary significantly in natural waters, reaching 30 mg/L in some regions of India [40], the monitoring of fluoride in water and food products is important.

The state of the art of fluoride determination was revised by Campbell [41] in 1987. Fluorine, like boron, does not enter into chemical reactions that are selective enough to permit its direct determination in the presence of elements with which it is

commonly associated [42]. Consequently, the major part of spectrophotometry or fluorescence methods are based on indirect determination [43–44].

A significant advance in the determination of fluoride was the development of the fluoride ion-sensitive electrode in 1966 [45]. Although ion-selective electrodes are convenient tools, they respond to the activity of fluoride ions, not concentration, and are affected by the hydroxide ions present. Consequently, they have to be used as end-point indicators in titrimetry when results traceable to g/L are required [45].

Mass spectrometry effectively addresses both the problem of measurement specificity and traceablity.

Derivatization of fluoride ions has traditionally been performed using silicon-based chemistry, such as the Me_3SiF [46–47] or Ph_3SiF [48]. The volatile fluorosilanes can be determined by gas chromatography following either liquid extraction with organic solvents or solid-phase microextraction from the headspace, achieving a detection limit of 6 µg/L in the latter case with Me_3SiF. Although the silicon-based chemistry produces volatile fluoro-compounds, the Si–F bond is not stable in aqueous solutions, especially at high pH. Consequently, Kage et al. [49] proposed alkylation of fluoride with pentafluorobenzylbromide (F_5BzBr), yielding volatile F_5BzF which can be determined by GC/MS in biological fluids. Although the stability of the obtained derivative is achieved, this derivatization chemistry suffers poor sensitivity ($\gamma(F^-)_{DL}$ = 0.5 mg/L).

Tertiary oxonium salts have recently been applied for the derivatization of inorganic anions, including chloride, bromide, iodide, cyanide, thiocyanate, sulfide, nitrite and nitrate [7]. Commercially available $Et_3O^+[BF_4]^-$ is not suitable for determination of fluoride, because tetrafluoroborate slowly hydrolyzes releasing fluoride ions. To overcome this drawback, the method proposed here employs triethyloxonium tetrachloroferrate(III). The resulting stable fluoroethane can be subjected to gas chromatography and detected with mass spectrometry. This method has unique advantages over the existing methods. Despite smaller throughput compared to

classical electrochemical determination, this novel ethyl-derivatization chemistry coupled with GC/MS gives better selectivity and specificity allowing the determination of fluoride free of spectral interferences. With respect to other GC/MS approaches, this method offers comparable (or better) sensitivity, but is considerably safer then silylation or alkylation with F_5BzBr because $Et_3O^+[FeCl_4]^-$ is a water soluble salt which undergoes complete hydrolysis in few hours and not a volatile liquid such as Me_3SiCl. Moreover, another important quality of the triethyloxonium derivatization over all the existing methods for the determination of fluoride is the ability of the former to deal with interference. All quantification methods for fluoride suffer severe matrix effects, especially for the presence of Al(III) and Fe(III). Here is demonstrated that large amount of those cations able to complex fluoride ions are not critical for the triethyloxonium derivatization and the negative effects can be accounted by using the method of the standard additions.

$Et_3O^+[FeCl_4]^-$ Derivatization. Unlike triethyloxonium tetrachloroferrate(III), which was selected in this work for determination of fluoride, the two commercially available oxonium salts, $Et_3O^+[BF_4]^-$ and $Et_3O^+[SbCl_6]^-$, are unsuitable analytical reagents for conversion of fluoride to fluoroethane,

$$Et_3O^+(aq) + F^-(aq) \rightarrow EtF(g) + Et_2O,$$

because $Et_3O^+[BF_4]^-$ releases fluoride ions during hydrolysis of the tetrafluoroborate [50]:

$$[BF_4]^- + H_2O \rightarrow [BF_3OH]^- + HF$$

whereas $Et_3O^+[SbCl_6]^-$ is not water soluble. Ethylation of fluoride with $Et_3O^+[FeCl_4]^-$ requires alkaline medium (pH = 10) because acid environment releases Fe(III) which

binds with fluoride ions. In addition, the alkalinity of the sample results in the precipitation of endogenous metal ions, removing them as potential interferences in the determination of fluoride. Moreover, alkaline conditions avoid the conversion of fluoride into gaseous hydrofluoric acid and this is indeed an advantage compared to the acidic silylation method, where potential analyte losses in the form of gaseous HF can occur. The ethylation reaction stops after the complete hydrolysis of Et_3O^+. Granik et al. [51] reported that complete hydrolysis of Et_3O^+ occurs in 80 min. From our previous research [7] and from similar experiment repeated here for $Et_3O^+[FeCl_4]^-$, we found that complete hydrolysis and equilibration of the headspace is complete in 3 h. After this time, the headspace can be sampled for analysis by GC/MS. Fluoroethane is a stable compound and was detected in the headspace even three days after the derivatization. The chemical yield for derivatization, achieved using the experimental conditions described herein, was 8%.

Figures of merit and applications. The determination of fluoride was undertaken on various liquid matrices, including rainwater, tap water, seawater, urine, beer, and soft drinks. In this work, a standard additions calibration approach was chosen for quantitation whereby the fluoroethane peak (m/z = 47 Da signal) was integrated and regressed against the amount of fluoride added. The mass concentration of fluoride in the sample was calculated from the linear regression plots. Headspace sampling and injection into GC/MS was performed manually; no internal standards were used to correct for variations that may occur during these operations. This methodology was validated using a simulated rainwater certified reference material sample (ERM®-CA408) yielding good agreement with the certified property value, as summarized in Table 1.2. Other matrices were then examined, including the City of Ottawa tap water, seawater (MOOS-2 NRC reference material), urine (from a healthy volunteer), beer, and two commercial soft drinks. Results are summarized in Table 1.3 and are based on the mean values of three independent measurements derived from four point

standard additions curves (in addition to the unspiked sample). For each measurement, the relation between the amount of fluoride added and the integrated signal was always linear and characterized by a coefficient of determination R^2 > 0.99. The concentration of fluoride determined in Ottawa drinking water, $\gamma(F^-)$ = 0.717 ± 0.063 mg/L, is in agreement with the target level of 0.70 mg/L recommended by Health Canada and adopted by the City of Ottawa [52]. With the exception of the two soft drinks that do not show the iron hydroxide precipitate, all samples show three phases after the derivatization with $Et_3O^+[FeCl_4]^-$: (1) a precipitate which contains $Fe(OH)_3$ and part of the matrix, (2) an aqueous phase wherein the fluoride is converted to fluoroethane, and (3) the upper gas phase from which the fluoroethane is sampled. Derivatization allows separation of the analyte from the matrix in vapor phase and enables the realization of extremely clean chromatograms. Fig. 1.3 shows the results from a urine sample; even with such a complex matrix, there are no interferences co-eluting with the analytical peaks.

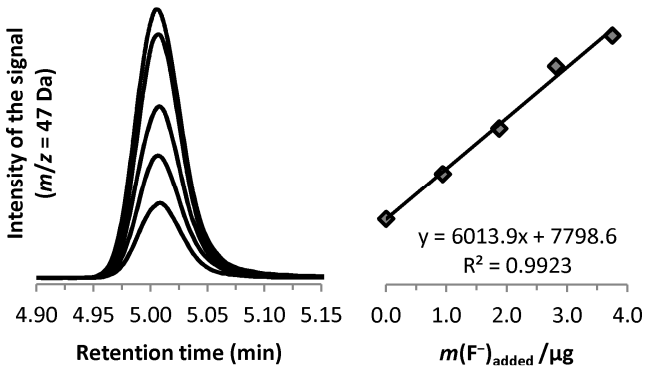

Figure 1.3 Analytical peaks for fluoroethane (at *m/z* = 47 Da) derived from a sample of incrementally spiked urine and the resulting standard additions calibration plot.

The instrumental limit of detection obtained by processing calibration solutions is $\gamma(F^-)_{DL}$ = 3.2 µg/L. This value is based on the signal-to-noise ratio calculated from the standard deviation of the baseline in proximity to the analyte peak (*i.e.* detection

limit is the concentration which produces a signal-to-noise-ratio of three). Standard solutions of $\gamma(F^-)$ = 123 µg/L and 531 µg/L give a signal-to-noise ratios of 115 and 492, respectively.

Table 1.2 Determination of fluoride in a simulated rainwater ERM®-CA408.[a]

run	$\gamma(F^-)$/(mg/L)
1	0.186 ± 0.034
2	0.196 ± 0.020
3	0.195 ± 0.017
4	0.199 ± 0.011
mean	**0.194 ± 0.012**
u_r	**6.5%**

[a] Certified property value: $\gamma(F^-)$ = 0.194 ± 0.008 mg/L.

Table 1.3 Determination of fluoride in various matrices

Matrix	$\gamma(F^-)$/(mg/L)
soft drink A	0.225 ± 0.019
soft drink B	0.213 ± 0.022
Beer	0.379 ± 0.038
Urine	0.594 ± 0.073
tap water	0.717 ± 0.063
Seawater	1.39 ± 0.09

Reported value is the mean of three independent determinations.

Interferences. Table 1.4 summarizes the interference arising from the presence of 10 mmol/L (240-650 mg/L) of several cations added to standard solutions containing 50 µmol/L of fluoride. This condition of large excess of interference, 200-fold higher than the analyte itself, was chosen in order to show the capacity of the methodology to keep under control the interference of metal cations, which frequently present a common interference for this kind of determination. When the sample is pretreated with NH_4OH and derivatized with $Et_3O^+[FeCl_4]^-$, signal suppression is observed in the presence of Mg(II), Ca(II), Fe(III), and Al(III). The latter exhibits the most severe interference and contributes to a decrease in the analytical signal of an order of magnitude as a consequence of its complexation capacity with fluoride. Negligible effects were evident with Zn(II), and Cu(II). The alkaline condition which arises after the pretreatment of the sample with aqueous NH_4OH, results in precipitation of most of these metal cations as hydroxides, allowing their separation from the solution and reducing their ability to complex fluoride. Al(III) hydroxide is redissolved in alkaline

condition because as the formation of the complex $Al(OH)_4^-$, and this could be at the origin of the severe interference effect of Al(III) on EtF formation. In this vein, the presence of $Al(OH)_4^-$ could accelerate the hydrolysis of the triethyloxonium or interact with the analyte in a reaction of ligand exchange such as:

$$Al(OH)_4^- + F^- \rightarrow AlF(OH)_3^- + OH^-$$

becoming a competitor with the derivatization itself.

Table 1.4 Interference effect arising from the presence of 10 mM metal ion in $c(F^-)$ = 0.05 mM/L standard solution.

Interference	S/S_0 [a]
None	1.00 ± 0.07
Al(III)	0.11 ± 0.09
Fe(III)	0.62 ± 0.07
Ca(II)	0.83 ± 0.03
Mg(II)	0.32 ± 0.02
Zn(II)	0.97 ± 0.06
Cu(II)	1.01 ± 0.06

[a] S/S_0 is the ratio between the analytical signal of the fluoride (S) in the presence of interference to that generated without interference (S_0). Three independent measurements were performed.

Conclusion. Triethyloxonium tetrachloroferrate(III) was successfully employed in this study for derivatization of fluoride ion into the stable and volatile fluoroethane. This allows its facile determination by GC/MS in matrixes of varying complexity. The method is analyte-specific, does not require the use of organic solvents, utilizes a water-solubleand solid derivatizing reagent, and offers low µg/L detection limits. Further improvement of the analytical figures of merit appears possible by employing

an automated purge-and-trap system for sampling which will quantitatively transfer the fluoroethane generated. In addition, bromide and iodide ions can be employed as ideal internal standards since they undergoes the same derivatization chemistry as fluoride. To this end, a standard addition approach with an endogenous internal standard [53], such as bromide, will greatly improve the method proposed here, providing better precision and ensuing traceability.

Experimental

Triethyloxonium tetrachloroferrate(III). $Et_3O^+[FeCl_4]^-$ was synthesized according to the procedure of Meerwein et al. [54]:

$$2Et_2O{\cdot}FeCl_3 + C_2H_3(O)CH_2Cl \rightarrow [Et_3O]^+[FeCl_4]^- + FeCl_2[(OCH(CH_2Cl)CH_2OEt].$$

For this purpose, 0.2 mol (32.4 g) anhydrous $FeCl_3$ was dissolved in 150 mL of dry diethyl ether and the formed solution was evacuated and filled with argon three times using a Schlenk line while keeping argon flowing during the reaction, and then 0.1 mol (9.25 g) 2-(chloromethyl)oxirane was added drop-wise using a syringe under magnetic stirring. The addition of 2-(chloromethyl)oxirane was controlled to keep the ether under constant boiling. After the addition, the resultant mixture was stirred for 5 min and then cooled to 0 °C using an ice/water bath and held at this temperature for 2 h with gentle magnetic stirring. The formed crystal was filtered on a Büchner funnel to recover the brown product, which was subsequently washed with dry ether twice; 23.2 g of $Et_3O^+[FeCl_4]^-$ was obtained (77% yield), enough to perform all the experiments described herein.
Although the triethyloxonium tetrachloroferrate(III) is soluble in water, it slowly undergoes hydrolysis. Aqueous solutions of this salt should therefore be prepared shortly before use. In this work, the $Et_3O^+[FeCl_4]^-$ solutions were prepared by dissolving 0.4 g $Et_3O^+[FeCl_4]^-$ in 16 mL of MilliQ water.

Sample preparation. A 2 mL volume of aqueous sample was introduced without pretreatment into five different vials; four of which were then spiked with 0.2 mL of different fluoride standard solutions whereas 0.2 mL of MilliQ water was added to the remaining vial. Quantitation of fluoride was based on the method of standard additions and the concentration of the standard was chosen so to observe a maximum of four-fold increase of the analytical signal compared to the un-spiked sample. The samples were spiked with a 50 µL volume of $w(NH_3)$ = 0.2 g/g ammonia solution, and then with a 1 mL volume of $Et_3O^+[FeCl_4]^-$ solution prepared as described above (the alkalinity of the sample entails the precipitation of $Fe(OH)_3$). After the addition of all reagents, the vials were quickly sealed with a screw-cap containing a PTFE/silicone septum and kept at room temperature for 3 h before sampling the headspace with a gas-tight syringe. Triethyloxonium converts F^- into fluoroethane which is gaseous at ambient temperature (t_{vap} = –37 °C). Therefore, in order to avoid analyte loss, it is important that unpunctured septa be used for sealing.

GC/MS analysis. A Hewlett-Packard 6890 gas chromatograph equipped with a Hewlett-Packard 5973 mass selective detector was operated at constant flow (0.9 mL He/min) . Pulsed split (5:1) injection mode was chosen, with a pulsed pressure of 172 kPa for 1 min and the inlet temperature was set at 100 °C. After the first isotherm at 30 °C (held for 7 min) the oven was heated at 20 °C/min to 200 °C. The transfer line temperature was 230 °C. The generated fluoroethane was manually sampled with a gas-

tight syringe from the vial headspace and a 250 µL volume injected into the GC/MS. To attain a clean chromatogram, a 60 m DB-624 column (6% cyanopropyl-phenyl 94% dimethyl polysiloxane) was chosen. Fluoroethane eluted at 5 min under the 30 °C isotherm. In addition, to improve the chromatographic performance, a narrow inlet liner designed for SPME and having an internal diameter of 0.75 mm was used.

The mass spectrometer was operated in electron impact mode (70 eV) using standard settings (ion source temperature 250 °C; quadrupole temperature 150 °C). The intensity of the molecular ion in the electron impact mass spectrum of fluoroethane (Fig. 1.4) is low (10% of the base peak) and the most abundant fluorine-containing ions are CH_2CH_2–F^+ (100%, *m/z* = 47 Da) and CH_2–F^+ (20%, *m/z* = 33 Da). Therefore, detection of fluoroethane was done by selected ion monitoring (SIM) using signals at *m/z* = 33 and 47 Da with 100 ms dwell time for each. The area of the peak extracted at *m/z* = 47 Da was used for quantitation purposes whereas the fragment ion at *m/z* = 33 Da was acquired for quality control.

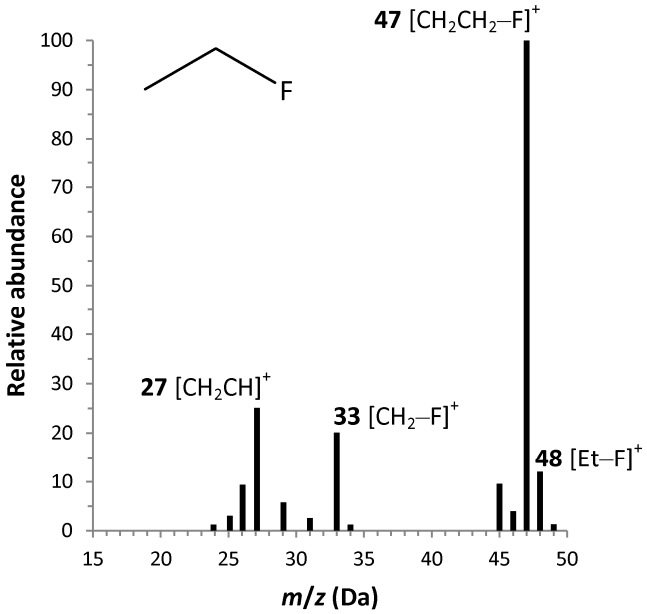

Figure 1.4 Electron impact mass spectrum of fluoroethane.

Part 2

Chemical generation of volatile hydrides: New mechanistic evidence

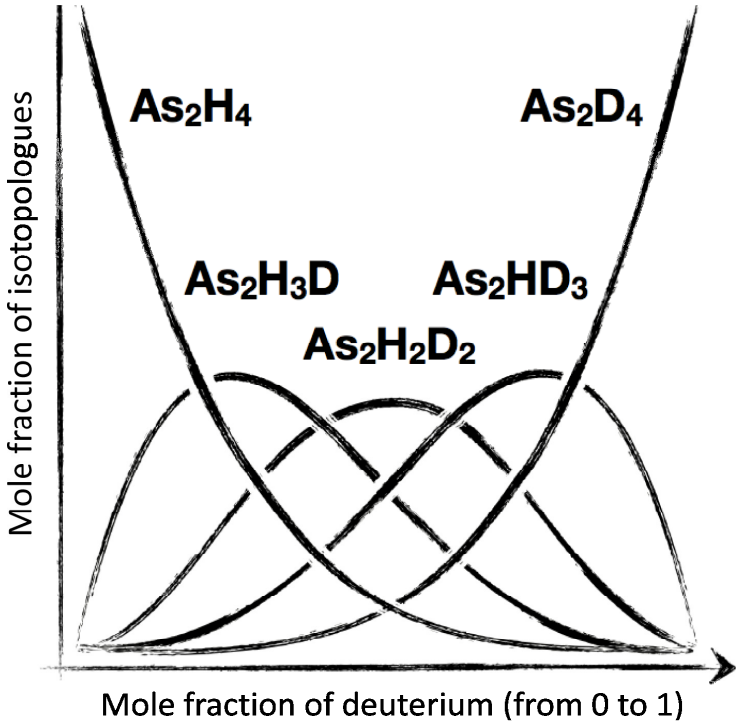

Predicted binomial distribution of chemical generated diarsane isotopologues - $As_2H_nD_{4-n}$

Chemical generation of volatile species of metallic or organometallic compounds by reactions with aqueous $NaBR_4$ (R = H, alkyl or phenyl group) or XBH_3 (X = NH_3, NR_3, CN^-) coupled with atomic or molecular spectroscopy or with mass spectrometry is among the most powerful analytical tools for trace element determination and speciation [55]. Despite the popularity of hydride generation by reaction with aqueous $NaBH_4$, the mechanism which rules this chemistry has received poor attention since few years ago [22]. Most of the more relevant mechanistic aspects of hydride generation has been collected using stable hydrides such as arsane and methyl arsanes and can be summarized as follows [22]:

1. The volatile hydrides is formed by direct transfer of hydrogen from boron to the analyte.
2. The volatile hydride is formed step-wise, i.e. all the hydrogens in the final hydride come from different borane molecules.
3. The hydride transfer takes place through the formation of analyte-borane complex intermediates.

The mechanism is valid when the analyte is very dilute ($< 10^{-5}$ mol/L), and $[BH_4]^-$ is in strong excess (> 0.1 mol/L). Therefore this mechanism can be called *analytical*.

In the course of the present work, it has been found that there are different conditions which entail a strong perturbation of this analytical mechanism. For example the presence of noble metals such as Au(III) and Pd(II) alters the mechanism of hydrogen transfer, while when the concentration of analyte increase, a gamut of condensation by-products is observed.

2.1

Papers attached: Annex II and V

Mechanistic interference of noble metals

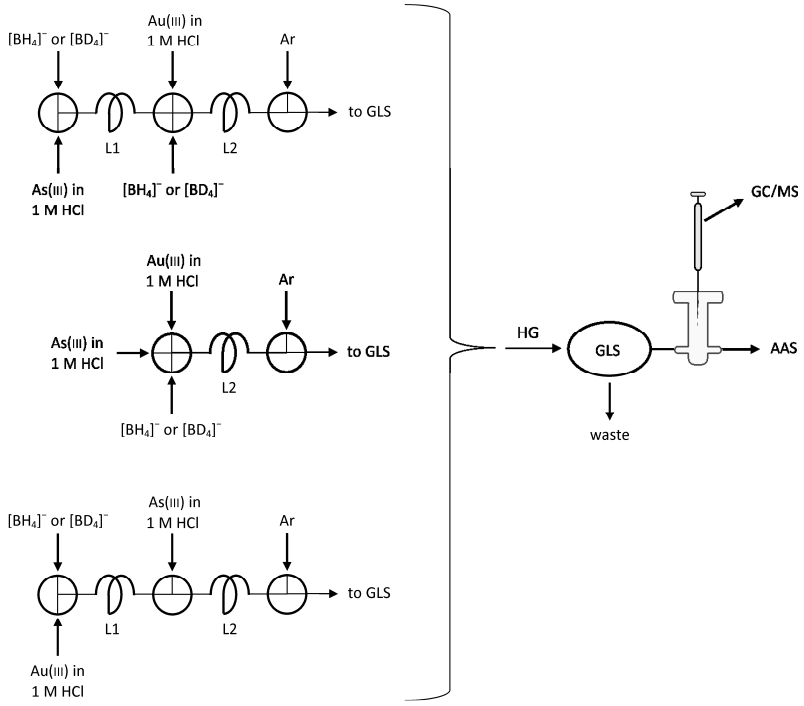

Reproduced in part from
Spectrochim. Acta Part B **2011**, *66*, 740–747
Copyright 2011 Elsevier B.V.

Introduction. Transition metals, and in particular noble metals, can produce severe interference in the generation of volatile arsane and other volatile hydrides by reaction with aqueous $NaBH_4$ [56–57]. The colloids which are formed by reduction of these transition metals can:

1. adsorb the already formed hydride.
2. decompose $[BH_4]^-$.

In both of these cases, the *interference* is seen as a process which contributes to decrease the amount of hydride reaching the detector. However, since the '70s it is clear that transition elements such as Co(II), Ni(II) [58] and Rh(III) [59] can modify

the reducing power of tetrahydroborate, allowing reduction of functional groups like nitriles, amides, and olefins, which cannot be reduced by $[BH_4]^-$ alone [60–61].

In this study the effect of several transition and noble metals on the mechanism of arsane generation by $[BH_4]^-$ was investigated. Batch and continuous flow hydride generation systems coupled with atomic absorption spectrometry and GC/MS were employed to measure the effect of Au(III), Pd(II), Pt(II), Rh(III), Ni(II) and Cu(II) (0.5–20 mg/L) on reaction yield and isotopic composition of arsane.

The results obtained herein show a perturbation in the mechanism of hydrogen transfer from the borano complex to the analytical substrate – i.e. a *mechanistic interference*.

Discussion and conclusion. In the absence of foreign species, the mechanism of arsane generation is due to the direct stepwise transfer of hydrogen from borane to arsenic. Using a mixed solution of $[BH_4]^-$ and $[BD_4]^-$ the isotopic composition of the generated arsane isotopologues is binomial:

$$x_{AsH_nD_{3-n}} = \frac{3!}{n!(3-n)!} \cdot x_D^{3-n} \cdot (1-x_D)^n$$

For a given value of x_D corresponds one and only one set of $x(AsH_nD_{3-n})$. This set describes the distribution of arsane isotopologues and cannot be achieved with other values of x_D.

The presence of Au(III), Pd(II) Pt(II), and Rh(III) induces a significant perturbation in the binomial mechanism of hydride generation, promoting the incorporation of a large amount of hydrogen derived from the solvent into the final arsane. Moreover, the experimental distribution of arsane isotopologues – $x(AsH_nD_{3-n})$ – generated in presence or in absence of these interferences changes significantly. An example is reported in Fig. 2.1 for Pt(II).

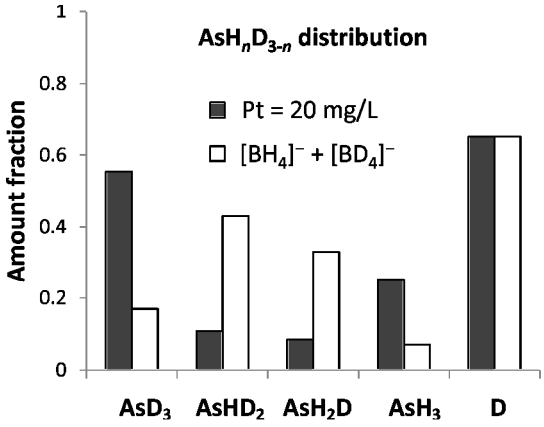

Figure 2.1 Arsane isotopologues generated by reaction of 1 mg/L As(III) with 0.2 M $[BD_4]^-$ in presence of 20 mg/L of Pt(II) (grey bars) and the corresponding binomial distribution calculated at the same level of deuterium incorporation (x_D = 0.63, white bars)

This perturbation of the binomial incorporation of hydrogen into the final hydride takes place at concentrations of metals which hardly affect the generation efficiency of the arsane and can likely be addressed to the action of intermediate species formed in the early stage of the reaction. The mechanistic interference reported here cannot be explained by H/D exchange of the borane complex before its reaction with the arsenite because in this case it would affect only the total amount fraction of deuterium incorporated, not the relative distribution of arsane isotopoloques.

A possible interpretation of this result can be achieved by considering the reductive process as the sum of two competing events: the reduction by $[BH_4]^-$ which is binomial, and the reduction by a hydride-borane-metal intermediate, present in the early stage of the reaction, and able to exchange hydrogen with the solvent. The postulation of the existence of a "new" reducing agent, with different reductive power respect to $[BH_4]^-$ alone is also supported by observation reported in the organic chemistry literature, as note earlier. This evidence reveals the existence of a new type of interference in chemical generation of volatile hydrides - a *mechanistic interference* - in addition to the already known yield interferences. Unfortunately, it was not possible to study how the mechanistic interference of these metal ions

propagates from arsane to di- and triarsane generated via the condensation cascades under non-analytical conditions (paragraph 2.2).

2.2

Paper attached: annex III

Condensation cascade and methyl transfer in arsane generation

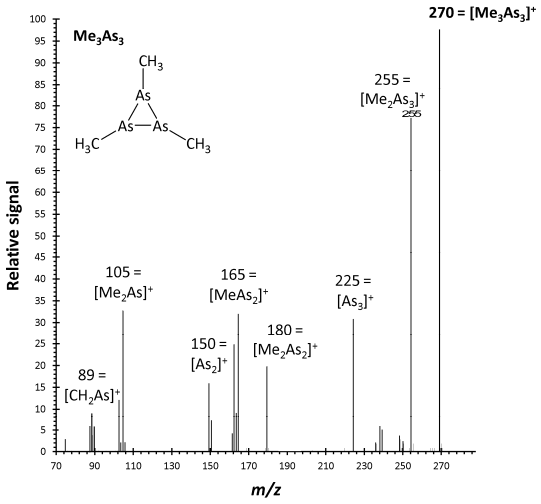

Reproduced in part from
Anal. Bioanal. Chem. **2012**, *402*, 921–933
Copyright 2011 Springer-Verlag

Discussion and conclusion. Under analytical conditions a large excess of aqueous $[BH_4]^-$ converts As(III), As(V), $MeAsO(OH)_2$, or $Me_2AsO(OH)$ to unique volatile arsanes (AsH_3, $MeAsH_2$ and Me_2AsH). In all of these cases it has been verified, by using deuterium labeled reagents, that the mechanism of formation is the same, i.e. direct stepwise transfer of hydrogen from boron to arsenic:

$Me_2AsO(OH)$ → **Me_2AsOH** → **Me_2AsH**

$MeAsO(OH)_2$ → $MeAs(OH)_2$ → $MeAsH(OH)$ → **$MeAsH_2$**

$AsO(OH)_3$ → $As(OH)_3$ → $AsH(OH)_2$ → $AsH_2(OH)$ → **AsH_3**

$As(OH)_3$ → $AsH(OH)_2$ → $AsH_2(OH)$ → **AsH_3**

where all compounds in bold have been identified.

When elevated concentrations of As(III), $MeAsO(OH)_2$ or $Me_2AsO(OH)$ are reacted by $NaBH_4$ in aqueous media, the formation of byproducts is visible, Fig. 2.2. From quantitative determination was possible to concluded that – under these conditions – the major part of the arsenic remains in condensed phase (65% for inorganic As(III) and As(V), and more than 98% for both methyl arsenates). For $Me_2AsO(OH)$, no precipitate was visible, but a white gas was generated upon the addition of $NaBH_4$ (Fig. 2.2).

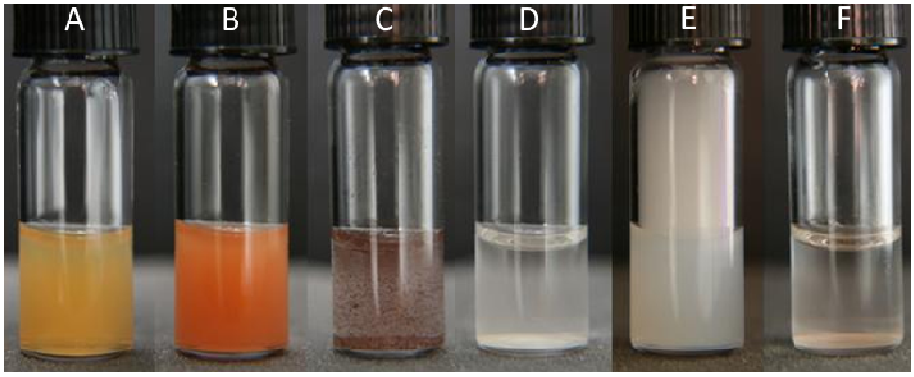

Figure 2.2 Visual change occurring during the reduction of As(III) (A-C) and $Me_2AsO(OH)$ (D-F) with $NaBH_4$ (color changes for As(III), As(V), and $MeAsO(OH)_2$ are similar). Images are taken approx. 1 s, 1 min, and 1 h after mixing the reagents, respectively. Experimental conditions: 1.4 mL of As solution (10 mM As in 0.1 M HCl) is reduced by 0.2 mL 0.2 M $NaBH_4$ in 0.1 M NaOH

In spite of the small amount fraction of volatile species that are formed under these conditions, their GC/MS identification gave interesting information about the reactions partaking in the liquid phase.

For inorganic As(III) and As(V) , the only observed volatile byproducts are diarsane (H_2AsAsH_2) and triarsane ($H_2AsAsHAsH_2$). A dedicated investigation on their formation is reported in paragraph 2.2.1. A gamut of volatile compounds was generated during the reduction of methyl arsenate. For $Me_2AsO(OH)$ only dimeric species were detected, but in non-analytical condition the most abundant volatile product was Me_3As, and not the expected Me_2AsH.

From all the observations collected (Annex III) it was concluded that the formation of these unwanted byproducts is due to the reaction between the intermediates formed during the reduction and the final hydride, i.e. condensation and methyl transfer reactions.

The condensations take place among arsenic species containing As-OH and As-H moieties. This leads to formation of AsAs chain by elimination of water. the following reaction explains the formation of diarsanes:

$$\mathbf{Me_2AsOH} + \mathbf{Me_2AsH} \rightarrow \mathbf{Me_2AsAsMe_2} + H_2O$$

$$MeAsH(OH) + \mathbf{MeAsH_2} \rightarrow \mathbf{MeHAsAsHMe} + H_2O$$

$$AsH_2(OH) + \mathbf{AsH_3} \rightarrow \mathbf{H_2AsAsH_2} + H_2O$$

where the species in bold where identified. Formation of triarsanes can be explained in a similar fashion. In general, when in solution are present at the same time elevate concentration of arsenates and arsanes (As–OH and H–As), the condensation reaction may proceed in cascade, bringing to the formation of linear or branched polymers:

$$2nH–(AsX)–OH \rightarrow H–(XAs–AsX)_n–OH + 2(n-1)H_2O$$

or cyclic As species,

$$H–(AsX)_n–OH \rightarrow (XAs)_n + H_2O$$

which remain in the solid phase.

This condensation pathways found an interesting confirmation also when the reduction of As(III) was performed in presence of Sb(III). In this case it was possible to identify by GC/MS the mixed dimer H_2AsSbH_2:

$$H_2AsOH + HSbH_2 \rightarrow H_2AsSbH_2 + H_2O \text{ and/or}$$

$$H_2SbOH + HAsH_2 \rightarrow H_2SbAsH_2 + H_2O$$

The reactivity of dimethyl arsenates can only be explained partially by this mechanism. The condensation reactions stop with the formation of $Me_2AsAsMe_2$ which does not undergo further condensations. However, the formation of Me_3As when non-analytical amounts of $Me_2AsO(OH)$ are reduced by $[BH_4]^-$, cannot be explained by condensation reactions. The formation of trimethylarsane is due to reaction of methyl transfer taking place among the intermediates (such as Me_2As-$AsMe_2$, and Me_2AsOH) and dimethy arsane. The presence of a methylating agent in this reaction system is also confirmed by the formation of $MeSbH_2$ during the simultaneous reduction of $Me_2AsO(OH)$ and Sb(III) under non-analytical conditions.

The addition of cysteine (RSH) supressed the formation of unwanted byproducts. The action of this masking agent was rather effective for $Me_2AsO(OH)$, where the formation of Me_3As was completely eliminated. It is well known that thiols reduce arsenic compounds to thiolates such as $As(SR)_3$, $MeAs(SR)_2$, and $Me_2As(SR)$ [62–65], which are quantitatively converted by $NaBH_4$ into the corresponding hydrides [66–67]. Consequently, intermediate hydroxyarsanes are not formed and the condensation reaction cannot take place.

2.2.1

Paper attached: annex V

Formation of $As_2H_nD_{4-n}$ and $As_3H_nD_{5-n}$

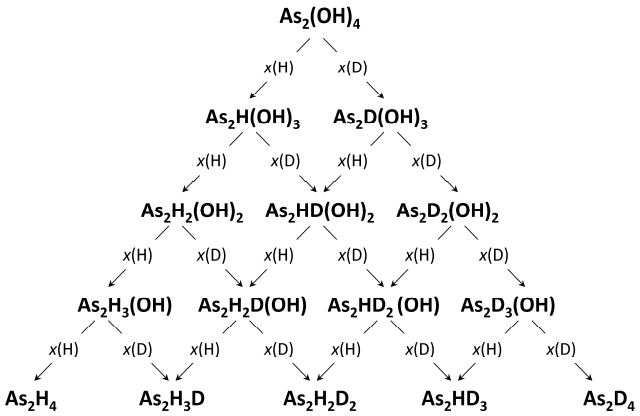

Reproduced in part from
J. Am. Soc. Mass Spectrom. **2012**, *25*, 2178-2186
Copyright 2012 Her Majesty the Queen in Right of Canada

Introduction. Mass spectra of arsenic hydride isotopologues show significant overlap (e.g., AsD^+ and AsH_2^+, etc.). Moreover, it is not feasible to synthesize pure partially deuterated isotopologues or separate them by conventional gas chromatography. Nevertheless, the determination of the amount fraction of each isotopologue in a mixture can be achieved mathematically [68–70].

A statistical model was employed to calculate the mass spectrum of each isotopologue $As_2H_nD_{4-n}$ and $As_3H_nD_{5-n}$ (Table 2.1 and 2.2). From this reconstructed spectra it is possible to determine the quantity of the various isotopologues from their mixtures. This is achieved using the relationship:

$$Y = FA$$

where Y is the mass spectrum (vector) of the mixture of isotopologues, F is the matrix reporting the mass spectra of the pure isotopologues (Tables 2.1 and 2.2) and A is the vector reporting the mole fraction of each component in the mixture.

Using this method it was possible to delineate the mechanism of formation of diarsane and triarsane in the As(III)/$[BH_4]^-$ system.

Table 2.1 Reconstructed mass spectra of $As_2H_nD_{4-n}$ isotopologues

(m/z)/Da	As_2H_4 [a]	As_2H_3D [b]	$As_2H_2D_2$ [b]	As_2HD_3 [b]	As_2D_4 [a]
150	0.478 ± 0.003	0.449 ± 0.022	0.431 ± 0.029	0.423 ± 0.023	0.425 ± 0.003
151	0.146 ± 0.002	0.109 ± 0.025	0.072 ± 0.029	0.036 ± 0.020	0.000
152	0.158 ± 0.002	0.121 ± 0.037	0.101 ± 0.037	0.100 ± 0.027	0.120 ± 0.003
153	0.003 ± 0.001	0.096 ± 0.022	0.125 ± 0.018	0.094 ± 0.018	0.000
154	0.215 ± 0.003	0.003 ± 0.001	0.039 ± 0.015	0.106 ± 0.026	0.208 ± 0.002
155	0.000	0.222 ± 0.003	0.003 ± 0.002	0.003 ± 0.001	0.000
156	0.000	0.000	0.229 ± 0.003	0.002 ± 0.001	0.004 ± 0.001
157	0.000	0.000	0.000	0.236 ± 0.004	0.000
158	0.000	0.000	0.000	0.000	0.243 ± 0.004

[a] Experimental mass spectrum. Each experimental set of data represents the mean of three independent determinations. Standard deviation of the results is reported in parentheses.

[b] Statistical model. Each set of data represents the mean of 5×10^7 simulations. Standard deviation of the results is reported.

Discussion and conclusion. Reduction of arsenite with boranes is a concerted multistep reaction wherein all –OH groups from the As-substrate are replaced by –H groups originating from different borane molecules:

$$As(OH)_3 + 3[BX_3H]^- \rightarrow AsH_3 + 3[BX_3OH]^- \ (X = H, OH),$$

As shown previously (paragraph 2.2), under non analytical condition the reduction of inorganic As(III) and As(V) by aqueous $[BH_4]^-$ brings to the formation of condensation byproducts such as diarsane and triarsane.

Table 2.2 Reconstructed mass spectra of $As_3H_nD_{5-n}$ isotopologues

(m/z)/Da	As_3H_5 [a]	As_3H_4D [b]	$As_3H_3D_2$ [b]	$As_3H_2D_3$ [b]	As_3HD_4 [b]	As_3D_5 [a]
225	0.360 ± 0.008	0.333 ± 0.017	0.310 ± 0.025	0.288 ± 0.024	0.269 ± 0.016	0.250 ± 0.006
226	0.327 ± 0.009	0.250 ± 0.024	0.183 ± 0.029	0.120 ± 0.025	0.060 ± 0.015	0.000
227	0.002 ± 0.002	0.078 ± 0.019	0.144 ± 0.027	0.206 ± 0.028	0.267 ± 0.021	0.330 ± 0.014
228	0.062 ± 0.004	0.028 ± 0.009	0.011 ± 0.005	0.004 ± 0.002	0.002 ± 0.001	0.000
229	0.000 ± 0.000	0.043 ± 0.008	0.040 ± 0.008	0.022 ± 0.008	0.007 ± 0.003	0.009 ± 0.003
230	0.250 ± 0.003	0.002 ± 0.001	0.022 ± 0.008	0.040 ± 0.008	0.037 ± 0.006	0.000
231	0.000	0.269 ± 0.005	0.003 ± 0.001	0.009 ± 0.004	0.027 ± 0.009	0.061 ± 0.009
232	0.000	0.000	0.288 ± 0.006	0.003 ± 0.001	0.003 ± 0.001	0.000
233	0.000	0.000	0.000	0.307 ± 0.008	0.002 ± 0.001	0.005 ± 0.001
234	0.000	0.000	0.000	0.000	0.326 ± 0.011	0.000
235	0.000	0.000	0.000	0.000	0.000	0.345 ± 0.015

[a] Experimental mass spectrum. Each experimental set of data represents the mean of three independent determinations. Standard deviation of the results is reported in parentheses.

[b] Statistical model. Each set of data represents the mean of 8×10^7 simulations. Standard deviation of the results is reported.

The incorporation of hydrogen into the final hydride can be monitored using tetrahydroborate enriched in deuterium via plots of the amount fraction of each isotopologue generated versus the amount fraction of deuterium in the tetrahydroborate reductant. The amount fraction of deuterium in the $NaBH_4$ and $NaBD_4$ mixtures was obtained gravimetrically and the mass spectra of the resultant di- and triarsanes were deconvoluted to obtain the mole fraction of each isotopologue generated. Results are shown in Figs. 2.3 and 2.4.

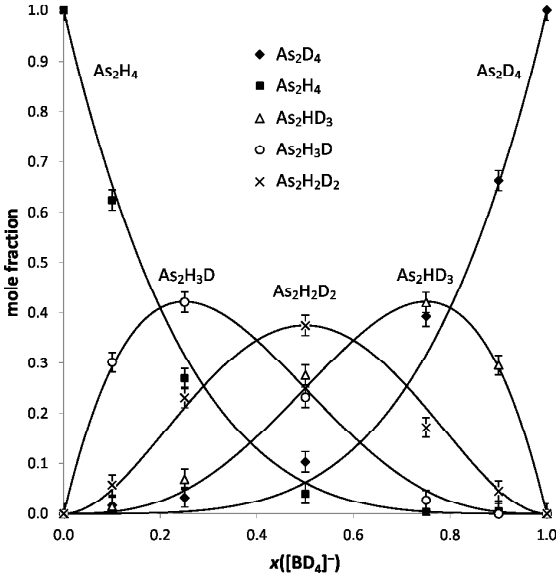

Figure 2.3 Amount fraction of diarsane isotopologues, $x(As_2H_nD_{4-n})$, generated using mixtures of $NaBH_4$ and $NaBD_4$. The continuous lines portray the theoretical trend based on a multistep direct hydrogen transfer from tetrahydroborate to the As-substrate

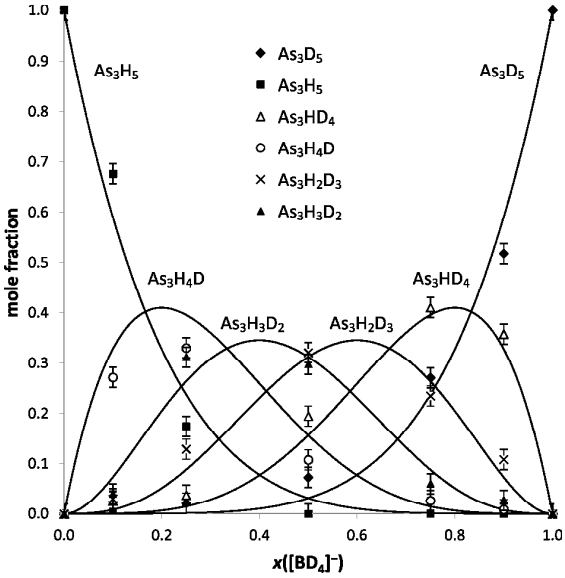

Figure 2.4 Amount fraction of triarsane isotopologues, $x(As_3H_nD_{5-n})$, generated using mixtures of $NaBH_4$ and $NaBD_4$. The continuous lines portray the theoretical trend based on a concerted multistep hydrogen transfer from tetrahydroborate to the As-substrate

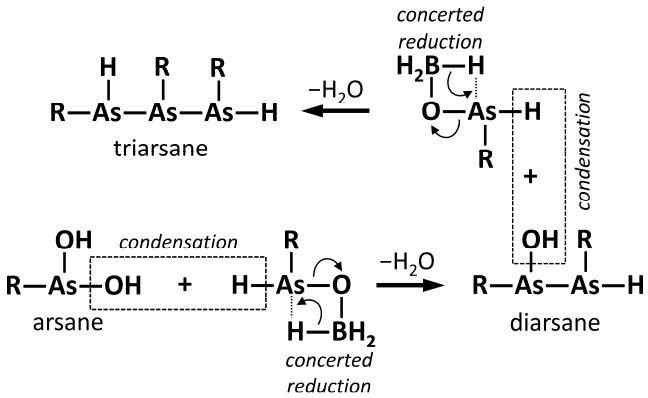

Scheme 2.1 Formation of di- and triarsanes in a concerted reduction and condensation cascade (R = H or OH).

It is evident that the incorporation of protium and deuterium in di- and triarsanes closely follows the binomial distribution, i.e.,

$$x_{As_2H_nD_{4-n}} = \frac{4!}{n!(4-n)!} \cdot x_D^{4-n} \cdot (1-x_D)^n$$

$$x_{As_3H_nD_{5-n}} = \frac{5!}{n!(5-n)!} \cdot x_D^{5-n} \cdot (1-x_D)^n$$

as illustrated by the continuous line in Figs. 2.3 and 2.4.The trends observed in the composition of diarsane and triarsane follow the hypothesis of a concerted multistep formation of arsane in a fashion already demonstrated for AsH_3 [22], and they further validate the proposed condensation cascade mechanism (paragraph 2.2). Therefore, the formation of di- and triarsanes can be described as a combination of two independent events: condensation of two hydroxoarsanes and their reduction by borohydrides via the concerted transfer of hydrogen to the arsenic substrate, as summarized in Scheme 2.1.

Conclusions

Results reported in this Ph.D. thesis contribute to an enhancement of the general knowledge of chemical vapor generation in Analytical Chemistry. Improvements have been achieved both for analytical applications and in comprehension of fundamental aspects concerning the mechanism of hydride generation by borane complexes.

Novel analytical methods have been developed for the determination of fluoride, nitrite and nitrate at ultra trace levels by gas chromatography-mass spectrometry. These analytes were converted with triethyloxonium salts ($Et_3O^+[FeCl_4]^-$ for fluoride, and $Et_3O^+[BF_4]^-$ for nitrite and nitrate) to their corresponding volatile ethyl-derivatives (EtF, EtONO and $EtONO_2$) prior to quantitation. These new approaches present several remarkable features which make the methodology very attractive, especially when high accuracy and precision are required. The triethyloxonium derivatization allows the determination of nitrite, nitrate and fluoride free from spectral interference, entails the possibility of using isotope dilution techniques (for nitrite an nitrate) and is suitable for the certification of reference materials.

In the field of chemical generation of volatile hydrides by aqueous phase reaction with boranes, new evidence has been collected based on a study of arsane (arising from inorganic As(III) and As(V) derivatization) and methylarsane (arising from mono- and dimethyl As(V) acids derivatization) as model compounds. It has been found that the recently reported reaction mechanism based on the stepwise, direct transfer of hydrogen from boron to arsenic is valid only in pure aqueous solutions, and under analytical conditions (arsenic at trace level and very high borane to arsenic mass ratio).

In particular, the presence of trace levels of noble metal ions, Au(III), Pd(II), Pt(II) and Rh(III), interferes with the mechanism of hydrogen transfer from boron to arsenic. Experiments with deuterium labeled reagents demonstrate that a large fraction of the hydrogen coming from the solvent can be incorporated into arsane in the presence of noble metal ions, which indicates that the noble metal is able to perturb the ideal analytical mechanism, playing a role in the reaction leading to the formation of the final volatile hydrides. This type of interference takes place at metal ion concentration levels of which do not significantly affect the generation yield of arsane, and it represents a new type of interference which is different from the classical analytical interference.

The use of non-analytical conditions (high arsenic concentration, lower borane- to-arsenic ratio, non-optimized pH conditions) gives rise to both volatile and non-volatile arsenic containing byproducts, the formation of which cannot be explained by the ideal analytical mechanism alone. According to the analytical mechanism, the stepwise formation of intermediate hydrides results in the unique final product. Under non-analytical conditions, reactions amongst intermediate hydrides, or intermediate hydrides and final products (condensation reaction) is competitive with the hydrogen transfer reaction, and yields polymeric species. In the case of methylated arsenic compounds, a methyl transfer reaction is also detected, which represents a further perturbation of the analytical mechanisms. The experimental evidence provides for a more general model for the mechanism of formation of volatile hydrides which is valid both under analytical and non-analytical conditions.

References

[1] Wells, R. J. Recent advances in non-silylation derivatization techniques for gas chromatography. *J. Chromatogr. A* **1999**, *843*, 1–18.

[2] Sturgeon, R. E.; Guo, X.; Mester, Z. Chemical vapor generation: are further advances yet possible? *Anal. Bioanal. Chem.* **2005**, *382*, 881–883.

[3] Marsh, J. Account of a method of separating small quantities of arsenic from substances with which it may be mixed. *Edinburgh New Philosophical Journal* **1836**, *21*, 229–236.

[4] Sturgeon, R. E.; Mester, Z. Analytical applications of volatile metal derivatives. *Appl. Spectrosc.* **2002**, *56*, 202A–213A.

[5] Wu, P.; He, L.; Zheng, C.; Hou, X.; Sturgeon, R. E. Applications of chemical vapor generation in non-tetrahydroborate media to analytical atomic spectrometry. *J. Anal. At. Spectrom.* **2010**, *25*, 1217–1246.

[6] Pagliano, E. *Applicazioni analitiche della derivatizzazione mediante sali di trialchilossonio: determinazione di specie anioniche/nucleofile a livello di tracce*; Master thesis, University of Pisa, Faculty of Chemistry, 2008.

[7] D'Ulivo, A.; Pagliano, E.; Onor, M.; Pitzalis, E.; Zamboni, R. Vapor generation of inorganic anionic species after aqueous phase alkylation with trialkyloxonium tetrafluoroborates. *Anal. Chem.* **2009**, *81*, 6399–6406.

[8] Manion, B. A.; Holbein, B. H.; Marcone, M. F.; Seetharaman, K. A new method for quantifying iodine in a starch-iodine matrix, *Carbohy. Res.* **2010**, *345*, 2698–2704.

[9] Manion, B.; Mei, Y.; Holbein, B. E.; Seetharaman, K. Quantification of total iodine in intact starches of different botanic origin exposed to iodine vapor at various water activities. *Carbohy. Res.* **2011**, *346*, 2482–2490.

[10] Meerwein, H.; Hinz, G.; Hofmann, P.; Kroning, E.; Pfeil, E. Über Tertiäre Oxoniumsalze, I. *J. Prakt. Chem.* **1937**, *147*, 257–285.

[11] Perst, H. *Oxonium Ions in Organic Chemistry*; Verlag Chemie GmbH: Weinheim, 1971.

[12] D'Ulivo, A.; Loreti, V.; Onor, M.; Pitzalis, E.; Zamboni, R. Chemical vapor generation atomic spectrometry using amine-boranes and cyanotrihydroborate(III) reagents. *Anal. Chem.* **2003**, *75*, 2591–2600.

[13] Braman, R. S. Membrane probe-spectral emission type detection system for mercury in water, *Anal. Chem.* **1971**, *43*, 1462–1467.

[14] Braman, R. S.; Justen, L. L.; Foreback, C. C. Direct volatilization-spectral emission type detection system for nanogram amounts of arsenic and antimony, *Anal. Chem.* **1972**, *4*, 2195–2199.

[15] Robbins, W. B.; Caruso, J. A. Development of hydride generation methods for atomic spectroscopic analysis. *Anal. Chem.* **1979**, *51*, 889A.

[16] Laborda, F.; Bolea, E.; Baranguan, M. T.; Castillo, J. R. Hydride generation in analytical chemistry and nascent hydrogen: when is it going to be over? *Spectrochim. Acta Part B* **2002**, *57*, 797–802.

[17] D'Ulivo, A.; Onor, M.; Pitzalis, E. Role of hydroboron intermediates in the mechanism of chemical vapor generation in strongly acidic media. *Anal. Chem.* **2004**, *76*, 6342–6352.

[18] D'Ulivo, A.; Baiocchi, C.; Pitzalis, E.; Onor, M.; Zamboni, R. Chemical vapour generation for atomic spectrometry. A contribution to the comprehension of reaction mechanisms in the generation of volatile hydrides using borane complexes, *Spectrochim. Acta Part B* **2004**, *59*, 471–486.

[19] D'Ulivo, A.; Mester, Z.; Meija, J.; Sturgeon, R. E. Mechanism of generation of volatile hydrides of trace elements by aqueous tetrahydroborate(III). Mass spectrometric studies on reaction products and intermediates, *Anal. Chem.* **2007**, *79*, 3008–3015.

[20] D'Ulivo, A.; Mester, Z.; Sturgeon, R. E. The mechanism of formation of volatile hydrides by tetrahydroborate(III) derivatization: a mass spectrometric study performed with deuterium labeled reagents. *Spectrochim. Acta Part B* **2006**, *60*, 423–438.

[21] D'Ulivo, A. Chemical vapor generation by tetrahydroborate(III) and other borane complexes in aqueous media. A critical discussion of fundamental processes and mechanisms involved in reagent decomposition and hydride formation, *Spectrochim. Acta Part B* **2004**, *59*, 793–825.

[22] D'Ulivo, A. Mechanism of generation of volatile species by aqueous boranes. Towards the clarification of most controversial aspects. *Spectrochim. Acta Part B* **2010**, *65*, 360–375.

[23] D'Ulivo, A.; Dědina, J.; Mester, Z.; Sturgeon, R. E.; Wang, Q.; Welz, B. Mechanisms of chemical generation of volatile hydrides for trace element determination. *Pure Appl. Chem.* **2011**, *83*,1283–1340.

[24] Olah, G. A.; Laali, K. K.; Wang, Q.; Surya Prakash, G. K. *Onium Ions*; Wiley: New York, 1998.

[25] Moorcroft, M. J.; Davis, J.; Compton, R. G. Detection and determination of nitrate and nitrite: a review. *Talanta* **2001**, *54*, 785–803.

[26] Jobgen, W. S.; Jobgen, S. C.; Li, H.; Meininger, C. J.; Wu, G. Analysis of nitrite and nitrate in biological samples using high-performance liquid chromatography. *J. Chromatogr. B* **2007**, *851*, 71–82.

[27] Helmke, S. M.; Duncan, M. W. Measurement of the NO metabolites, nitrite and nitrate, in human biological fluids by GC-MS, *J. Chromatogr. B* **2007**, *851*, 83–92.

[28] Nydahl, F. On the optimum conditions for the reduction of nitrate by cadmium. *Talanta* **1976**, *23*, 349–357.

[29] Dhar, N. R.; Tandon, S. P.; Biswas, N. N.; Bhateacharya, A. K. Photo-oxidation of nitrite to nitrate. *Nature* **1934**, *133*, 213–214.

[30] Mudgal, P. K.; Bansal, S. P.; Gupta, K. S. Kinetics of atmospheric oxidation of nitrous acid by oxygen in aqueous medium. *Atmos. Environ.* **2007**, *41*, 4097–4105.

[31] Tsikas, D. Simultaneous derivatization and quantification of the nitric oxide metabolites nitrite and nitrate in biological fluids by gas chromatography/mass spectrometry. *Anal. Chem.* **2000**, *72*, 4064–4072.

[32] Pagliano, E.; Meija, J.; Sturgeon R.E.; Mester, Z.; D'Ulivo, A. Negative chemical ionization GC/MS determination of nitrite and nitrate in seawater using exact matching double spike isotope dilution and derivatization with triethyloxonium tetrafluoroborate. *Anal. Chem.* **2012**, *84*, 2592–2596.

[33] Pagliano, E.; Onor, M.; Pitzalis, E.; Mester, Z.; Sturgeon, R.E.; D'Ulivo, A. Quantification of nitrite and nitrate in seawater by triethyloxonium tetrafluoroborate derivatization – Headspace SPME GC–MS, *Talanta* **2011**, *85*, 2511–2516.

[34] Henrion, A. Reduction of systematic errors in quantitative analysis by isotope dilution mass spectrometry (IDMS): an iterative method. *Fresenius J. Anal. Chem.* **1994**, *350*, 657–658.

[35] Meija, J.; Mester, Z. Paradigms in isotope dilution mass spectrometry for elemental speciation analysis. *Anal. Chim. Acta* **2008**, *607*, 115–125.

[36] Verkerk, R. H. J. The paradox of overlapping micronutrient risks and benefits obligates risk/benefit analysis. *Toxicology* **2010**, *278*, 27–38.

[37] Harrison, P. T. C. Fluoride in water: A UK perspective. *J. Fluorine Chem.* **2005**, *126*, 1448–1456.

[38] Levy, S. M. Total fluoride intake and implications for dietary fluoride supplementation. *J. Public Health Dent.* **1999**, *59*, 211–223.

[39] Ekstrand, J. Fluoride Intake in Early Infancy. *J. Nutr.* **1989**, *119*, 1856–1860.

[40] Meenakshi; Maheshwari, R. C. Fluoride in drinking water and its removal *J. Hazard. Mat.* **2006**, *137*, 456–463.

[41] Campbell, A. D. Determination of fluoride in various matrices. *Pure & Appl. Chem.* **1987**, *59*, 695–702.

[42] Lundell, G. E. F.; Hoffman J. I. *Outlines of Methods of Chemical Analysis*; Wiley: New York, 1948.

[43] Williams, W. J. In *Handbook of Anion Determination*; Butterworth; London, 1979; pp 335–373.

[44] Bayón M. M.; Rodríguez Garcia, A.; García Alonso, J. I.; Sanz-Medel, A. Indirect determination of trace amounts of fluoride in natural waters by ion chromatography: a comparison of on-line post-column fluorimetry and ICP-MS detectors. *Analyst* **1999**, *124*, 27–31.

[45] Frant, M. S.; Ross, J. W. Electrode for sensing fluoride ion activity in solution. *Science* **1966**, *154*, 1553–1555.

[46] Wejnerowska, G.; Karczmarek, A.; Gaca, J. Determination of fluoride in toothpaste using headspace solid-phase microextraction and gas chromatography–flame ionization detection. *J. Chromatogr. A* **2007**, *1150*, 173–177.

[47] Tashkov, W.; Benchev, I.; Rizov, N.; Kolarska, A. Fluoride determination in fluorinated milk by headspace gas chromatography. *Chromatographia* **1990**, *29*, 544–546.

[48] Musijowski, J.; Szostek, B.; Koc, M.; Trojanowicz, M. Determination of fluoride as fluorosilane derivative using reversed-phase HPLC with UV detection for determination of total organic fluorine. *J. Sep. Sci.* **2010**, *33*, 2636–2644.

[49] Kage, S.; Kudo, K.; Nishida, N.; Ikeda, H.; Yoshioka, N.; Ikeda, N. Determination of fluoride in human whole blood and urine by gas chromatography-mass spectrometry. *Forensic Toxicol.* **2008**, *26*, 23–26.

[50] Morales, R.; West, P. W. The precipitation of calcium fluoride from homogeneous solution. *Anal. Chim. Acta* **1966**, *35*, 526–529.

[51] Granik, V. G.; Pyatin, B. M.; Glushkov, R. G. The chemistry of trialkyloxonium fluoroborates. *Russ. Chem. Rev.* **1971**, 40, 747–759.

[52] Health Canada (2010) Guidelines for Canadian Drinking Water Quality: Guideline Technical Document - Fluoride. Health Canada, Ottawa, Ontario.

[53] Hauswaldt, A-L.; Rienitz, O.; Jährling, R.; Fischer, N.; Schiel, D.; Labarraque, G.; Magnusson, B. Uncertainty of standard addition experiments: a novel approach to include the uncertainty associated with the standard in the model equation. *Accred. Qual. Assur.* **2012**, *17*, 129–138.

[54] Meerwein, H.; Battenberg, E.; Gold, H.; Pfeil, E.; Willfang, G. Über tertiäire Oxoniumsalze, II. *J. Prakt. Chem.* **1939**, *154*, 83–156.

[55] Dědina, J.; Tsalev, D. L. *Hydride Generation Atomic Absorption Spectroscopy*; Wiley: Chichester, 1995.

[56] Welz, B.; Melcher, M. Mechanisms of transition metal interferences in hydride generation atomic-absorption spectrometry. Part 1. Influence of cobalt, copper, iron and nickel on selenium determination. *Analyst* **1984**, *109*, 569–572.

[57] Bax, D.; Agterdenbos, J.; Worrell, E.; Beneken Kolmer, J. The mechanism of transition metal interference in hydride generation atomic absorption spectrometry. *Spectrochim. Acta B* **1988**, *43*, 1349–1354.

[58] Satoh, T.; Suzuki, S.; Suzuki, Y.; Miyaji, Y.; Imai, Z. Reduction of organic compounds with sodium borohydride-transition metal salt systems: reduction of organic nitrile, nitro and amide compounds to primary amines. *Tetrahedron Lett.* **1969**, *10*, 4555–4558.

[59] Nishiki, M.; Miyataka, H.; Niino, Y.; Mitsuo, N.; Satoh, T. Facile hydrogenation of aromatic nuclei with sodium borohydride-rhodium chloride in hydroxylic solvents. *Tetrahedron Lett.* **1982**, *23*, 193–196.

[60] Hinzman, S. W.; Ganem, B. The mechanism of sodium borohydride-cobaltous chloride reductions. *J. Am. Chem. Soc.* **1982**, *104*, 6801–6802.

[61] Osby, J. O.; Heinzman, S. W.; Ganem, B. Studies on the mechanism of transitionmetal-assisted sodium borohydride and lithium aluminum hydride reductions. *J. Am. Chem. Soc.* **1986**, *108*, 67–72.

[62] Raab, A.; Meherag, A. A.; Jaspars, M.; Genney, D. R.; Feldmann, J. Arsenic–glutathione complexes—their stability in solution and during separation by different HPLC modes. *J. Anal. At. Spectrom.* **2004**, *19*, 183–190.

[63] Rey, N. A.; Howarth, O. W.; Pereira-Maia, E. C. J. Equilibrium characterization of the As(III)–cysteine and the As(III)–glutathione systems in aqueous solution. *Inorg. Biochem.* **2004**, *98*, 1151–1159.

[64] Scott, N.; Hatlelid, K. M.; MacKenzie, N. E.; Carter, D. E. Reactions of arsenic(III) and arsenic(V) species with glutathione. *Chem. Res. Toxicol.* **1993**, *6*, 102–106.

[65] Spuches, A. M.; Kruszyma, H. G.; Rich, A. M.; Wilcox, D. E. Thermodynamics of the As(III)−thiol interaction: arsenite and monomethylarsenite complexes with glutathione, dihydrolipoic acid, and other thiol ligands. *Inorg. Chem.* **2005**, *44*, 2964–2972.

[66] Le, X-C.; Cullen, W. R.; Reimer, K. J. Effect of cysteine on the speciation of arsenic by using hydride generation atomic absorption spectrometry. *Anal. Chim. Acta* **1994**, *285*, 277–285.

[67] Tsalev, D. L.; Sperling, M.; Welz, B. Flow-injection hydride generation atomic absorption spectrometric study of the automated on-line pre-reduction of arsenate, methylarsonate and dimethylarsinate and high-performance liquid chromatographic separation of their l-cysteine complexes. *Talanta* **2000**, *51*, 1059–1068.

[68] Meija, J.; Mester, Z.; D'Ulivo, A. Mass spectrometric separation and quantitation of overlapping isotopologues. $H_2O/HOD/D_2O$ and $H_2Se/HDSe/D_2Se$ mixtures. *J. Am. Soc. Mass Spectrom.* **2006**, *17*, 1028–1036.

[69] Meija, J.; Mester, Z.; D'Ulivo, A. Mass spectrometric separation and quantitation of overlapping isotopologues. Deuterium containing hydrides of As, Sb, Bi, Sn, and Ge. *J. Am. Soc. Mass Spectrom.* **2007**, *18*, 337–345.

[70] Pagliano, E.; D'Ulivo, A.; Mester, Z.; Sturgeon, R.E.; Meija, J. The binomial distribution of hydrogen and deuterium in arsanes, diarsanes, and triarsanes generated from As(III)/$[BH_nD_{4-n}]^-$ and the effect of trace amounts of Rh(III) ions, *J. Am. Soc. Mass Spectrom.* **2012**, *25*, 2178–2186.

Annex I

Pagliano, E. (ca); Onor, M.; Pitzalis, E.; Mester, Z.; Sturgeon, R.E.; D'Ulivo, A.

Quantification of nitrite and nitrate in seawater by triethyloxonium tetrafluoroborate derivatization – Headspace SPME GC–MS

Talanta **2011**, *85*, 2511-2516

Copyright 2011 Elsevier B.V.

Talanta 85 (2011) 2511–2516

Contents lists available at ScienceDirect

Talanta

journal homepage: www.elsevier.com/locate/talanta

Quantification of nitrite and nitrate in seawater by triethyloxonium tetrafluoroborate derivatization—Headspace SPME GC–MS

E. Pagliano[a,*], M. Onor[b], E. Pitzalis[b], Z. Mester[c], R.E. Sturgeon[c], A. D'Ulivo[b]

[a] Scuola Normale Superiore, Piazza dei Cavalieri, 7, 56126, Pisa, Italy
[b] CNR, Consiglio Nazionale delle Ricerche, Istituto di Chimica dei Composti Organometallici, Via G. Moruzzi, 1, 56124 Pisa, Italy
[c] National Research Council of Canada, 1200 Montreal Road, Ottawa, ON K1A 0R6, Canada

ARTICLE INFO

Article history:
Received 4 March 2011
Received in revised form 27 July 2011
Accepted 29 July 2011
Available online 5 August 2011

Keywords:
Vapor generation
Trialkyloxonium tetrafluoroborate
Nitrite
Nitrate
Enriched isotope
Gas chromatography mass spectrometry
Water analysis

ABSTRACT

Triethyloxonium tetrafluoroborate derivatization combined with direct headspace (HS) or SPME-gas chromatography–mass spectrometry (GC–MS) is proposed here for the simultaneous determination of nitrite and nitrate in seawater at micromolar level after conversion to their corresponding volatile ethyl-esters (EtO-NO and EtO-NO_2). Isotopically enriched nitrite [^{15}N] and nitrate [^{15}N] are employed as internal standards and for quantification purposes. HS-GC–MS provided instrumental detection limits of 0.07 μM NO_2^- and 2 μM NO_3^-. Validation of the methodology was achieved by determination of nitrite and nitrate in MOOS-1 (Seawater Certified Reference Material for Nutrients, NRC Canada), yielding results in excellent agreement with certified values. All critical aspects connected with the potential inter-conversion between nitrite and nitrate (less than 10%) were evaluated and corrected for by the use of the isotopically enriched internal standard.

© 2011 Elsevier B.V. All rights reserved.

1. Introduction

Nitrite and nitrate are ubiquitous and the availability of analytical methods for their simultaneous determination at trace and ultra-trace levels in complex matrices is important for understanding aspects of environmental and biological processes. They reflect the final states of a variety of N-compounds in many metabolic pathways occurring in living systems [1,2]. Issues related to their speciation in body fluids are explored in order to understand the role of NO as a regulatory molecule in the vascular system, in the brain, and in the immune system [3]. Direct determination of NO gas is a challenge for Analytical Chemistry and the use of nitrite and nitrate as NO metabolic products are exploitable for this purpose.

Environmental contamination by nitrite and nitrate can occur through industrial and domestic combustion and from agricultural sources; their monitoring has gained increasing importance [1].

The state of the art of their analytical determination has been reviewed by Moorcroft [1] and Jobgen [4] who focused their attention on liquid-phase molecular spectroscopy (determination by UV–vis and chemiluminescence) and electrochemical detection. Both techniques are often used in combination with chromatographic separation or capillary electrophoresis in order to perform on-line detection which suffers, in general, from limited selectivity and sensitivity, especially due to high matrix effects. One additional drawback is related to the derivatization step: many reactions have been proposed to convert nitrite to a suitable molecule for detection whereas little attention has been given to the less reactive nitrate, which can be only determined following a critical reduction. This separation step suffers matrix effects when real samples are processed, especially proteinaceous materials. Tsikas [5] presented an overview of currently available assays for nitrate and nitrite based on the Griess reaction.

The use of GC–MS in this field has also been proposed and recently reviewed by Helmke [3]. GC–MS strategies for the analysis of these two anions include nitration using aromatic compounds and alkylation with pentafluorobenzyl bromide (PFB-Br). The first approach is applicable only for the direct determination of nitrate ion as nitrite does not react under the specified conditions; for its detection a critical oxidation step is required. The latter approach is able to achieve simultaneous determination of both anions [6]. In any case, derivatization of nitrate ion by PFB-Br requires demanding reaction conditions such as elevated temperature and high PFB-Br concentration [3]. Tsikas [7] published the first method for the determination of nitrite by GC–MS which was free of derivatization, but it has not been used for the determination of nitrate.

Recently, analytical application of triethyloxonium tetrafluoroborate salt (TEOT) has been proposed by the authors for the chemical vapor generation (CVG) of Cl^-, Br^-, I^-, CN^-, SCN^-, S^{2-},

* Corresponding author. Tel.: +39 340 84 28735.
E-mail addresses: e.pagliano@sns.it, e.pagliano@libero.it (E. Pagliano).

0039-9140/$ – see front matter © 2011 Elsevier B.V. All rights reserved.
doi:10.1016/j.talanta.2011.07.098

NO_3^-, NO_2^- [8]. Trialkyloxonium "Meerwein" reagents [9,10] have proven capable of aqueous phase alkylation of several inorganic substrates, allowing their separation from the reaction matrix as volatile or semi-volatile reaction products of defined chemical composition [8]. The TEOT method has been validated by determination of bromide in BCR-612 reference material and has been applied to the determination of iodine and iodate [8].

TEOT converts nitrite and nitrate to their corresponding ethyl esters through an O-alkylation reaction. These molecules present suitable volatility and stability to be determined by GC–MS.

In this work we propose, for the first time, application of a CVG-GC–MS methodology for the simultaneous determination of nitrite and nitrate at micromolar level. The procedure is simple and the use of isotopically enriched internal standards confers ruggedness to the method. Validation has been achieved by analysis of a "Seawater Certified Reference Material for Nutrients", MOOS-1. Results reported here demonstrate the analytical potentialities and usefulness of aqueous phase alkylation with TEOT for the determination of anionic species by CVG.

2. Experimental

2.1. Reagents and materials

Aqueous solutions of isotopically enriched nitrite and nitrate were prepared by dissolution of sodium nitrite (^{15}N, 98%+) and potassium nitrate (^{15}N, 99%), respectively (Cambridge Isotope Laboratories, Inc.) in ultrapure water in order to obtain final concentrations of 200 mg/L $^{15}NO_3^-$ and 20 mg/L $^{15}NO_2^-$. An alkylating solution of TEOT (triethyloxonium tetrafluoroborate) was prepared by dissolving the reagent (Fluka: TEOT >97%) in ultrapure water; the quantity of solid salt required to ensure 40 mg of reactant in 100 μL solution. Aqueous oxonium salts are unstable, so the solution is prepared just prior to sample derivatization. Working solutions of nitrite and nitrate were prepared by dilution of Fluka concentrates (Fluka: nitrate, certified anion standard solution 1001 mg/L ± 2 mg/L; nitrite standard for IC 1000 mg/L ± 4 mg/L) with ultrapure water. All standard solutions were stored at 4 °C.

2.2. GC–MS methods

GC–MS experiments were performed using an Agilent GC 6850 equipped with an Agilent 5975 C MS detector. For the HS-GC–MS procedure, manual sample injection was employed using a 250 μL sample volume. The oven program consisted of the following: isothermal (10 min) at 30 °C, 5 °C/min to 100 °C maintained for 4 min, 25 °C/min to 240 °C maintained for 10 min. Inlet setup: inlet mode is pulsed split with split ratio 8:1, pulsed pressure 200 kPa and temperature 150 °C. A model J&W 122-1364E DB-624 column (6% Cyanopropyl-phenyl 94% dimethyl polysiloxane) was used in constant flow mode at 0.7 mL He/min. Mass spectrometry detection (70 eV electron impact, transfer line 260 °C, ion source 250 °C) was performed in SIM mode monitoring *m*/*z* 30–31–60–61 (dwell time 100 ms for each *m*/*z*) for nitrous acid ethyl ester and *m*/*z* 46–47–76–77 for nitric acid ethyl ester (same dwell time).

For the SPME-GC–MS procedure, a 57310-U df 65 μm polydimethylsiloxane/divinylbenzene (PDMS/DVB) Supelco SPME fiber assembly was used. The fiber was exposed to the headspace of the vial for 10 min at ambient temperature whereas the desorption process required 1.5 min in the GC inlet. The oven program consisted of: isothermal (10 min) at 30 °C, 10 °C/min to 80 °C, 25 °C/min to 200 °C maintained for 10 min. Inlet setup: inlet mode is pulsed split with split ratio 5:1, pulsed pressure 180 kPa and temperature 170 °C. A model J&W 122-1364E DB-624 column (6% Cyanopropyl-phenyl 94% dimethyl polysiloxane) was operated in constant flow mode at 1 mL He/min. Mass spectrometry detection (70 eV electron impact, transfer line 260 °C, ion source 250 °C) was performed in SIM mode monitoring *m*/*z* 30–31–60–61 (dwell time 100 ms for each *m*/*z*) for nitrous acid ethyl ester and *m*/*z* 46–47–76–77 for nitric acid ethyl ester (same dwell time).

2.3. Sample preparation

A 2 mL sample was introduced without any pretreatment into a 4 mL vial and isotope enriched spike (100 μL) added. After sealing, 100 μL aqueous TEOT was injected through the septum. GC–MS analysis was performed after 3 h reaction time at 23 °C; the HS procedure required the injection of 250 μL of headspace; SPME entails the exposure of the fiber in the headspace for 10 min.

3. Results and discussion

3.1. Identification

Nitrite and nitrate are converted to their corresponding ethyl esters by TEOT. TEOT is a strong alkylating agent which is able to perform alkylation in aqueous solution and to react with anions in neutral substrates. In the present case, O-alkylation of the substrate occurs with the formation of nitrous and nitric ethyl ester:

No volatile products arising from N-alkylation of nitrite and nitrate have been observed. Nitrite and nitrate ethyl esters are suitable for GC–MS analysis and their corresponding EI mass spectra are reported in Figs. 1–2. In the case of the nitrite ethyl ester (Fig. 1), we note the absence of a molecular ion and the fragmentation produced $[CH_2NO_2]^+$ ion (*m*/*z* 60) which corresponds to the loss of 15 amu (methyl loss) and the ion $[NO]^+$ (*m*/*z* 30) which corresponds to loss of 45 amu (ethoxy loss). For the nitrate ethyl ester (Fig. 2), the interpretation of the mass spectrum is similar to the nitrite ethyl ester, and the EI spectrum is the same as reported in the NIST05 library. Unfortunately, there is no possibility of making a similar comparison for the nitrite ethyl ester. Mass spectra reported in our previous work [8] were obtained using a Varian 3400CX GC equipped with a 1077 split–splitless injector directly interfaced to a Saturn3 ion trap mass spectrometer (Varian). Mass spectra presented here are obtained with a different apparatus and tune setting. As a consequence, some small differences in relative intensities of the fragment ions can be noted. With the actual settings of the MS, the mass spectra are of better quality with a view to analytical determination of nitrite and nitrate.

3.2. Quantification method and inter-conversion of nitrite and nitrate

With the proposed method, the problem arising from the potential chemical inter-conversion of nitrite and nitrate during the derivatization step has been evaluated. It has been proven that no detectable conversion of nitrate to nitrite arises whereas the conversion of nitrite to nitrate is observed and occurs to the extent of about 10% at the 0.2 mM NO_2^- concentration level. This problem likely originates with the presence of dissolved atmospheric oxygen [11,12] and the strong acidic conditions that arise from the acid hydrolysis of TEOT. This interfering effect can be corrected for by the use of the isotopically enriched internal standard.

The following equations describe the methodology used for the elaboration of the data. The algorithm proposed is similar to that

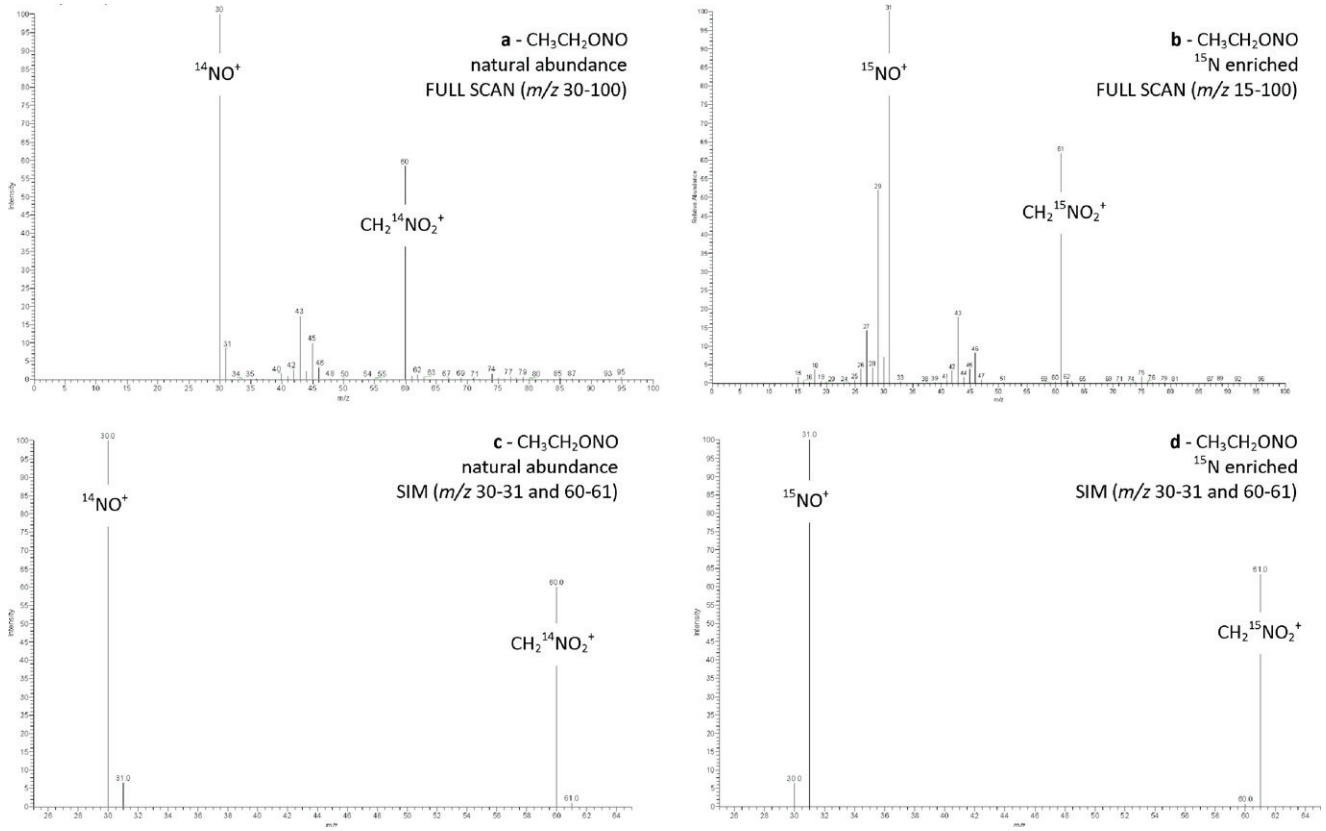

Fig. 1. Nitrous acid ethyl ester, CH_3CH_2ONO. (a) Full scan mass spectra (m/z 30–100) of the standard of natural origin. (b) Full scan mass spectra (m/z 15–100) of the ^{15}N enriched standard. (c) SIM mass spectra (m/z 30–31 and 60–61) of the standard of natural origin. (d) SIM mass spectra (m/z 30–31 and 60–61) of the ^{15}N enriched standard.

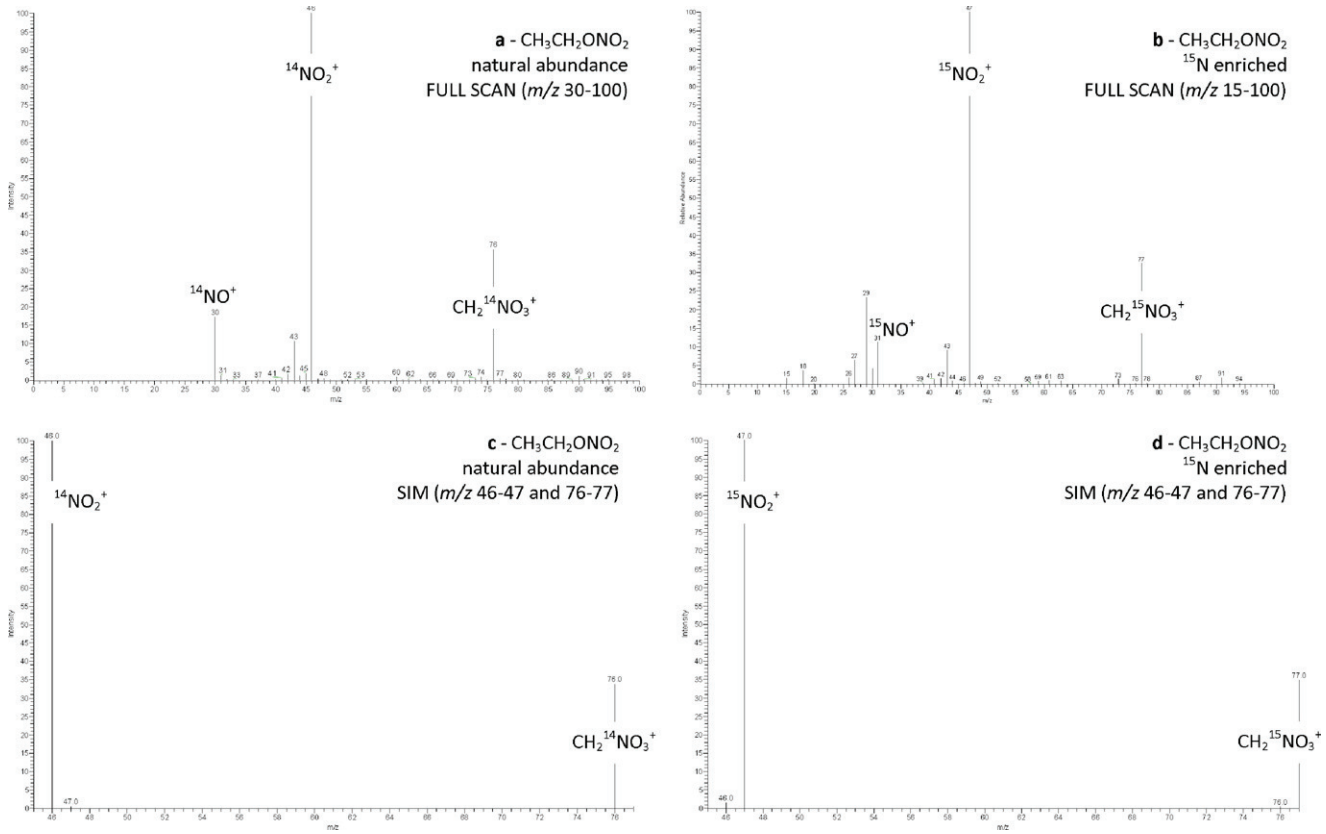

Fig. 2. Nitric acid ethyl ester, $CH_3CH_2ONO_2$. (a) Full scan mass spectra (m/z 30–100) of the standard of natural origin. (b) Full scan mass spectra (m/z 15–100) of the ^{15}N enriched standard. (c) SIM mass spectra (m/z 46–47 and 76–77) of the standard of natural origin. (d) SIM mass spectra (m/z 46–47 and 76–77) of the ^{15}N enriched standard.

use for classical isotope dilution methodology, but here some considerations have been given to correct for the problem of conversion of NO_2^- to NO_3^- and the instrumental mass bias which results in isotope ratios different from their values expected from the natural and enriched abundances of ^{14}N and ^{15}N.

Defining N_x and N_y as the signals (m/z 30 and 31) measured from 10 mg/l NO_2^- standard of natural origin and E_x and E_y as the signals (m/z 30 and 31) measured from 10 mg/l NO_2^- isotopically enriched species, it is possible to define the following parameters (^xA_N, ^xA_E, ^yA_N, ^yA_E):

$$\begin{cases} {}^xA_N = \dfrac{N_x}{N_x + N_y} \\ {}^xA_E = \dfrac{E_x}{E_x + E_y} \\ {}^yA_N = \dfrac{N_y}{N_x + N_y} \\ {}^yA_E = \dfrac{E_y}{E_x + E_y} \end{cases} \quad (1)$$

If the MS signals are not affected by mass bias, the above definitions of ^xA_N, ^xA_E, ^yA_N, ^yA_E will be simply the relative abundances of ^{14}N and ^{15}N in the natural and enriched samples.

Defining X_1 and Y_1 as the signals (m/z 30 and 31) measured from the blend of the sample spiked with isotopically enriched standard and N_1 and E_1 as the fraction of analyte from natural and enriched origin in this blend, we can write:

$$\begin{cases} X_1 = {}^xA_N \cdot N_1 + {}^xA_E \cdot E_1 \\ Y_1 = {}^yA_N \cdot N_1 + {}^yA_E \cdot E_1 \end{cases} \quad (2)$$

The concentration of the analyte C_A in the sample is related to the concentration of enriched standard C_E and is given by:

$$C_A = C_E \cdot \frac{N_1}{E_1} \quad (3)$$

An approximate value for C_A should be obtained based on the value of C_E calculated from the gravimetric preparation of the enriched standard. In any case, the best results are obtained by measuring the value of C_E using the same method in order to take into consideration the effects which arise from the conversion of nitrite and from mass bias. In other words, C_E becomes an empirical quantification parameter.

Its value can be calculated by reverse isotope dilution, for which a second blend prepared from a standard of nitrite with a known concentration C_A^0 close to that of the sample C_A, and spiked with the same amount of enriched standard is processed. If there are no significant matrix effects, the response of this second blend and of the sample must be similar. Additionally, the chemical behavior and interferences will also be similar.

Defining X_2 and Y_2 as the signals (m/z 30 and 31) measured from this standard spiked with isotopically enriched compounds and N_2 and E_2 as the fraction of analyte from natural and enriched origin present, it is possible to write:

$$\begin{cases} X_2 = {}^xA_N \cdot N_2 + {}^xA_E \cdot E_2 \\ Y_2 = {}^yA_N \cdot N_2 + {}^yA_E \cdot E_2 \end{cases} \quad (4)$$

The concentration of the standard C_A^0 is accurately known, so the concentration of enriched standard C_E is given by:

$$C_E = C_A^0 \cdot \frac{E_2}{N_2} \quad (5)$$

The final equation is obtained by substitution of C_E from (5) into (3):

Table 1
Summary of results for determination of nitrite and nitrate in MOOS-1.

Nitrite (μM)		Nitrate (μM)	
HS-GC–MS	SPME-GC–MS	HS-GC–MS	SPME-GC–MS
3.15	3.19	21.7	21.3
3.15	3.42	22.3	23.5
3.20	3.48	22.3	23.8
3.15	3.21	22.4	23.4
3.16 ± 0.03	**3.3 ± 0.2**	**22.2 ± 0.3**	**23 ± 1**

Certified values: nitrite 3.06 ± 0.15 μM; nitrite and nitrate: 23.7 ± 0.9 μM.
Bold line reports the mean of four independent measurements performed using HS and SPME. The results are coherent and provide evidence that the precision achieved with the HS method is better than that with SPME. The overall mean between these data is given by: nitrite 3.2 ± 0.1 μM; nitrate 22.6 ± 0.9 μM; nitrite and nitrate: 26 ± 1 μM.

$$C_A = C_E \cdot \frac{N_1}{E_1} = C_A^0 \cdot \frac{E_2}{N_2} \cdot \frac{N_1}{E_1} = C_A^0 \cdot \frac{{}^yA_N \cdot X_2 - {}^xA_N \cdot Y_2}{{}^yA_N \cdot X_1 - {}^xA_N \cdot Y_1} \cdot \frac{{}^yA_E \cdot X_1 - {}^xA_E \cdot Y_1}{{}^yA_E \cdot X_2 - {}^yA_E \cdot Y_2} \quad (6)$$

Defining:

$$\begin{cases} \theta_N = \dfrac{{}^xA_N}{{}^yA_N} \\ \theta_E = \dfrac{{}^xA_E}{{}^yA_E} \end{cases} \quad (7)$$

the formalism of (6) becomes:

$$C_A = C_A^0 \cdot \frac{X_2 - \theta_N \cdot Y_2}{X_1 - \theta_N \cdot Y_1} \cdot \frac{X_1 - \theta_E \cdot Y_1}{X_2 - \theta_E \cdot Y_2} \quad (8)$$

The above discussion is focused on nitrite, but the same is valid for nitrate (m/z 46 and 47). Equation (8) presents the final formula used for the calculation. This is not a conventional way of employing an isotopically enriched standard for quantification purposes; indeed, equation (8) does not depend on the concentration of enriched standard or on the relative abundances of $^{14}N/^{15}N$ in the sample and in the internal standard. From this point of view, this procedure is quite different from a rigorous isotope dilution methodology. Here, calibration is achieved through the values of θ_N, θ_E and X_2, Y_2, which are empirical parameters obtained from measurements performed in a particular instrumental setting characteristic of the experiments. In all measurements, a solution containing 2.17 μM NO_2^- and 16.1 μM NO_3^- was used in the reverse experiment for calibration purposes (X_2, Y_2 value).

3.3. Quantification of nitrite and nitrate in MOOS-1

Quantitative data related to analytical content of nitrite and nitrate in MOOS-1 (Seawater Certified Reference Material for Nutrients) are summarized in Table 1. The related chromatogram is presented in Fig. 3. In order to perform quantification, ion extraction at m/z 30–31 and at m/z 46–47 was carried out for nitrite and nitrate respectively; peak heights were employed for all calculations. All data reported are obtained applying equation (8). Other experiments not reported here, based on the classical internal standard (IS) and on standard additions (SA), provided results in accord with those summarized in Table 1. Furthermore, the slopes of both SA and IS plots were consistent, suggesting that matrix effects were accounted for by the use of the enriched standard.

Regarding analytical figures of merit, instrumental detection limits (concentration of the analyte that produces a peak with a signal-to-noise ratio of 3) with HS-GC–MS are 0.07 μM for NO_2^- and 2 μM for NO_3^- and with SPME are 0.3 μM for NO_2^- and 2 μM for NO_3^-. Analytical performance can be improved by increasing

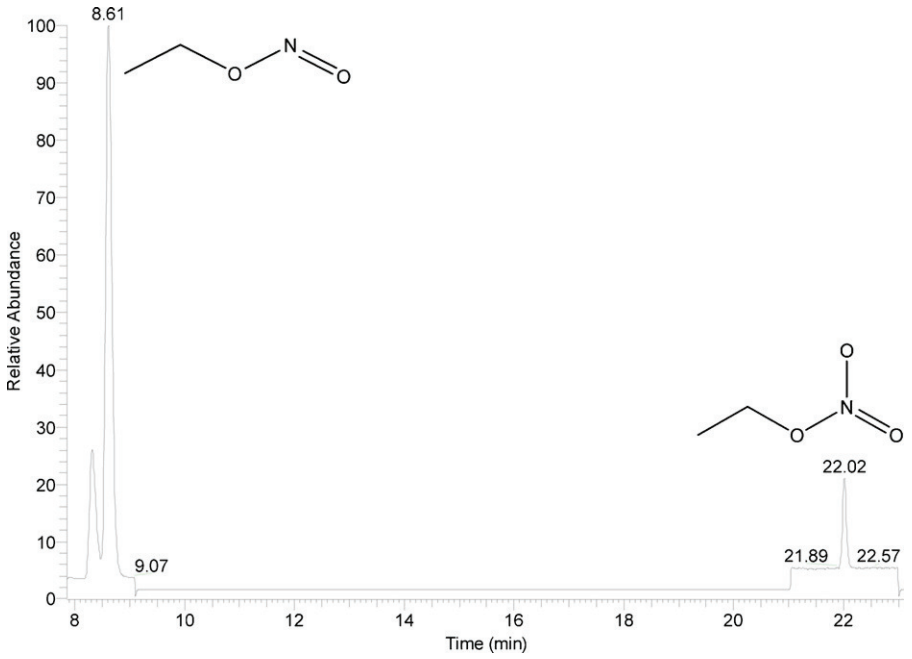

Fig. 3. HS-GC–MS chromatogram collected in SIM mode during analysis of MOOS-1 sample. Nitrite ion: converted into ethyl ester nitrous acid, retention time 8.61 min, mass extracted 30. Nitrate ion: converted into ethyl ester nitric acid, retention time 22.02 min, mass extracted 46. The peak eluting in front of ethyl nitrite is methoxyethane, an impurity arising from the triethyloxonium tetrafluoroborate.

Table 2
Recovery test performed on MOOS-1.

Nitrite (μM)				Nitrate (μM)			
Added	Expected	Found	Rec. (%)	Added	Expected	Found	Rec. (%)
0	3.06	3.21	105.0	0	20.6	22.2	107.6
0	3.06	3.17	103.5	0	20.6	22.4	108.5
2.72	5.78	5.77	99.8	20.2	40.8	44.8	109.8
2.72	5.78	5.75	99.6	20.2	40.8	43.2	105.7
5.43	8.49	8.09	95.2	40.4	61.0	62.9	103.1
5.43	8.49	8.10	95.3	40.4	61.0	62.1	101.7
10.87	13.93	12.91	92.7	80.8	101.4	106.5	105.1
10.87	13.93	13.27	95.3	80.8	101.4	106.3	104.8

The recovery (Rec., %) has been calculated as the ratio of measured response (found) and concentration expected (expected). A bias of less than 10% is evident.

Table 3
Recovery test performed on mineral water.

Nitrite (μM)			Nitrate (μM)
Added	Found	Rec. (%)	Found
0	n.d.	–	121.3
0.22	0.20	92.3	117.5
2.15	2.15	99.8	120.7
21.52	21.06	97.9	116.8
215.21	203.95	94.8	107.7

Calibration in based in all cases on reverse calibration performed with a solution of 2.17 μM NO_2^- and 16.1 μM NO_3^-.

the temperature of the HS, the amount of HS injected and time of exposure of the SPME fiber to the HS.

From Table 1, it is evident that there are no significant differences between the concentrations of nitrite and nitrate obtained using HS-GC–MS and SPME-GC–MS procedures. The overall mean of the results for the concentration of nitrite is 3.2 ± 0.1 μM (RSD 4.0%, $n = 8$) and for the concentration of nitrate is 22.6 ± 0.9 μM (RSD 4.0%, $n = 8$). The sum of nitrite and nitrate can be calculated to be 26 ± 1 μM (RSD 4.0%, $n = 8$). These results are in excellent agreement with the certified values for MOOS-1, i.e. 3.06 ± 0.15 μM for nitrite and 23.7 ± 0.9 μM for nitrite and nitrate.

Table 2 reports results for a recovery test performed on MOOS-1; the values obtained confirm not only the accuracy of this analytical method but that it is able to correct for the conversion of nitrite to nitrate. Finally, Table 3 presents recovery data for nitrite from a mineral water containing no detectable concentration of nitrite. Four additions at different concentrations of nitrite were performed spanning more than three orders of magnitude of concentration. Despite calculation of X_2 and Y_2 from equation (8) being based in all cases on the reverse experiment performed on a solution of 2.17 μM NO_2^- and 16.1 μM NO_3^-, no errors are evident for the recovery of nitrite and quantification of nitrate was satisfactory: 117 ± 5 μM (RSD 4.7%, $n = 5$) against 105 μM as the expected value. All instrumental and chemical problems possibly arising with this procedure are well corrected for by the use of the enriched standard and by the selected method of quantification, which demonstrates the ruggedness that the use of an enriched standard imparts to an analytical procedure.

4. Conclusion

Aqueous phase alkylation with TEOT has been applied to the determination of nitrite and nitrate in a sample of seawater certified reference material (MOOS-1) by CVG-GCMS. Nitrite and nitrate were converted to their corresponding volatile ethyl esters and could be simultaneously detected and determined using different approaches, including HS-GC–MS and SPME-GC–MS. The two procedures provide similar analytical figures of merit and direct HS is preferred for analysis when manual injection is performed, while SPME should be selected when the automation of the procedure is required. The results obtained for MOOS-1 using an isotopically enriched internal standard for quantification provided results in excellent agreement internally and with the certified values. The problem of chemical inter-conversion of nitrite to nitrate (less than 10%) is well accounted for using the present method. To the best of our knowledge, this is the first CVG method developed for the simultaneous determination of nitrite and nitrate: CVG offers the advantages of good analytical

figures of merit while separating the derivatized analytes from the sample matrix. Moreover, use of enriched isotopes makes available the ultimate primary calibration technique of isotope dilution. A reverse spike against a primary natural abundance standard affords traceability, making the method suitable for certification purposes and promising for application to samples of different origin.

References

[1] M.J. Moorcroft, J. Davis, R.G. Compton, Talanta 54 (2001) 785–803.
[2] J.O. Lundberg, E. Weitzberg, M.T. Gladwin, Nat. Rev. Drug Discov. 7 (2008) 156.
[3] S.M. Helmke, M.W. Duncan, J. Chromatogr. B 851 (2007) 83–92.
[4] W.S. Jobgen, S.C. Jobgen, H. Li, C.J. Meininger, G. Wu, J. Chromatogr. B 851 (2007) 71–82.
[5] D. Tsikas, J. Chromatogr. B 851 (2007) 51–70.
[6] D. Tsikas, Anal. Chem. 72 (2000) 4064–4072.
[7] D. Tsikas, A. Böhmer, A. Mitschke, Anal. Chem. 82 (2010) 5384–5390.
[8] A. D'Ulivo, E. Pagliano, M. Onor, E. Pitzalis, R. Zamboni, Anal. Chem. 81 (2009) 6399–6406.
[9] H. Meerwein, G. Hinz, P. Hofmann, E. Kroning, E. Pfeil, J. Prakt. Chem. 147 (1937) 257–285.
[10] V.G. Granik, B.M. Pyatin, R.G. Glushkov, Russ. Chem. Rev. 40 (9) (1971) 747–759.
[11] P.K. Mudgal, S.P. Bansal, K.S. Gupta, Atmos. Environ. 41 (2007) 4097–4105.
[12] N.R. Dhar, S.P. Tandon, N.N. Biswas, A.K. Bhateacharya, Nature 133 (1934) 213–214.

Annex II

Pagliano, E.; Onor, M.; Meija, J.; Mester, Z.; Sturgeon, R.E.;
D'Ulivo, A.

Mechanism of hydrogen transfer in arsane generation by aqueous tetrahydridoborate: interference effects of Au^{III} and other noble metals

Spectrochim. Acta Part B **2011**, *66*, 740-747
Copyright 2011 Elsevier B.V.

Spectrochimica Acta Part B 66 (2011) 740–747

Contents lists available at SciVerse ScienceDirect

Spectrochimica Acta Part B

journal homepage: www.elsevier.com/locate/sab

Mechanism of hydrogen transfer in arsane generation by aqueous tetrahydridoborate: Interference effects of Au^{III} and other noble metals

Enea Pagliano [a], Massimo Onor [b], Juris Meija [c], Zoltan Mester [c], Ralph E. Sturgeon [c], Alessandro D'Ulivo [b,*]

[a] Scuola Normale Superiore, Piazza dei Cavalieri, 7, 56126, Pisa, Italy
[b] CNR, Consiglio Nazionale delle Ricerche, Istituto di Chimica dei Composti Organometallici, Via G. Moruzzi, 1, 56124 Pisa, Italy
[c] National Research Council of Canada, Institute of National Measurements Standard, 1200 Montreal Road, Ottawa, ON K1A 0R6, Canada

ARTICLE INFO

Article history:
Received 25 July 2011
Accepted 27 September 2011
Available online 2 October 2011

Keywords:
Hydride generation
Tetrahydridoborate
Noble metal
Reaction mechanism
Mechanistic interference

ABSTRACT

The generation of arsane by reaction of either $NaBH_4$ (THB) or $NaBD_4$ (TDB) in aqueous solution with As^{III} (1 mg L^{-1}) has been studied in the presence of several transition and noble metals at trace levels. A continuous flow generation system coupled with both atomic absorption spectrometry (AAS) and gas chromatography mass spectrometry (GC-MS) were employed to measure the effect of Au^{III} (0.5 – 20 mg L^{-1}) on reaction yield and isotopic composition of arsane. In a different set of batch experiments, GC-MS was employed to measure the effect of Au^{III}, Pd^{II}, Pt^{II}, Ni^{II} and Cu^{II} on the isotopic composition of arsane. Au^{III}, Pd^{II} and Pt^{II} induce a significant perturbation in the mechanism of hydride generation, promoting the incorporation of a large amount of hydrogen derived from the solvent into the final arsane. This effect takes place at metal concentration levels which hardly affect the generation efficiency of arsane and can likely be addressed by the action of intermediate species formed in the early stage of the reaction between the metal ion and the TDB-arsenic complex. Nanoparticles and colloids arising from the interaction of the metal and TDB are able to capture the final arsane but they do not promote H/D exchange on the already formed arsane. This evidence reveals the existence of a new type of interference in chemical generation of volatile hydrides - a "mechanistic interference" - in addition to the already known yield interferences.

© 2011 Elsevier B.V. All rights reserved.

1. Introduction

The chemical generation of volatile species by aqueous phase reaction of tetrahydridoborate and other borane complexes coupled with atomic or mass spectrometry is one of the most powerful techniques used for trace element determination and speciation [1,2]. Chemical vapor generation can be considered a consolidated method for hydride forming elements and increasing attention has recently addressed the mechanistic aspects [3,4]. In chemical vapor generation, the presence of transition metals can produce severe interference problems [2,5,6] and the mechanisms which are recognized to play a role are essentially two: *(i)* adsorption of the already formed hydrides by finely dispersed reduced metal particles, which are generated by reaction of the metal ions with THB; *(ii)* catalytic decomposition of THB by metal ions and/or their reaction products; in both of these cases, the *"interference"* is seen as a process which contributes to a decreased amount of hydride reaching the detector. On the other hand, the reaction of THB with transition and noble metals has been usefully employed in many other fields as, for example, the metal catalyzed hydrolysis of THB for hydrogen production [7] and the determination of transition and noble metals by chemical vapor generation at trace levels [1,8]. However, many mechanistic aspects of the reaction between THB and transition and noble metals remain to be clarified.

In the analytical field, the mechanism of reduction of metal ions resulting in the formation of volatile metal species is of significant interest. Recently, it has been reported that, in the case of Ag [9] and possibly also Au[10], these metals are released from the reaction solution in the form of nanoparticles. The capability of borane complexes to react with transition metals transforming them from their ionic form to nanoparticles has earlier been reported and Van Hyning and Zukoski [11] discussed the mechanism of formation and aggregation of silver particles by reaction with tetrahydridoborate. However, no evidence has been presented to date on the possible mechanism involved in the reduction of the metal ion to the zerovalent oxidation state. The most reasonable hypothesis is that it follows a similar route to that for formation of the volatile hydrides: direct, stepwise transfer of hydrogen from borane to analyte following the formation of an analyte-borane complex. This leads to formation of hydridometal complexes as intermediate reaction products in which the ligands of the coordination sphere of the analyte are sequentially replaced by hydrogen to produce the final product [3].

The interaction between THB and transition metals has received much attention due to its relevance in the field of hydrogen storage

* Corresponding author.
E-mail address: dulivo@pi.iccom.cnr.it (A. D'Ulivo).

0584-8547/$ – see front matter © 2011 Elsevier B.V. All rights reserved.
doi:10.1016/j.sab.2011.09.009

where the hydrolysis of THB to produce molecular hydrogen is catalyzed by the presence of transition metal species [12,13]. The metal catalysts modify the mechanism of hydrolysis, as evident from deuterium labeled experiments. Under alkaline conditions, the acid catalyzed hydrolysis of THB in D_2O produces almost pure HD (>98%), whereas significant H/D exchange is observed when this reaction occurs in the presence of Pd/C and Pt/C [14]. Guella et al. [15] investigated the mechanism of hydrolysis of tetrahydridoborate in the presence of Pd/C with deuterium labeled experiments, concluding that the hydrolysis is caused by the electron-withdrawing and electron-releasing effect of the palladium atoms on the catalyst surface via the putative species Pd-BH_3^- and Pd-H. Glavee et al. [16] discussed the reduction of some transition metals in aqueous media and in diglyme, concluding that in the latter solvent rather stable $M(BH_4)_{2,3}$ complexes were generated with copper and iron. Moreover, the reduction by tetrahydridoborate in the presence of transition metals has been employed in organic chemistry to reduce functional groups such as nitriles, amides and alkenes, which are inert to THB alone [17,18].

In this work, some simple experiments are reported which indicate that the interaction of THB with Au^{III} and other noble and transition metal ions during generation of arsane is more complex than expected on the basis of earlier presumed mechanisms of interference. The presence of these noble metals significantly changes the chemistry of the system and strongly perturbs the mechanism of generation of arsane.

2. Experimental

2.1. Chemicals

Solutions of 1 mg L^{-1} As^{III} in 1 M HCl were prepared by dilution of 1000 mg L^{-1} As (Fluka, As_2O_3). Solutions of metal ions were prepared in 1 M HCl by dilution of a 1000 mg L^{-1} Merck concentrates (for Au^{III}, Pd^{II}, Ni^{II} and Cu^{II}) and 950 mg L^{-1} Pt^{II} (from K_2PtCl_4, Sigma Aldrich). As the reducing agent, a 0.25 M solution of $NaBH_4$ (THB) (Sigma Aldrich, assay>98.5%) was employed in continuous flow experiments coupled with atomic absorption spectrometry (AAS) for detection and a 0.25 M solution of $NaBD_4$ (TDB) (Sigma Aldrich $NaBD_4$, 98% D) solution was employed in continuous flow experiments coupled with GC-MS. A second 0.2 M solution of TDB was prepared with a reagent of higher isotopic purity (Cambridge Isotope Laboratories, $NaBD_4$, 99% D) and employed in batch experiments. All TDB and THB solutions were stabilized in 0.1 M NaOH and stored at 4 °C. All other chemicals were reagent grade.

2.2. Instrumentation and Apparatus

2.2.1. Continuous flow hydride generation experiments

A schematic representation of the lines employed in continuous flow-HG experiments is shown in Fig. 1. Three different chemifold setups were required to realize different mixing sequences of reagents. The continuous flow was achieved by a peristaltic pump (Ismatec pump head MS/CA4-12 fitted on a Masterflex L drive) and all chemicals and

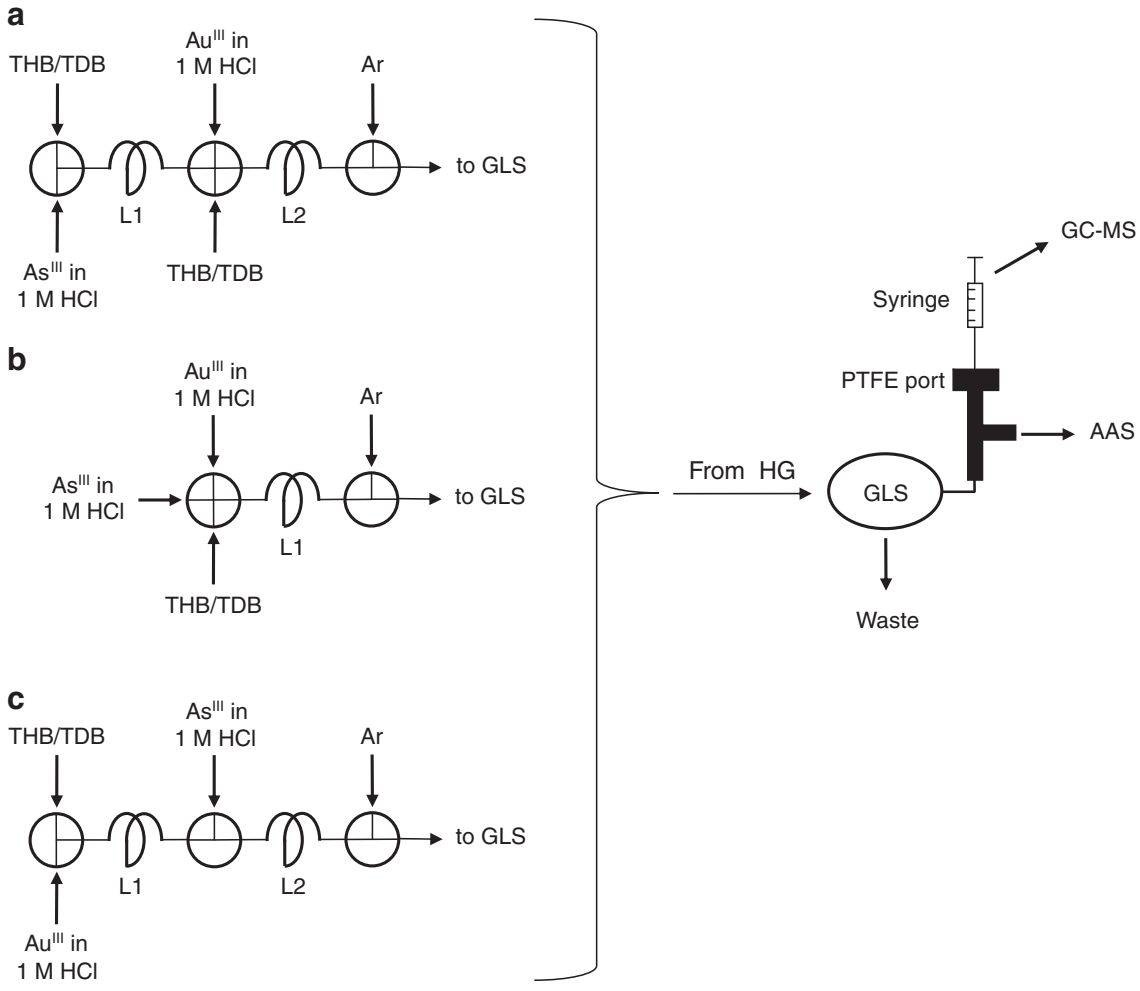

Fig. 1. Schematic of experimental setups used in continuous flow generation of arsane coupled with AAS and GC-MS detection. The volatile products which are formed using the different mixing sequences (A or B or C) are delivered to a gas–liquid separator (GLS) coupled with the detection system.

waste sample solutions were propelled by Tygon microtubes of appropriate diameters (i.d. 0.76-1.14 mm). Mixing T-junctions and X-junctions were purchased from Ismatec (Kel-F, 0.8-mm i.d.) and reaction loops consisted of PTFE tubing.

A Perkin-Elmer model 2380 atomic absorption spectrometer was employed to evaluate the interference of Au^{III} on the relative yield of arsane generation. An electrodeless discharge lamp (EDL System II, Perking-Elmer) was used to detect As at a wavelength of 193.7 nm (spectral bandwidth 0.7 nm). The lamp was operated at the current level recommended by the manufacturer. The atomizer was a miniaturized Ar/H_2 diffusion flame [19] supported in a quartz tube (6.5 mm internal diameter).

An Agilent GC 6850 equipped with an Agilent 5975 C MS detector was employed to evaluate the interference by Au^{III} on the mechanism of hydrogen transfer from boron to arsenic. A manual sample injection of headspace gas (100 μL) was performed. The oven program consisted of the following: isothermal (6 min) at 25 °C, 25 °C/min to 200 °C maintained for 5 min. Inlet setup: inlet mode is pulsed split mode with split ratio 10:1, pulsed pressure 220 kPa and temperature 200 °C. A model J&W 122-1364E DB-624 column (6% cyanopropylphenyl 94% dimethyl polysiloxane) was used in constant flow mode at 0.8 mL He/min. Mass spectrometry detection (70 eV electron impact, transfer line 260 °C, ion source 250 °C) was performed in SCAN mode (55–350 *m/z*).

2.2.2. Batch-hydride generation experiments

Batch-HG was used in order to estimate, by GC-MS, the isotopic composition of arsane which was produced by reaction of As^{III} by TDB in aqueous solution and in the presence of trace amounts of Au^{III}, Pd^{II}, Pt^{II}, Ni^{II} and Cu^{II}. Screw cap reaction vials fitted with PTFE/silicone septa (4 mL, borosilicate glass, Pierce Chemical Co.) were employed. GC-MS conditions were similar to those used for continuous flow-HG (section 2.2.1) with the following exceptions: 0.5 mL sample was injected in a splitless mode into a 30 m × 0.25 mm i.d. capillary column (1 μm Valcobond VB-1).

2.3. Procedures

2.3.1. Continuous Flow-Hydride Generation Experiments

Continuous flow-HG experiments were accomplished using the chemifold setups shown in Fig. 1. The As^{III} concentration was 1 mg L^{-1} and the Au^{III} concentration was varied from 0.5 to 20 mg L^{-1}. Both As^{III} and Au^{III} were prepared in 1 M HCl. Three different experimental protocols were investigated, namely *Exp-A* (Fig. 1a), *Exp-B* (Fig. 1b) and *Exp-C* (Fig. 1c).

Exp-A: As^{III} was first mixed with THB (or TDB) in a T-junction and the hydride generation continued in loop L1 (volume 116 μL). The arsane preformed in L1, together with As^{III} and other As species not fully reacted, merged in an X-junction with additional THB (or TDB) and Au^{III} in 1 M HCl. After reaction in loop L2 (volume 500 μL) this solution underwent gas–liquid separation (assisted by Ar stripping) and the volatile compounds were analyzed by GC-MS and AAS.

Exp-B: As^{III}, Au^{III} and TDB solutions were mixed simultaneously in an X-junction. The reaction took place in loop L1 (volume 116 μL), after which the solution underwent gas–liquid separation (assisted by Ar stripping) and the volatile compounds were analyzed by GC-MS and AAS. This experiment most closely resembled that used analytically and the absorbance signal measured in the absence of interference - S_0 - was taken as the reference signal.

Exp-C: Au^{III} was first mixed with THB (or TDB) in a T-junction and the reduction took place in loop L1 (volume 116 μL). The reaction products from L1 were merged in a T-junction with As^{III}. After reaction in loop L2 (volume 500 μL), this solution underwent gas–liquid separation (assisted by Ar stripping) and the volatile compounds were analyzed by GC-MS and AAS.

In all experiments, the steady-state signal intensity was employed for absorbance measurement. The signal generated between 40 and 90 s after the start of reaction was averaged and taken as the signal intensity. For GC-MS measurements, the arsane was sampled through the PTFE port (Fig.1) in the time interval between 40 and 90s after the start of the reaction.

2.3.2. Batch-HG experiments

Exp-1: A 1 mL solution of 1 mg L^{-1} As^{III} in 1 M HCl was placed in the reaction vial and spiked with an appropriate amount of metal ion. The vial was sealed, purged with nitrogen and kept under magnetic stirring. A 0.5 mL volume of 0.2 M TDB in 0.1 M NaOH was then added. GC-MS analysis of 0.5 mL of headspace was performed at varying time intervals.

Exp-2: AsD_3 was generated in a vial by reacting 10 mg L^{-1} As^{III} in 1 M HCl with TDB in 0.1 M NaOH. In another vial containing the metal ion solution in 1 M HCl, a 0.5 mL volume of 0.2 M TDB was injected (a needle was inserted in the septum to remove the hydrogen over pressure). The needle was removed and 2 mL of the headspace containing the AsD_3 generated in the first vial were injected. The solution was maintained under shaking and GC-MS analysis of the headspace was performed at different times after injection of the TDB solution.

In all these experiments, the concentration of arsane in the headspace was considered proportional to the integrated area of the arsane peak (total ion current) obtained by GC-MS analysis.

2.4. Estimation of the amount fraction of AsH_nD_{3-n} isotopologues ($n = 0 - 3$) in a gaseous mixture

The separation of the different isotopologues AsH_nD_{3-n} ($n = 0 - 3$) cannot be performed using conventional capillary GC. Moreover, they cannot be separated in the mass domain since their electron impact mass spectra substantially overlap. Additionally, there are no experimental strategies to obtain pure isotopologues, such as AsH_2D and $AsHD_2$. In this work, the relative abundances $y(AsH_nD_{3-n})$ ($n = 0, 1, 2, 3$) generated experimentally in different conditions, were estimated theoretically using the method described by Meija et al. [20].

3. Results and discussion

As shown in Fig. 1 and described in the experimental section, the continuous flow experiments were undertaken in an effort to understand the relevance of the mixing sequence on generation of arsane by THB (or TDB) in the presence of gold;

Exp-B provides conditions closest to an analytical situation wherein the analyte and the interference are present at the same time at the moment reduction by THB (or TDB) occurs.

Exp-A and *Exp-C* can be viewed as perturbations of *Exp-B* in that arsane is reacted with Au^{III}/THB (or Au^{III}/TDB) in *Exp-A* and the preformed Au-colloid/THB (or Au-colloid/TDB) is reacted with arsane during generation in *Exp-C*.

Continuous flow experiments were conducted in order to investigate the effect of gold on the yield of arsane and on the mechanism of hydrogen transfer.

Batch experiment *Exp-2* provides information on the role of the metal colloid on the H/D exchange in pre-formed AsD_3, whilst *Exp-1* is the batch version of *Exp-B* wherein analyte and interference are present together in the system at the moment of reduction by TDB.

3.1. Interference by Au^{III} during continuous flow-HG: AAS experiments

The most important results generated by the continuous flow-*HG* experiments are presented in Fig. 2. Fig. 2a reports an interference plot obtained using THB. The magnitude of the interference is relatively low (signal depression < 10%) for both *Exp-A* and *Exp-B*. An interesting effect is observed with *Exp-C*. In the absence of gold, the signal is lower than that obtained during *Exp-A* and *Exp-B*. This is in agreement with

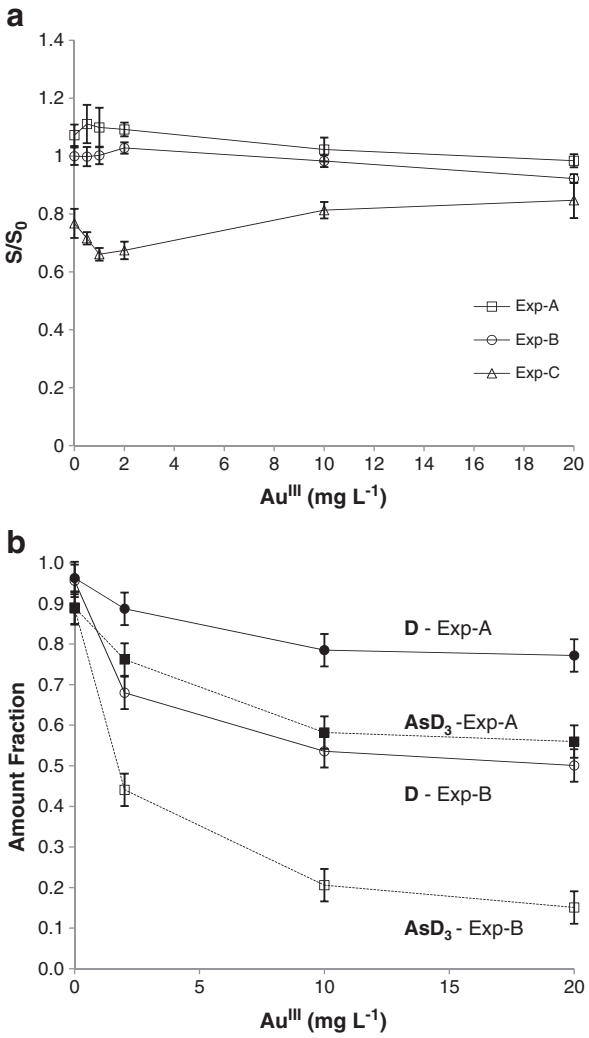

Fig. 2. Effect of concentration of Au^{III} on the HG of arsane. Conditions: 1 mg L^{-1} As^{III} in 1 M HCl reacting with 0.25 M THB (or TDB) in 0.1 M NaOH. Plots *Exp-A*, *Exp-B* and *Exp-C* were obtained using experimental setups of Fig. 1a, 1b and 1c. (a) Effect of Au^{III} concentration on the generation efficiency of arsane. *S* is the adsorbance signal and S_0 is the absorbance signal obtained in the absence of interference using the mixing sequence shown in Fig. 1b. (b) Effect of Au^{III} concentration on the isotopic composition of arsane; D represents the total amount fraction of deuterium incorporated into arsane and AsD_3 is the amount fraction of the heavy arsane. Uncertainties are SD, N = 3.

previously reported evidence [21] wherein arsane is generated with reduced efficiency when As^{III} is reacted with hydridoboron intermediates (formed in L1, Fig. 1c). By increasing the gold concentration, the signal obtained in *Exp-C* reached its maximum at 20 mg L^{-1}, which is close to the response obtained in *Exp-A* and *Exp-B*. The result of *Exp-C* (Fig. 2a) suggests that, under these conditions, gold is able to improve the HG efficiency by playing an active role in the hydrogen transfer from the borane complex to the substrate. We propose that THB-Au^{III} intermediates are more efficient for HG than the hydridoboron species formed without the metal. However, considering that Au^{III} and its reaction products can also exert an interference effect on the yield of arsane, it is concluded that both positive and negative effects are present at the same time in the experiments reported in Fig. 2a. Coincidentally, at 20 mg L^{-1} Au^{III}, the two opposing effects result in a similar generation efficiency of arsane for the experiments reported in Fig. 2a.

An additional interesting observation is the effect of Au^{III} on the shape of the absorbance-time signals: *Exp-A* and *Exp-B* are not perturbed by the presence of gold in the range 0–20 mg L^{-1} Au^{III}. On the other hand, the shapes of the signals obtained in *Exp-C* are strongly affected by the presence of Au^{III}. In this case, the signals lose their typical steady-state profiles and tend to decrease with time. Moreover, strong memory effects derived from the action of the metal are evident from the pronounced tailing of the signals and from the signal enhancement which remains even in the absence of Au^{III}. This peculiar positive memory interference effect is not easy to explain but the possibility cannot be ruled out that some gold compounds retained in the HG system continue to exert an enhancement effect on the efficiency of arsane generation (Fig. 2a, *Exp-C*). Accumulation of gold compounds in the HG apparatus was evident from the light blue color of deposits adhering to the inner wall of the PTFE tubing. After the generation of the arsane in the presence of gold (2–20 mg L^{-1} Au^{III}), the baseline noise level of the blank (1 M HCl and 0.25 M THB, without Au, *Exp-C*, Fig.1) remained higher than the original level measured before experiments. If 1 M HCl is replaced by 20 mg L^{-1} Au^{III} in 1 M HCl, a transient peak is observed due to arsane generation and the baseline is restored in less than 3 minutes. These qualitative observations indicate the different reactivity of the reducing species which are formed by hydrolysis of THB in the presence and in the absence of Au^{III}. These reducing species are more effective than those generated by hydrolysis of THB in 1 M HCl and this is in agreement with the evidence presented in Fig. 2a, *Exp-C*.

From this set of experiments, it is clear that the role played by gold during generation of arsane is not only associated with the suppression of generation efficiency, but also by strong interaction with the THB-As^{III} system, rendering positive effects on HG under select conditions.

3.2. Interference by Au^{III} during continuous flow-HG: deuterium labeled experiments

The experiments summarized in Fig. 2a were repeated using TDB and the isotopic composition of the arsanes generated in the presence of Au^{III} was determined; results are reported in Fig. 2b for *Exp-A* and *Exp-B*. The presence of Au^{III} in the reaction system produces a remarkable decrease in the amount fraction of deuterium which is incorporated into the generated arsane, even at the lowest concentration of gold (As/Au mole ratio equal to 1.3). The effect is particularly evident with AsD_3, which tends to disappear. *Exp-C* and *Exp-A* yield comparable results with $y(D) = 0.90$ and 0.93 at 2 mg L^{-1} Au^{III}, respectively. In general, the collected evidence indicates that gold interferes with the mechanism of hydrogen transfer from boron to arsenic.

The most pronounced effect is observed when all reagents are mixed together (*Exp-B*, Fig. 1b); this indicates that gold plays a role in the early stages of formation of arsane. Under conditions in which the arsane has already formed in L1 (*Exp-A*, Fig.1a) and can interact with those gold compounds formed during the Au^{III}-TDB reaction, the H/D exchange is considerably reduced. The same is evident when the formation of arsane takes place in the presence of gold compounds which are formed after prolonged reaction time with TDB in L1 (*Exp-C*, Fig. 1c).

It is noteworthy that H/D exchange is promoted at gold concentrations which produce either a moderate depletion of the reaction efficiency (signal depression < 10%) or no effect at all.

There is no correlation between the magnitude of the interference and the magnitude of the H/D exchange, as illustrated by results presented in Fig. 2, wherein *Exp-B* produces less pronounced interference (Fig. 2a) but more pronounced H/D exchange (Fig. 2b).

The results presented in this section indicate that Au^{III} participates in the generation of arsane and this occurs during the early stages of the following reaction sequence:

$$Au^{III} + THB \rightarrow intermediates \rightarrow Au^{0} \rightarrow Au(nanoparticles) \rightarrow Au(colloids) \quad (1)$$

Concerning the nature of the intermediates, formation of transient species containing Au-H, Au-B-H and B-Au-H bonds [17,22–24] as

intermediate states through which gold passes during the reduction from Au^{III} to Au^{0} cannot be excluded.

3.3. Interference by Au^{III} and other metal ions during batch-HG: deuterium labeled experiments

In addition to Au^{III}, the effect of other metal ions (Pd^{II}, Pt^{II}, Ni^{II} and Cu^{II}) was tested during batch-HG of arsane. When TDB was added to a solution containing both As^{III} and the metal ion (*Exp-1*) a remarkable H/D exchange was produced by Au^{III}, Pd^{II} and Pt^{II}, whereas the effects produced by Ni^{II} and Cu^{II} were of little relevance. For these three elements, a more detailed investigation was conducted through *Exp-1* and *Exp-2* and the results are reported in Fig. 3 for Au^{III}, Pd^{II}, and Pt^{II}, respectively.

The gradual decrease of arsane concentration with time (Fig. 3a, 3c and 3e) is due to the sequestration of hydride on the surface of the

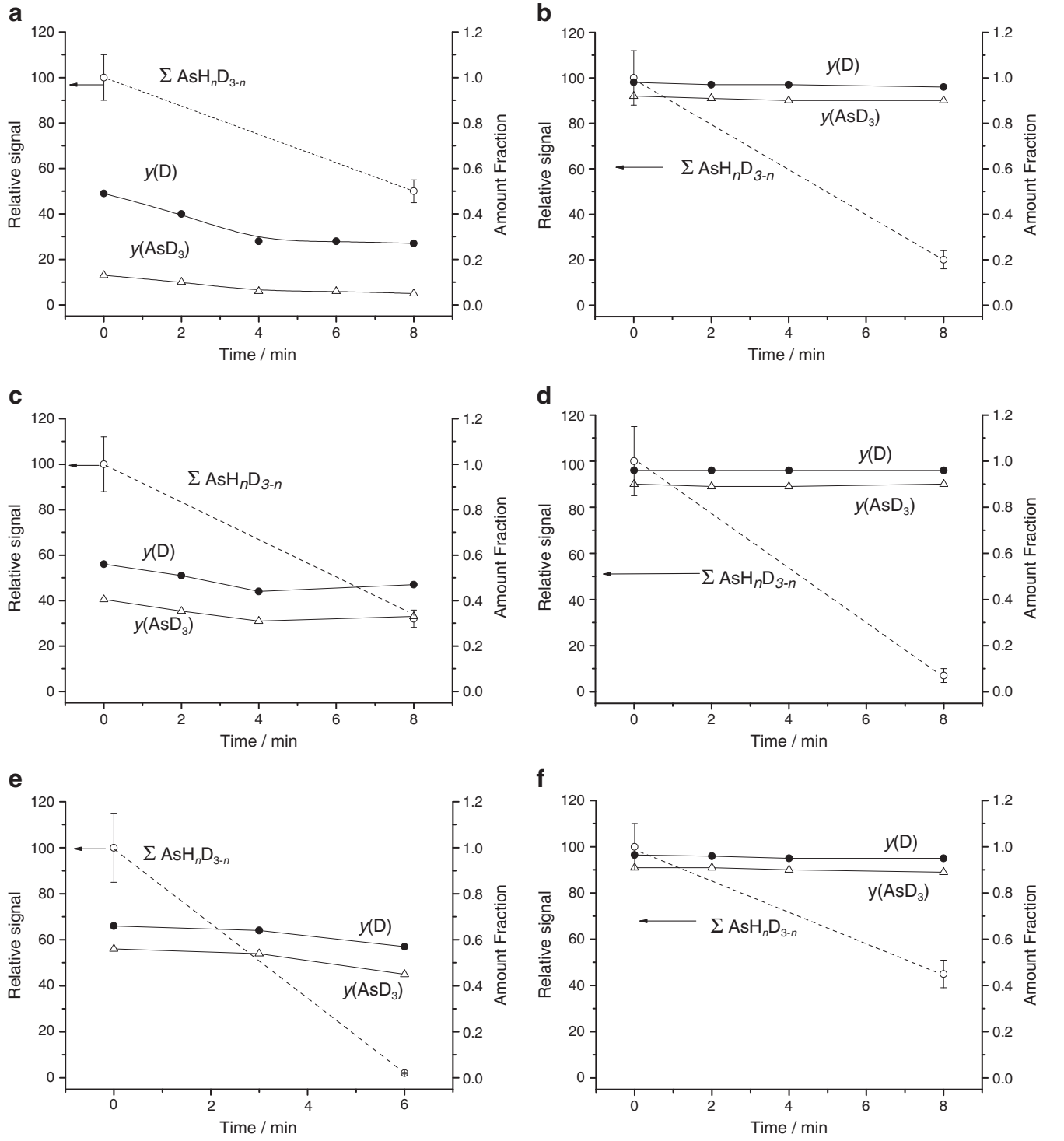

Fig. 3. Effect of noble metal ions Au^{III}, Pd^{II} and Pt^{II} on the isotopic composition of arsane and on its total concentration (ΣAsH_nD_{3-n}) in the reaction headspace. Arsane generated by reaction of 1 mg L^{-1} As^{III} in 1 M HCl with 0.2 M TDB in 0.1 M NaOH. Several samples were collected at different times after the start of reaction: (a) Arsane generated in the presence of 20 mg L^{-1} Au^{III}. (b) Preformed AsD_3 injected into the vial just after reaction of 20 mg L^{-1} Au^{III} with TDB. (c) Arsane generated in the presence of 2 mg L^{-1} Pd^{II}. (d) Preformed AsD_3 injected into the vial just after reaction of 20 mg L^{-1} Pd^{II} with TDB. (e) Arsane generated in the presence of 20 mg L^{-1} Pt^{II}. (f) Preformed AsD_3 injected into the vial just after reaction of 20 mg L^{-1} Pt^{II} with TDB. Standard deviation on amount fractions is less than 0.02.

(nano)particles formed by the reduction of the metal ions by TDB. However, the presence of metal particles did not produce further notable changes in the isotopic composition of arsane during the observed reaction time span, with the exception of gold, for which additional H/D exchange is observed within 4 minutes (Fig. 3a). However, most of the H/D exchange occurs just after the addition of TDB. The interaction of the metal reaction products with preformed AsD_3 (*Exp-2*) did not produce significant H/D exchange, as shown in Fig. 3b, 3d and 3f. This confirms the observations emerging from continuous flow-HG experiments and rules out the possibility that AsD_3 undergoes H/D exchange in the presence of metal colloids.

3.4. Effect of metal ions on the mechanism of hydrogen transfer

In the absence of foreign species, the mechanism of arsane generation is due to the direct stepwise transfer of hydrogen from borane to arsenic, and takes place with moderate isotopic effects [25]. Using a mixed solution of THB and TDB [25] the isotopic composition of the generated arsane is similar to that reported in Fig.4. From Fig. 4, it is possible to estimate that a mixed THB + TDB reductant solution of composition $x(TDB)$ $(0 \le x \le 1)$ generates a mixture of arsane isotopologues AsH_3, $AsHD_2$, AsH_2D and AsD_3. The distribution of abundances of the arsane isotopologues is described by a set of four amount fractions $y(AsH_3)$, $y(AsHD_2)$, $y(AsH_2D)$ and $y(AsD_3)$ $(0 \le y \le 1)$. The cumulative amount fraction of deuterium incorporated into the generated arsane is $y(D)$ [where $y(D) < x(TDB)$ because of the isotopic effect] and

$$y(D) = \sum_{n=0}^{3} (3-n) \cdot y(AsH_nD_{3-n}).$$

In pure aqueous solution, a given value of $y(D)$ corresponds to one and only one set of $y(AsH_3)$, $y(AsHD_2)$, $y(AsH_2D)$ and $y(AsD_3)$. This set describing the distribution of abundances of the arsane isotopologues cannot be achieved with other values of $y(D)$ and vice versa; for every $y(D)$ there is a unique set of abundances of the arsane isotopologues, evident from the abundance distributions reported in Fig. 4.

The presence of trace amounts of some transition metal ions can produce dramatic changes in both $y(D)$ and the distribution of abundances of arsane isotopologue. Ni^{II} and Cu^{II} produced only a minimal effect on the distribution, whereas Au^{III}, Pt^{II} and Pd^{II} result in a dramatic perturbation. The results obtained for these noble metals are compared in Figs. 5 and 6.

In general, the presence of Au^{III}, Pt^{II} and Pd^{II} at trace levels results in the generation of arsanes in which the total deuterium incorporated decreases from 98% to about 65 – 45%, depending on the metal and its concentration. This is clearly the consequence of an H/D exchange processes with the reaction environment which could occur during different steps of the reaction pathways. Excluding the H/D exchange on the already formed arsane (section 3.3), one hypothesis could be a catalytic role of the metal promoting H/D exchange on TDB before the hydrogen transfer step. This would change the isotopic composition of the borane complex, reducing the amount fraction of deuterium in it, and giving reaction conditions similar to those achievable by the use of a mixed THB + TDB reductant. In this case, from Fig. 4, it is possible to determine the isotopic composition of arsane produced for a given fractional amount of total deuterium, $y(D)$, which is obtained with a reductant of composition $x(TDB)$. In Fig. 5b, it is evident that the presence of Pt^{II} produces arsane with $y(D) = 0.65$ and that the same level of deuterium incorporation could be obtained in the absence of the metal by using a mixed THB + TDB with $x(TDB) = 0.725$. The same is valid for Pd^{II}, producing arsane with $y(D) = 0.55$ and that the same level of deuterium incorporation could be obtained in the absence of the metal by using mixed THB + TDB with $x(TDB) = 0.635$. However, the distributions of arsane isotopologues for the same level of $y(D)$ show dramatic differences. In particular, the presence of Pt^{II} and Pd^{II} considerably increases the formation of fully hydrogenated and deuterated isotopologues, AsH_3 and AsD_3, thus inverting the distribution obtained by mixed THB + TDB reductant for which the prevailing species formed in the absence of these metal ions are the mixed isotopologues AsH_2D and $AsHD_2$. The formation of only AsH_3 and AsD_3 species is expected in a mechanism in which the H or D atoms come from the same borane molecule [25]. The presence of Pt^{II} and Pd^{II} could promote the formation of borane-metal intermediates according to same scheme of reaction 1. In this case, formation of arsane could also take place with a partial contribution of a reaction pathway in which all the three H or D atoms come from the same borane-metal intermediate.

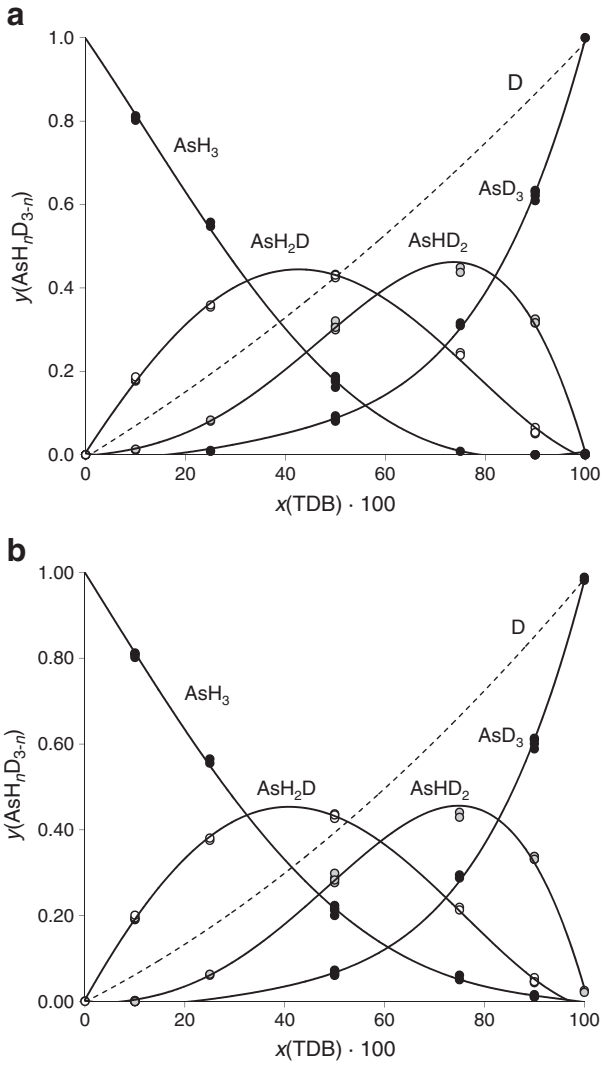

Fig. 4. Abundance distribution of arsane isotopomers and total amount fraction of deuterium obtained during generation of arsane with mixed THB and TDB: (a) Statistical deconvolution. (b) Entropy minimization.

The effect of Au^{III} (Fig. 6c), while strongly influencing the amount fraction of incorporated deuterium [$y(D) = 0.46$], is less pronounced on the distribution of arsane isotopologues. However, the increase of $y(AsD_3$ from 0.09 to 0.21 and the decrease of $y(AsH_2D)$ from 0.41 to 0.31 are significant, and indicate that, in this case as well, the presence of metal changes the abundance distribution of arsane isotopologues.

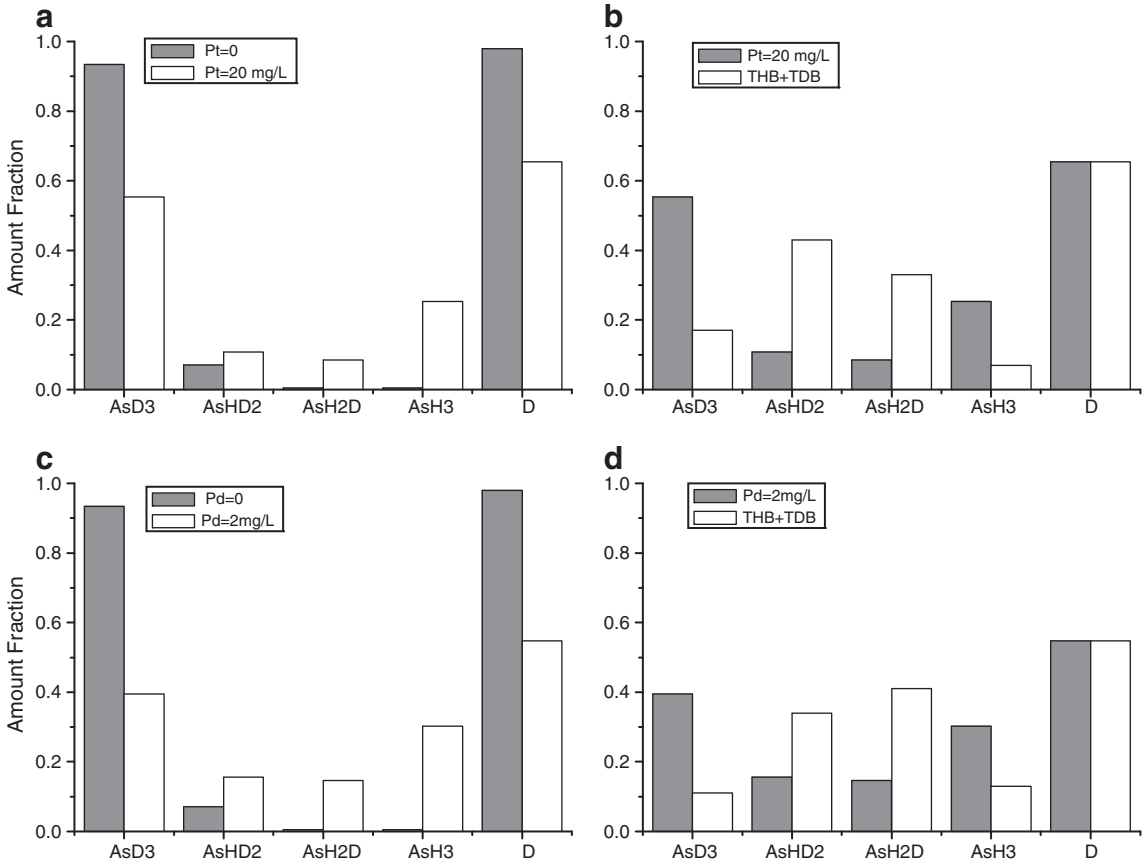

Fig. 5. Comparison of abundance distribution of arsane isotopologues and total deuterium obtained during batch generation of arsane from 1 mg L^{-1} As^{III} in 1 M HCl (Exp-1, section 2.3.2). (a) arsane generated by reaction with 0.2 M TDB in the absence and in the presence of 20 mg L^{-1} Pt^{II}; (b) arsane generated by reaction with 0.2 M TDB in the presence of 20 mg L^{-1} Pt^{II} (grey histograms) and arsane generated in the absence of metal ion by using 0.2 M (THB + TDB) with x(TDB) = 0.725, according to abundance distribution reported in Fig. 4 (white histograms); (c) arsane generated by reaction with 0.2 M TDB in the absence and in the presence of 2 mg L^{-1} Pd^{II}; (d) arsane generated by reaction with 0.2 M TDB in the presence of 20 mg L^{-1} Pd^{II} (grey histograms) and arsane generated in the absence of metal ion by using 0.2 M (THB + TDB) with x(TDB) = 0.635, according to abundance distribution reported in Fig. 4 (white histograms). D represents the total amount fraction of deuterium incorporated into arsane and AsD_3 is the amount fraction of the heavy arsane. Standard deviation on amount fractions is less than 0.02.

The evidence reported above casts doubt on a mechanism based on the sole hypothesis that the metal promotes a preliminary H/D exchange on the borane complex before the reaction of borane with As^{III}.

These data illustrate that the presence of some metal ions at trace levels are able to change the mechanism of incorporation of hydrogen into the final hydride and that their interaction with the borane-analyte reaction system is much faster than the complex of reactions leading to the formation of the final arsane in the absence of these noble metals [25]. This represents a new type of interference in HG technique, which can be termed a "mechanistic interference" in order to distinguish it from the already know "reaction yield interference".

4. Conclusion

A new type of interference - herein termed "mechanistic interference" - has been identified in HG of arsane by aqueous tetahydridoborate. It is induced by the presence of some noble metal ions such as Au^{III}, Pd^{II} and Pt^{II}. Concentrations of these metal ions at the micromolar level are able to change the mechanism of hydrogen transfer from the borane complex to arsenic, allowing the incorporation of a larger amount of hydrogen derived from the solvent to the final arsane. This mechanistic interference appears independent of the reaction yield interference, at least for the investigated case of arsane generation in the presence of Au^{III}, Pd^{II} and Pt^{II}. It is remarkable that the mechanistic interference takes place during the early stages of the reaction and under conditions in which the As/metal mole ratio is in the range from 0.5 to 15 and the borane reagent concentration is several orders of magnitude higher than both As and the metal ions. This is a new evidence with respect to the mechanism proposed for hydride generation in the absence of foreign species, essentially based on the direct stepwise hydrogen transfer from the borane complex to the substrate. The mechanistic interference reported here cannot be explained by H/D exchange of borane before its reaction with the arsenic substrate and thus clarification of the mechanism associated with this type of interference requires further detailed investigations.

More evidence on the effect of Au^{III} on arsane generation indicates that the metal can interact with the borane-As reaction system at concentrations much lower than those producing depletion of reaction yield of arsane. In some cases, the intermediate products which are formed in the early stages of the Au^{III}-THB-H_3O^+ reaction pose peculiar reactivity with respect to those formed during the THB-H_3O^+ reaction.

This work sheds new light on the role played by metal ions during the chemical vapour generation of volatile hydrides and contributes to the general knowledge of THB, a classical reducing agent in chemistry and a molecule actually under investigation by the scientific community for its potentialities for hydrogen storage.

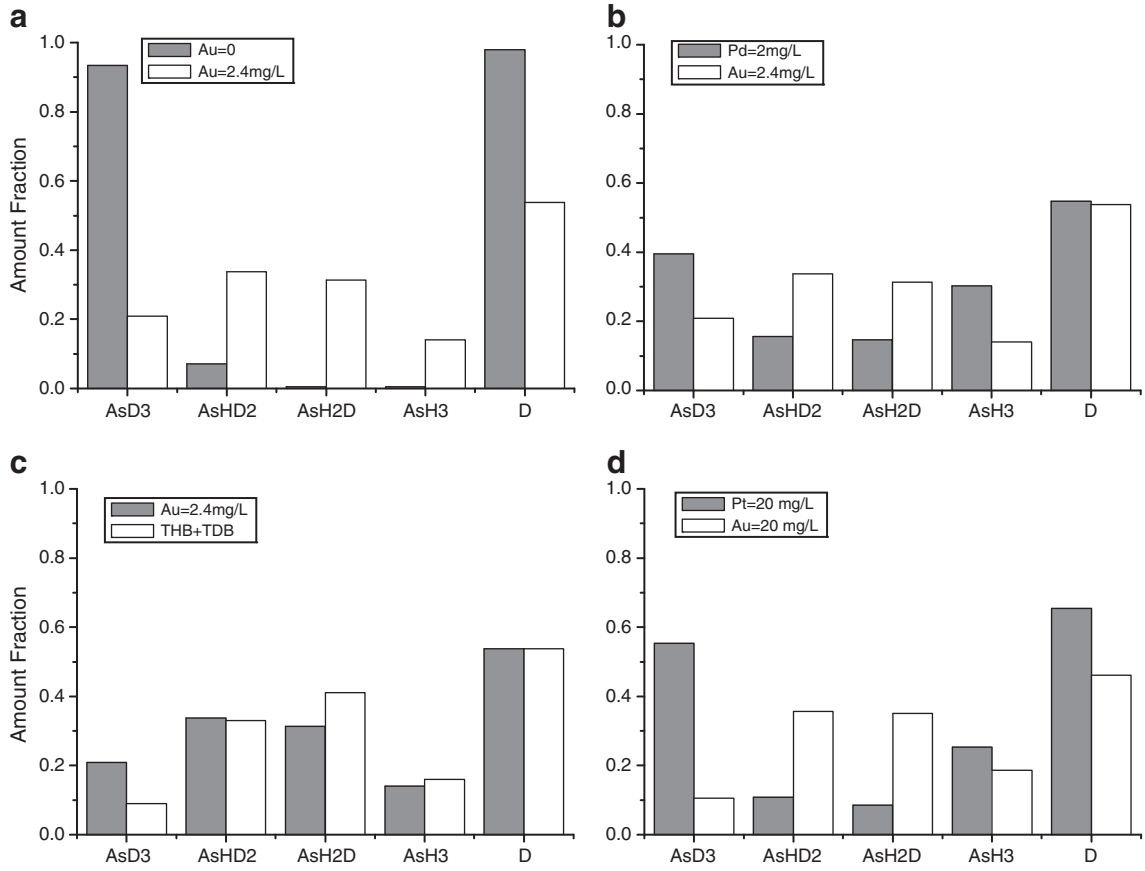

Fig. 6. Comparison of abundance distribution of arsane isotopologues and total deuterium, obtained by batch generation of arsane from 1 mg L^{-1} As^{III} in 1 M HCl (Exp-1, section 2.3.2). (a) arsane generated by reaction with 0.2 M TDB in the absence and in the presence of 2.4 mg L^{-1} Au^{III}; (b) arsane generated by reaction with 0.2 M TDB in the presence of 2 mg L^{-1} Pd^{II} (grey histograms) and 2.4 mg L^{-1} Au^{III} (white histograms); (c) arsane generated by reaction with 0.2 M TDB in the presence of 2.4 mg L^{-1} Au^{III} (grey histograms) and arsane generated in the absence of metal ion by using 0.2 M (THB + TDB) with x(TDB) = 0.545, according to abundance distribution reported in Fig. 4 (white histograms). (d) arsane generated by reaction with 0.2 M TDB in the presence of 20 mg L^{-1} Pt^{II} (grey histograms) and 20 mg L^{-1} Au^{III} (white histograms). D represents the total amount fraction of deuterium incorporated into arsane and AsD_3 is the amount fraction of the heavy arsane. Standard deviation on amount fractions is less than 0.02.

References

[1] R.E. Sturgeon, Z. Mester, Analytical Applications of Volatile Metal Derivatives, Appl. Spectrosc. 56 (2002) 202A–213A.
[2] J. Dědina, D.L. Tsalev, Hydride Generation Atomic Absorption Spectroscopy, Wiley, Chichester, 1995.
[3] A. D'Ulivo, Mechanism of generation of volatile species by aqueous boranes. Towards the clarification of most controversial aspects, Spectrochim. Acta Part B 65 (2010) 360–375.
[4] A. D'Ulivo, J. Dědina, Z. Mester, R.E. Sturgeon, Q. Wang, B. Welz, Mechanism of generation of volatile hydrides for trace element determination (IUPAC Technical Report), Pure Appl. Chem. 83 (2011) 1283–1340.
[5] B. Welz, M. Melcher, Mechanisms of transition metal interferences in hydride generation atomic-absorption spectrometry. Part 1. Influence of cobalt, copper, iron and nickel on selenium determination, Analyst 109 (1984) 569–572.
[6] D. Bax, J. Agterdenbos, E. Worrell, J. Beneken Kolmer, The mechanism of transition metal interference in hydride generation atomic absorption spectrometry, Spectrochim. Acta Part B 43 (1988) 1349–1354.
[7] S.S. Muir, X. Yao, Progress in sodium borohydride as hydrogen storage material: development of hydrolysis catalysts and reaction systems, Int. J. Hydrogen Energy 36 (2011) 5893–5997.
[8] P. Pohl, B. Prusisz, Chemical vapor generation of noble metals for analytical spectrometry, Anal. Bioanal. Chem. 388 (2007) 753–762.
[9] S. Musil, J. Kratzer, M. Vobecký, J. Hovorka, O. Benada, T. Matoušek, Chemical vapor generation of silver for atomic absorption spectrometry with the multiatomizer: Radiotracer efficiency study and characterization of silver species, Spectrochim. Acta Part B 64 (2009) 1240–1247.
[10] Y. Arslan, T. Matoušek, J. Kratzer, S. Musil, O. Benada, M. Vobecký, O.Y. Ataman, J. Dědina, Gold volatile compound generation: optimization, efficiency and characterization of the generated form, J. Anal. At. Spectrom. 26 (2011) 828–837.
[11] D.L. Van Hyning, C.F. Zukoski, Formation mechanisms and aggregation behavior of borohydride reduced silver particles, Lagmuir 14 (1998) 7034–7046.
[12] C.-H. Liu, B.-H. Chen, C.-L. Hsueh, J.-R. Ku, M.-S. Jeng, F. Tsau, Hydrogen generation from hydrolysis of sodium borohydride using Ni–Ru nanocomposite as catalysts, Int. J. Hydrogen Energy 34 (2009) 2153–2163.
[13] N. Patel, R. Fernandes, A. Miotello, Hydrogen generation by hydrolysis of $NaBH_4$ with efficient Co–P–B catalyst: A kinetic study, J. Power. Sources 188 (2009) 411–420.
[14] R.E. Davis, J.A. Bloomer, D.R. Cosper, A. Saba, Boron hydrides. The metal ion catalyzed hydrolysis of sodium borohydride in heavy water, Inorg. Chem. 3 (1964) 460–461.
[15] G. Guella, C. Zanchetta, B. Patton, A. Miotello, New insights on the mechanism of palladium-catalyzed hydrolysis of sodium borohydride from ^{11}B NMR measurements, J. Phys. Chem. B 110 (2006) 17024–17033.
[16] G.N. Glavee, K.J. Klabunde, C.M. Sorensen, G.C. Hadjipanayis, Borohydride reduction of nickel and copper ions in aqueous and nonaqueous media. Controllable chemistry leading to nanoscale metal and metal boride particles, Langmuir 10 (1994) 4726–4730.
[17] S.W. Hinzman, B. Ganem, The mechanism of sodium borohydride-cobaltous chloride reductions, J. Am. Chem. Soc. 104 (1982) 6801–6802.
[18] J.O. Osby, S.W. Heinzman, B. Ganem, Studies on the mechanism of transition-metal- assisted sodium borohydride and lithium aluminum hydride reductions, J. Am. Chem. Soc. 108 (1986) 67–72.
[19] J. Dědina, A. D'Ulivo, L. Lampugnani, T. Matoušek, R. Zamboni, Selenium hydride atomization, fate of free atoms and spectroscopic temperature in miniature diffusion flame atomizer studied by atomic absorption spectrometry, Spectrochim. Acta Part B 53 (1998) 1777–1790.
[20] J. Meija, Z. Mester, A. D'Ulivo, Mass spectrometric separation and quantitation of overlapping isotopologues. Deuterium containing hydrides of As, Sb, Bi, Sn, and Ge, J. Am. Soc. Mass Spectrom. 18 (2007) 337–345.
[21] A. D'Ulivo, M. Onor, E. Pitzalis, Role of hydroboron intermediates in the mechanism of chemical vapor generation in strongly acidic media, Anal. Chem. 76 (2004) 6342–6352.
[22] H.D. Kaesz, R.B. Saillant, Hydride complexes of the transiction metals, Chem. Rev. 72 (1972) 231–281.
[23] J. Aggett, Y. Hayashi, Observation of the interference by copper(II), cobalt(II) and nickel(II) on the determination of arsenic by arsine generation atomic absorption spectrometry, Analyst 112 (1987) 277–282.
[24] E. Ługowska, I.D. Brindle, Potentiometric investigation of Ni, Fe and Co interferences in the generation of selenium hydride by sodium tetrahydridoborate(III), Analyst 122 (1997) 1559–1568.
[25] A. D'Ulivo, Z. Mester, J. Meija, R.E. Sturgeon, Mechanism of generation of volatile hydrides of trace elements by aqueous tetrahydridoborate (III). Mass spectrometric studies on reaction products and intermediates, Anal. Chem. 79 (2007) 3008–3015.

Annex III

D'Ulivo, A.; Meija, J.; Mester, Z.; **Pagliano, E.**; Sturgeon R.E.

Condensation cascades and methylgroup transfer reactions during the formation of arsane, methyl- and dimethylarsane by aqueous borohydride and (methyl) arsenates

Anal. Bioanal. Chem **2012**, *402*, 921-933

Copyright 2011 Springer-Verlag

Anal Bioanal Chem (2012) 402:921–933
DOI 10.1007/s00216-011-5503-4

ORIGINAL PAPER

Condensation cascades and methylgroup transfer reactions during the formation of arsane, methyl- and dimethylarsane by aqueous borohydride and (methyl) arsenates

Alessandro D'Ulivo · Juris Meija · Zoltán Mester · Enea Pagliano · Ralph E. Sturgeon

Received: 4 August 2011 / Revised: 12 October 2011 / Accepted: 13 October 2011 / Published online: 30 October 2011
© Springer-Verlag 2011

Abstract The formation of volatile products during the reaction of As(III), As(V), $MeAsO(OH)_2$, and $Me_2AsO(OH)$ with aqueous $NaBH_4$ has been investigated, and the formation of arsanes, diarsanes, and triarsanes has been detected. The presence of triarsanes is reported here for the first time. Diarsanes and triarsanes are likely formed in condensation cascade reactions, whereas trimethylarsane arises via the transfer of a methyl group. The formation of volatile by-products is considerably reduced by increasing the acidity of the medium and the concentration of $NaBH_4$ or by the addition of thiols, such as cysteine. A reaction scheme is proposed which reconciles the evidence reported herein and elsewhere in the literature that is valid for both analytical (trace analysis) and non-analytical reaction conditions.

Keywords Arsenic · Monomethyarsonic acid · Dimethylarsinic acid · Tetrahydridoborate · Diarsanes · Triarsanes

A. D'Ulivo (✉)
CNR, Consiglio Nazionale delle Ricerche,
Istituto di Chimica dei Composti Organometallici,
Via G. Moruzzi, 1,
56124 Pisa, Italy
e-mail: dulivo@pi.iccom.cnr.it

J. Meija · Z. Mester · R. E. Sturgeon
Institute for National Measurement Standards,
National Research Council Canada,
Ottawa, ON K1A 0R6, Canada

E. Pagliano
Scuola Normale Superiore,
Piazza dei Cavalieri, 7,
56126 Pisa, Italy

Introduction

Chemical generation of volatile species (CGVS) of metallic or organometallic compounds by reactions with aqueous $NaBR_4$ (R=H, alkyl or phenyl group) or XBH_3 (X=NH_3, NR_3, CN^-) coupled with atomic or molecular spectroscopy or with mass spectrometry is among the most powerful analytical tools for trace element determination and speciation [1–3]. Despite the widespread analytical application of volatile hydride formation for the determination of trace amounts of elements such as arsenic, antimony, bismuth, germanium, tin, lead, selenium, tellurium, and mercury, the mechanism by which they are formed has been debated for many years. In particular, perpetuation of the notorious two-century-old incorrect hypothesis that free atomic (nascent) hydrogen is somehow involved in this reaction needs to be dispelled [4, 5].

Recent studies have shown that the aqueous phase reaction of $NaBH_4$ with oxoacid species of elements such as arsenic occurs through a concerted (direct) transfer of hydrogen atoms from boron to the element, thus forming the hydride, AsH_3 [6]. The generation of EH_n-type hydrides is an *n*-step process wherein each of the *n* hydrogen atoms in the hydride originates from different borane molecules [7]. In addition, acid hydrolysis of $NaBH_4$ is not necessary for the formation of hydrides [8, 9]. Analyte–borane intermediates have also been detected, as in the case of the reaction of $Me_2AsO(OH)$ with aqueous aminoboranes [7]. Certain aspects of the generation of the volatile hydrides, however, are not fully understood. An additional problem that arises from the incomplete understanding of this reaction is the assumption that the reaction of $NaBH_4$ with aqueous ions of the hydride-forming elements leads to the formation of a *unique* volatile hydride. It is well known,

however, that with the increased concentration of the analytical substrate, many elements are partially converted to solid reaction products [10–12]. This diminishes the yield of volatile hydride and leads to a curvature in calibration plots at higher concentrations of analyte [11, 12]. At trace levels (sub-milligrams per liter), inorganic As (III) and As(V), $MeAsO(OH)_2$, and $Me_2AsO(OH)$ react with an excess of aqueous $NaBH_4$, forming AsH_3, $MeAsH_2$, and Me_2AsH, respectively [2]. As the concentration of the analytical substrate increases or the $NaBH_4$-to-analyte amount ratio decreases, various volatile by-products, such as diarsanes or Me_3As, are formed [7]. This phenomenon is of great importance to analytical chemists. For example, it casts doubt on whether diarsane and monomethyl diarsane are indeed present in the environment, as recently reported [13], or they only appear as artifacts of the analytical method, as will be demonstrated here.

This study is devoted to a clarification of the mechanism of arsane generation from inorganic and methyl arsenates under analytical and non-analytical conditions. A series of experiments was performed with deuterium-labeled reagents using gas chromatography coupled with mass spectrometry for the identification of the reaction products. The mass spectra of the hydrides were mathematically deconvoluted in order to obtain the amount fractions of isotopologues AsH_nD_{3-n} (n=0–3), $MeAsH_nD_{2-n}$ (n=0–2), and $Me_2AsH_nD_{1-n}$ (n=0–1) and the amount fraction of deuterium incorporated into the final hydrides [14].

Experimental section

Instrumentation

A Hewlett-Packard 6890 gas chromatograph (GC) operated in splitless mode and equipped with a Hewlett-Packard 5973 mass selective detector (MS) was fitted with a 30-m capillary GC column (Valcobond VB-1, 1-μm film thickness, 0.25-mm internal diameter) for the acquisition of the mass spectra of arsane and methylated arsane isotopologues. The GC was operated under the following conditions: injector temperature, 160 °C; oven temperature program, 35 °C; hold for 4 min; and heated to 200 °C at 15 °C min^{-1}. The initial transfer line temperature was 150 °C, heated at 30 °C min^{-1} to 250 °C. For the separation and identification of the less volatile arsenic species, a different GC capillary column was employed (DB-5; 30-m length, 5-μm film thickness, 0.25-mm internal diameter), and it was operated under the following conditions: injector temperature, 160 °C; oven temperature program, 35 °C; hold for 4 min; heated to 200 °C at 15 °C min^{-1}. The initial transfer line temperature was 150 °C, heated at 30 °C min^{-1} up to 250 °C. Gas-tight syringes (1 and 5 mL, Hamilton) were employed for sampling gases from the reaction vial headspace. Screw cap vials (4 mL) fitted with PTFE/silicone septa (borosilicate glass, Pierce Chemical Co.) were used. The carrier gas was He at 1.2 mL min^{-1}. Mass spectral deconvolution of the results was undertaken.

Chemicals

$NaBH_4$ pellets (Alfa Aesar, Word Hill, MA), $NaBD_4$ powder (isotopic purity, x_D=99%; Cambridge Isotope Laboratories, Cambridge, MA), 37% DCl in D_2O (x_D=99.5%; Aldrich), 30% NaOD in D_2O (x_D=99%; Aldrich), and D_2O (x_D=99.9%; Aldrich) were used. Arsenic standard solutions (2,000 μg As mL^{-1}) were prepared from K_3AsO_4 (>99.0% purity, Baker's Analyzed), $MeAsO(ONa)_2$ (99.0% purity, ChemService, PA, USA), and cacodylic acid, $Me_2AsO(OH)$ (99.3% purity, Sigma Aldrich). A 1 mol L^{-1} bromide/0.2 mol L^{-1} bromate solution was prepared from analytical grade solid reagents (Carlo Erba). L-Cysteine solution (γ=10 gL^{-1}) was prepared by dissolving the solid reagent (Fluka) in 0.1 M HCl. A hydrazine solution (w=250 mg g^{-1}, $NH_2NH_2{\cdot}H_2O$; Fluka) was employed without further dilution. All other chemicals were reagent grade. Stock solutions of 1 M $NaBH_4$ or $NaBD_4$, prepared in H_2O, were stabilized with 0.5 M NaOH. A stock solution of 0.2 M $NaBD_4$ was prepared in D_2O and stabilized with 0.1 M NaOD. All $NaBH_4$ or $NaBD_4$ solutions were stored at 4 °C and were stable for a week. Working solutions for reactions were prepared by dilution of the stocks just before use.

Generation of arsanes

For the generation of different volatile arsanes, 1 mL of HCl solution (0.01–0.20 M) was placed into a 4-mL reaction vial and spiked with the required amount of the arsenic standard (5–400 μL of 2,000 μg As mL^{-1}). The vial was sealed, purged with nitrogen, and kept under magnetic stirring. An aliquot (0.1–1.0 mL) of 0.2 M $NaBH_4$ (or $NaBD_4$) in 0.1 M NaOH (or NaOD) was then added with a syringe. After the addition of the reducing agent, the headspace of the vial (approx. 0.25 mL) was sampled at different reaction times (from 5 s to 20 min) and analyzed by GC-MS.

For H/D exchange experiments, pure hydrogenated or deuterated arsanes were prepared shortly before their use from fully hydrogenated or deuterated media following the above procedure. After reaction, 5 mL of the headspace gas was sampled and then injected into another vial containing the exchange solution, H_2O or D_2O, at the required acidity. The vial was continuously shaken and the headspace (approx. 0.25 mL) was periodically sampled over an interval of 5 min.

Arsenic remaining in the liquid phase

Solutions resulting from the reaction of 10 mM As(III) or $MeAsO(OH)_2$ or $Me_2AsO(OH)$ in 1.4 mL 0.1 M HCl with 0.2 mL 0.2 M $NaBH_4$ in 0.1 M NaOH were analyzed following the same procedure described above for arsanes. During the reaction, several changes are observed for the different arsenic compounds; these are illustrated in Fig. 1. After 30 min, the headspace of the reaction vial was flushed with nitrogen in order to remove volatile products. The solution was analyzed for both the arsenic dissolved in the liquid phase and for the total arsenic (liquid phase + solid phase).

For the determination of arsenic dissolved in the liquid phase, 0.05 mL of the solution was diluted to 100 mL with 0.1 M HCl and 0.1 M cysteine solution. After 30 min, the solution was analyzed using arsane generation with detection by atomic absorption spectrometry (HG-AAS) [15]. For the determination of total arsenic, the solution containing the precipitate was acidified with 0.8 mL of 12 M HCl, and then bromine was developed in situ by the addition of 10 μL of a bromide/bromate solution. The solution was heated at 95 °C for 1 h in a heating block, and after cooling, the bromine was reduced with 10 μL of hydrazine solution. The determination of arsenic was achieved by HG-AAS, following the same procedure described for dissolved arsenic.

Amount fraction of arsane isotopologues

Separation of the arsane isotopologues AsH_nD_{3-n} (n=0–3), $MeAsH_nD_{2-n}$ (n=0–2), and $Me_2AsH_nD_{1-n}$ (n=0–1) cannot be accomplished using conventional capillary GC. Their separation, however, can be accurately performed in the mass domain since their mass spectra are different. For dimethylarsane, estimation of the Me_2AsH and Me_2AsD amount fractions can be performed from the fragments at m/z 106 and 107, respectively. Isotopologues of arsane and monomethyarsane, however, cannot be treated in a similar manner since the electron impact mass spectra of these hydrides overlap substantially. Additionally, there are no experimental strategies for obtaining pure AsH_2D, $AsHD_2$, or MeAsHD. In this case, relative abundances of the arsane and monomethylarsane isotopologues were estimated using mathematical deconvolution techniques previously developed for the quantitation of hydrides EH_2 (E=O, Se) [16], EH_3 (E=As, Sb, Bi), and EH_4 (E=Ge, Sn) [14]. The electron impact mass spectra of the pure arsane isotopologues are given below:

AsH_nD_{3-n}, m/z=75–81: 0.145, 0.420, 0.105, 0.328, 0.000, 0.000, 0.000 (n=3); 0.139, 0.262, 0.177, 0.079, 0.343, 0.000, 0.000 (n=2); 0.135, 0.086, 0.324, 0.006, 0.103, 0.346, 0.000 (n=1) and 0.136, 0.000, 0.431, 0.000, 0.088, 0.000, 0.345 (n=0) [14]
$MeAsH_nD_{2-n}$, m/z=90–94: 0.481, 0.079, 0.434, 0.006, 0.000 (n=2); 0.434, 0.151, 0.026, 0.389, 0.000 (n=1) and 0.350, 0.172, 0.068, 0.018, 0.392 (n=0)
$Me_2AsH_nD_{1-n}$, m/z=106–107: 1.000, 0.000 (n=1) and 0.000, 1.000 (n=0)

Results and discussion

H/D exchange of hydridic hydrogen in methylarsanes

As reported recently, neither AsH_3 nor AsD_3 undergoes H/D exchange when in contact with acidic solutions (pH, or pD, in the range from 0 to 7) for several minutes [17]. In contrast, methylarsanes undergo fast H/D exchange in

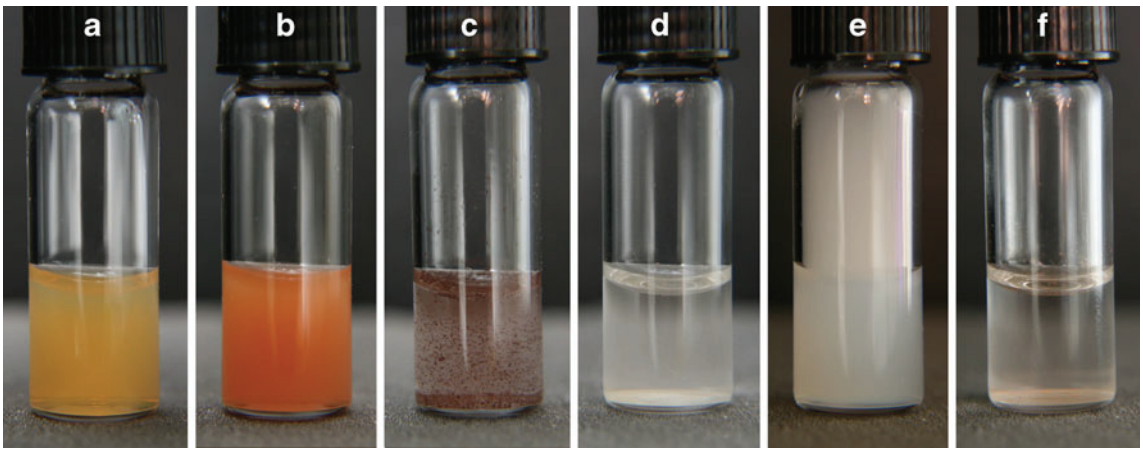

Fig. 1 Visual change occurring during the reduction of As(III) (**a**–**c**) and $Me_2AsO(OH)$ (**d**–**f**) with $NaBH_4$ (color change for As(III), As(V), and $MeAsO(OH)_2$ is similar). Images are taken approx. 1 s, 1 min, and 1 h after mixing the reagents, respectively. Experimental conditions: 1.4 mL of As solution (10 mM As in 0.1 MHCl) is reduced by 0.2 mL 0.2 M $NaBH_4$ in 0.1 M NaOH

acidic media [18]. Both $MeAsH_2$ and $MeAsD_2$ undergo a rapid H/D exchange in strongly acidic or alkaline conditions; however, no significant H/D exchange is observed in the interval of pH, or pD, from 6 to 10 for contact times with the liquid phase of up to 30 s, as evident from Fig. 2. The generation of $MeAsD_2$ at a final pH 9 results in a 95% isotopic purity of $MeAsD_2$ with only 4% of MeAsHD and 1% $MeAsH_2$. With the objective of evaluating the mechanism of hydrogen transfer, this was considered a tolerable level of H/D exchange. Both Me_2AsH and Me_2AsD undergo H/D exchange in strongly acidic media (pH, pD=1), yet are stable at pH, or pD, in the range from 6 to 13, where no significant exchange (<8%) takes place in the first 5 min. However, pure Me_2AsD could be obtained only in a strongly basic medium (pH>12), as shown in Fig. 3. In order to avoid any H/D exchange with the solvent, a final pH 13 was considered more appropriate, even though dimethylarsane is generated quite slowly under these conditions.

The identification of the pH regions where the arsanes are stable against H/D exchange with the media (HCl/H_2O) allowed the development of experimental designs in which the integrity of the isotopic composition of the generated volatile arsanes could be maintained. This, in turn, allowed probing the mechanism of hydride generation.

Mechanism of the hydrogen transfer from borohydride

Arsenic hydride generation experiments with pure $NaBD_4$ or from mixtures of $NaBD_4$ and $NaBH_4$ are useful for deciphering the origin of the hydrogen and, more importantly, the nature of the hydrogen transfer from the borohydride to arsenic. Most notably, it is among the simplest of means to dismiss the atomic hydrogen hypothesis of arsane generation [7]. Experiments with $NaBH_4$ and $NaBD_4$ mixtures can also differentiate between the single- and multistep transfer of hydrogen atoms from borohydride as these two scenarios result in different patterns of arsane isotopologues, as evident in Fig. 4.

In the multistep hydrogen transfer, the hydrogen atoms in the final hydride arise from different borane molecules, whereas in the case of a single-step hydrogen transfer, all hydrogen atoms in the final hydride derive from the same borane molecule. In the reaction of $MeAsO(OH)_2$ with a 1:1 mixture of $NaBH_4/NaBD_4$, the single-step hydrogen transfer would result in two hydrides, $MeAsH_2$ and $MeAsD_2$, both in equal amounts. In contrast, a two-step hydrogen transfer would result in a mixture of $MeAsH_2$, MeAsHD, and $MeAsD_2$ in a ratio of 1:2:1, as coefficients in the Pascal triangle. Comparison of the experimental and expected distributions of monomethylarsane isotopologues, shown in Fig. 4c, d, clearly favors the two-step transfer of hydrogen from boron to arsenic, analogous to the three-step transfer observed in the formation of AsH_3, SbH_3, or BiH_3 [7].

Isotope effects

The expected isotopologue distributions were calculated without considering the H/D isotope effect. Indeed, there is

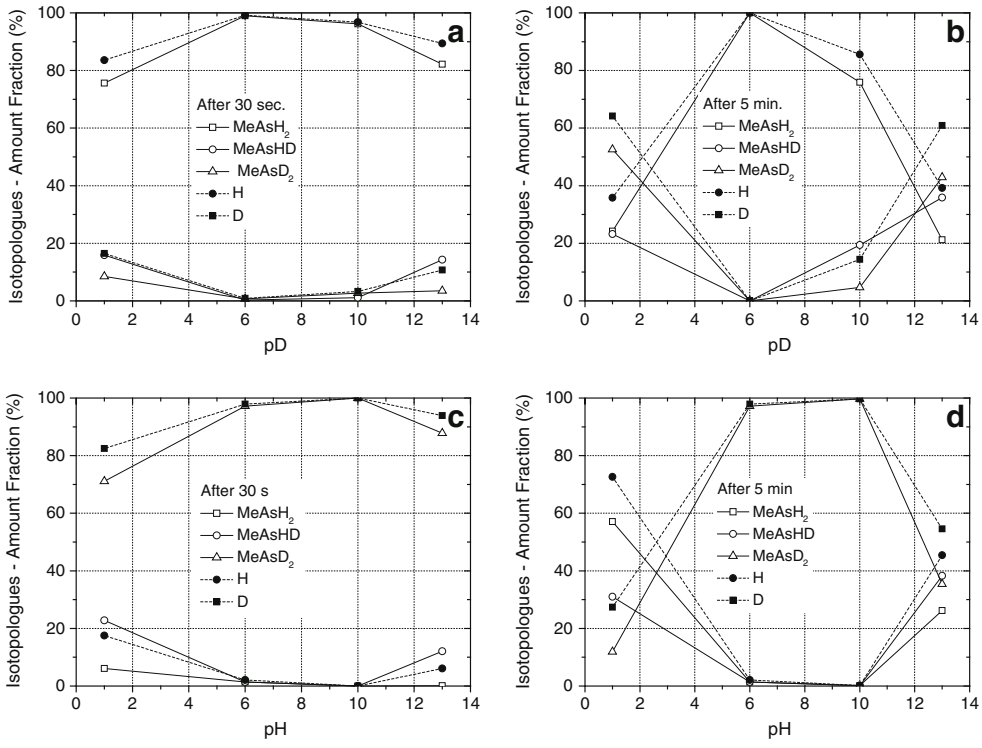

Fig. 2 H/D exchange of monomethylarsane. Pre-formed Me_2AsD (Me_2AsH) was placed in contact with the exchange media under various conditions. The amount fractions of $MeAsH_nD_{(2-n)}$ (n=0, 1, 2) detected in the headspace at different acidities are reported. **a** $MeAsH_2$ in D_2O at different pD values, 30-s contact time. **b** Same as (**a**), but with a 5-min contact time. **c** $MeAsD_2$ in H_2O at different pH values, 30-s contact time. **d** Same as (**c**), but with a 5-min contact time

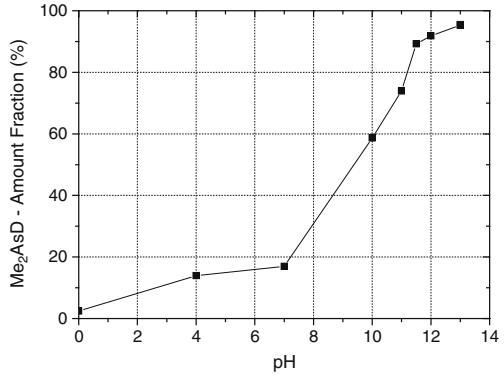

Fig. 3 Synthesis of dimethylarsane. 0.1 mM $Me_2AsO(OH)$ placed in a completely hydrogenated media was reduced with 0.2 M $NaBD_4$. The isotopic composition of dimethylarsane evolved has been followed against the acidity of the resulting solution. The amount fraction of Me_2AsD is reported at different pH values

no evidence of a significant isotope effect in the formation of dimethylarsane (Fig. 4a). In contrast to this, the isotopologue distributions of arsane (Fig. 4e) and monomethylarsane (Fig. 4c) are slightly skewed toward a more favorable incorporation of H over D, even if it appears of little relevance. Considering that no isotope effect is observed during the formation of dimethylarsane, this skew is likely due to a secondary isotope effect. This secondary isotope effect is reasonably due to the fact that the incorporation rate of an incoming H or D is dependent on the coordination sphere of arsenic, say to the presence of As–H or As–D bonds which are already formed in the preceding transfer step. In sum, the kinetic isotope effect, which has been observed by replacing H with D in $NaBH_4$, indicates that hydrogen transfer is not the rate-determining step in the formation of volatile arsanes.

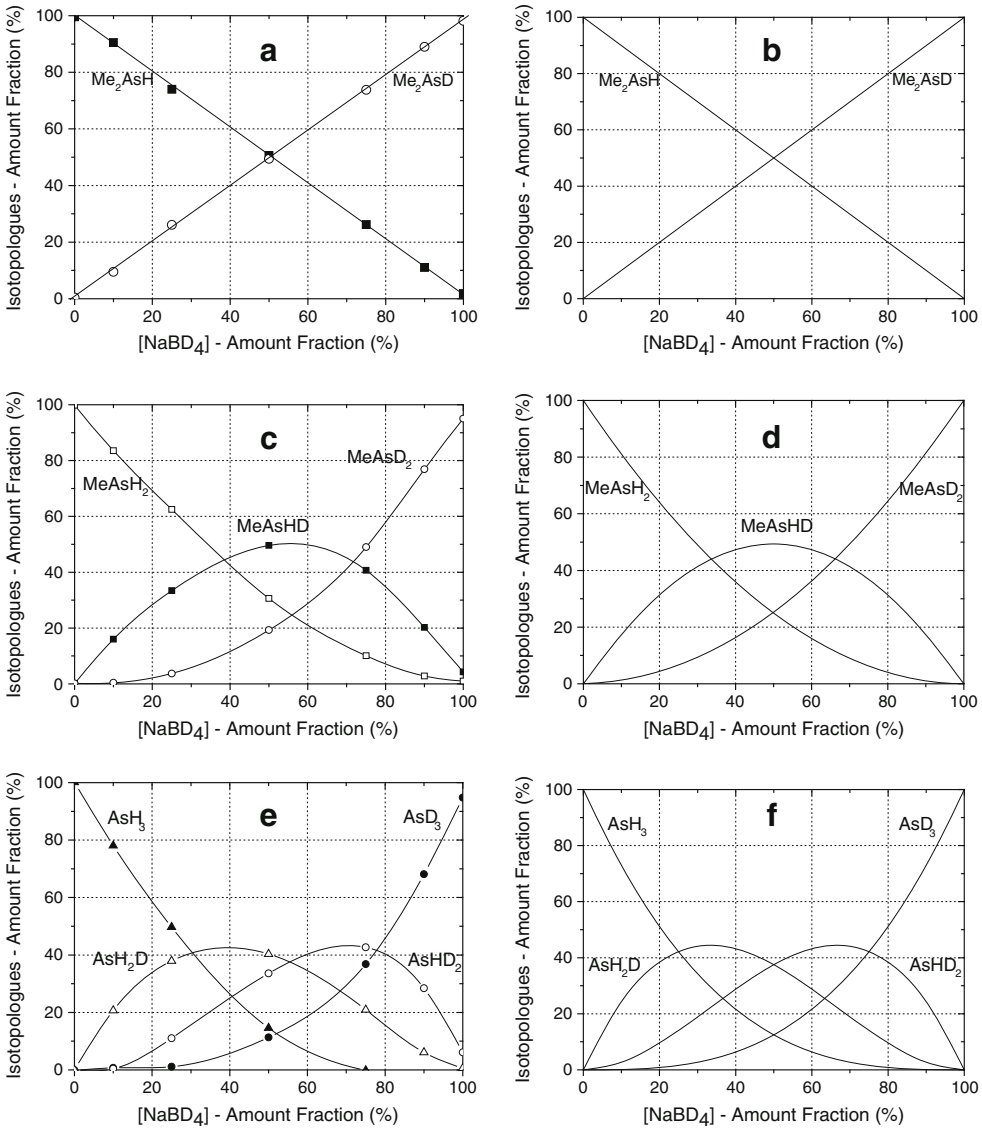

Fig. 4 Experimental (**a**, **c**, **e**) and predicted (**b**, **d**, **f**) distributions of arsane and methylated arsane isotopologues arising from the reduction of the corresponding pentavalent arsenic compounds. **a** Dimethylarsane. Conditions: 1 mL 60 μM $Me_2AsO(OH)$ in 1 mM HCl was reduced with 0.5 mL of 0.2 M ($NaBH_4$ + $NaBD_4$) in 0.1 M NaOH; all reagents were prepared in H_2O. **b** Predicted distribution of dimethylarsane isotopologues based on the direct hydrogen transfer from borohydride to arsenic. **c** Monomethylarsane. Conditions: 1 mL of 60 μM $MeAsO(OH)_2$ in 0.1 M HCl was reduced with 0.5 mL of 0.2 M ($NaBH_4$ + $NaBD_4$) in 0.1 M NaOH; all reagents were prepared in H_2O. **d** Predicted distribution of monomethylarsane isotopologues based on the direct hydrogen transfer from borohydride to As: two-step hydrogen transfer. **e** Arsane. Conditions: 1 mL of 60 μM $AsO(OH)_3$ in 1 M HCl was reduced with 0.5 mL of 0.2 M ($NaBH_4$ + $NaBD_4$) in 0.1 M NaOH; all reagents were prepared in H_2O. **f** Predicted distribution of arsane isotopologues based on the direct hydrogen transfer from borohydride to As: three-step hydrogen transfer

Volatile reaction by-products

Under analytical conditions and at ultra-trace levels of arsenic, hydride generation is commonly assumed to yield a single volatile product: AsH_3 from As(III) and As (V), $MeAsH_2$ from $MeAsO(OH)_2$, and Me_2AsH from $Me_2AsO(OH)$. To test this assumption, various experiments were conducted under analytical and non-analytical conditions wherein the concentration of the arsenic substrates was varied in the range from 10^{-2} to 10 mM (the typical analytical working range is from 1 nM to 1 μM of arsenic). While at the ultra-trace level the arsenic compounds are indeed converted to unique volatile arsanes, as mentioned above, the formation of other volatile arsanes is evident at a higher analyte concentration, as summarized in Tables 1 and 2. In certain cases, these by-products even become the major components of the headspace.

At arsenic concentrations up to 1 mM, the formation of a reddish suspended particulate matter is also evident for inorganic As and $MeAsO(OH)_2$, suggesting that they are not completely converted into volatile species (Fig. 1c). For $Me_2AsO(OH)$, no particulate matter is formed, but a white gas is generated upon the addition of $NaBH_4$, and it is clearly visible in the headspace of the reaction vial (Fig. 1e). At the highest concentration level of arsenic (10 mM), quantitative experiments indicate that a large fraction of arsenic remains in the vial after reaction with $NaBH_4$. For the inorganic arsenic compounds, about 65% of the total As remains in the condensed phase (45% in solution and 20% as solid precipitate). For both $MeAsO(OH)_2$ and $Me_2AsO(OH)$, the amount fraction of the total As remaining in solution as non-volatile compounds is >98%, but in the latter, no precipitate is visible. In spite of the small fraction amount of volatile species that are formed under these reaction conditions, their identification can give interesting information about the reactions which took place in the liquid phase.

For inorganic arsenic, the only observed volatile by-products are diarsane ($H_2As–AsH_2$) and triarsane ($H_2As–AsH–AsH_2$). A gamut of volatile compounds was produced during the reduction of methylated arsenic acids by $NaBH_4$, including dimeric and trimeric arsenic species. A summary of dimeric and trimeric arsenic species which have been detected in the headspace is reported in Table 4. The mass spectra of trimeric species are reported in Figs. 5, 6, 7, 8, and 9.

A rather interesting behavior is exhibited by the reaction of $Me_2AsO(OH)$ with $NaBH_4$/HCl, which, under certain conditions, can give Me_3As as the most abundant volatile product (Table 2). Experimental evidence indicates that Me_3As is formed simultaneously with the disappearance of Me_2AsH. In general, the formation of volatile by-products is more pronounced with increased reaction time, As/

Table 1 Volatile arsenic compounds detected during the reaction of inorganic As^{III}, As^{V}, or $MeAsO(OH)_2$ with $NaBH_4$

Compound	As/$NaBH_4$ (μmol/μmol)	Conditions[a]	Time (min)	Volatile arsenic species[b]							
				AsH_3	$MeAsH_2$	Me_2AsH	Me_3As	Me_2AsCl	As_2H_4	H_2As_2MeH	$As_2(HMe)_2$
$AsO(OH)_3$	2.7/20	pH 3	0.2	100	–	–	–	–	9.5	–	–
	2.7/100	pH 9	0.2	100	–	–	–	–	–	–	–
$As(OH)_3$	2.7/20	pH 3	0.2	100	–	–	–	–	1.4	–	–
	2.7/100	pH 9	0.2	100	–	–	–	–	0.2	–	–
$MeAsO(OH)_2$	10.8/8	pH 3–4	0.2	–	100	–	–	–	–	–	–
			30	–	100	–	–	–	–	–	–
	2.7/20	pH 3	0.2	2.1	100	0.2	–	0.1	–	0.1	4.9
			20	7.4	100	0.6	0.3	–	–	–	–
	1.3/100	pH 9	0.2	1.3	100	0.14	–	–	–	–	0.83
			0.2	2.4	100	0.18	–	–	–	–	3.5
	2.7/100	pH 9	0.2	0.16	100	0.14	–	–	–	–	0.6
		0.2 M Cys	20	0.14	100	0.37	–	–	–	–	0.27
		pH 6	0.2	0.17	100	0.14	–	–	–	–	0.35
		0.2 M Cys	20	0.21	100	0.35	–	–	–	–	–
	0.27/100	pH 9 0.2 M Cys	0.2	0.1	100	–	–	–	–	–	–

[a] $NaBH_4$ (0.5 mL) added to 1 mL sample solution. Final pH is given

[b] Relative signals are the integrated area of the TIC peaks. Relative signals <0.1 are not reported

$NaBH_4$ amount ratio, or acidity. It is interesting to note that the reaction of $Me_2AsO(OH)$ with metallic zinc in HCl generates the same volatile reaction products as with $NaBH_4$ (Table 3).

The addition of cysteine (R–SH) supressed the formation of unwanted by-products (Tables 1 and 2). In particular, it was rather effective for $Me_2AsO(OH)$ where the formation of Me_3As was completely eliminated (Table 2). It is well known that thiols reduce arsenic compounds to thiolates such as $As(SR)_3$, $MeAs(SR)_2$, and $Me_2As(SR)$ [19–22], which are quantitatively converted by $NaBH_4$ into the corresponding hydrides [23, 24]. Consequently, cold vapor generation by $NaBH_4$ in the presence of thiols presents an attractive way to estimate the purity of the methylarseno compounds.

Mechanism of volatile by-product formation: condensation reactions

The formation of volatile by-products is a result of the interaction between the reduction intermediates and the volatile arsanes. For example, pure Me_2AsH (prepared separately from $MeAsO(OH)_2/NaBH_4$ in the presence of cysteine), when injected into a vial containing aqueous $Me_2AsO(OH)$, does not result in the formation of Me_3As, nor diarsanes. According to the evidence collected herein, it can be assumed that the stepwise formation of arsanes proceeds through a series of intermediates, as summarized in reactions 1–4:

$$\mathbf{Me_2AsO(OH)} \rightarrow \mathbf{Me_2AsOH} \rightarrow \mathbf{Me_2AsH} \quad (1)$$

$$\mathbf{MeAsO(OH)_2} \rightarrow MeAs(OH)_2 \rightarrow MeAsH(OH) \rightarrow \mathbf{MeAsH_2} \quad (2)$$

$$\mathbf{AsO(OH)_3} \rightarrow As(OH)_3 \rightarrow AsH(OH)_2 \rightarrow AsH_2(OH) \rightarrow \mathbf{AsH_3} \quad (3)$$

$$\mathbf{As(OH)_3} \rightarrow AsH(OH)_2 \rightarrow AsH_2(OH) \rightarrow \mathbf{AsH_3} \quad (4)$$

Here, the reagents and all identified compounds are shown in bold. In each of the reaction sequences (1–4), arsenic becomes progressively less reactive toward the transfer of hydrogen from boron as a result of the decreasing number of oxygen atoms bound to it. The intermediates involved in the last hydrogen transfer step are, therefore, the least reactive toward the hydride attack in their relevant reaction sequences. Likewise, the reactivity toward the transfer of hydrogen from $NaBH_4$ is expected to decrease in the order $AsH_2(OH)<MeAsH(OH)<Me_2AsOH$.

Table 2 Volatile arsenic compounds detected during the reaction $Me_2AsO(OH)$ with $NaBH_4$

As/$NaBH_4$ (μmol/μmol)	Conditions[a]	Time (min)	Volatile arsenic species[b]								
			AsH_3	$MeAsH_2$	Me_2AsH	Me_3As	Me_3AsO	Me_2AsOH	Me_2AsCl	$As_2(O)Me_4$	As_2Me_4
0.27/100	pH 3	0.2	–	8.1	100	7.1	–	–	–	–	–
		20	–	15.1	6.9	100	–	–	–	–	–
0.13/100	pH 9	5	0.3	4.32	100	9.0	–	–	–	–	–
	pH 13	5	–	–	100	–	–	–	–	–	–
2.7/20	pH 3	4	0.1	0.1	1.5	100	–	0.2	2.1	0.13	0.2
		20	–	–	–	100	–	–	0.5	–	0.3
0.27/100	pH 9	0.2	–	4	100	2.9	–	–	–	–	0.9
		20	26	11	59	100	–	–	–	–	–
10.8/8	pH 2	0.2	–	1.3	–	100	0.7	1.1	0.9	5.6	5.0
		30	–	–	–	100	0.2	7.9	1.5	9.4	4.2
	pH 4	20	–	–	–	100	0.2	6.4	1.3	8.5	5.4
		20	–	–	16	100	0.6	2.2	0.9	9.8	7.0
0.27/100	pH 3	0.2	4	0.3	100	–	–	–	–	–	–
	0.2 M Cys	20	–	0.3	100	0.1	–	–	–	–	–
	pH 9	0.2	–	0.1	100	–	–	–	–	–	–
	0.2 M Cys	20	–	0.1	100	0.1	–	–	–	–	–
0.4/100	pH 9 0.2 M Cys	0.2	–	0.2	100	–	–	–	–	–	–

[a] $NaBH_4$ (0.05–0.5 mL) added to 1 mL sample solution. Final pH is given

[b] Relative signals are the integrated area of the TIC peaks. Relative signals <0.1 are not reported

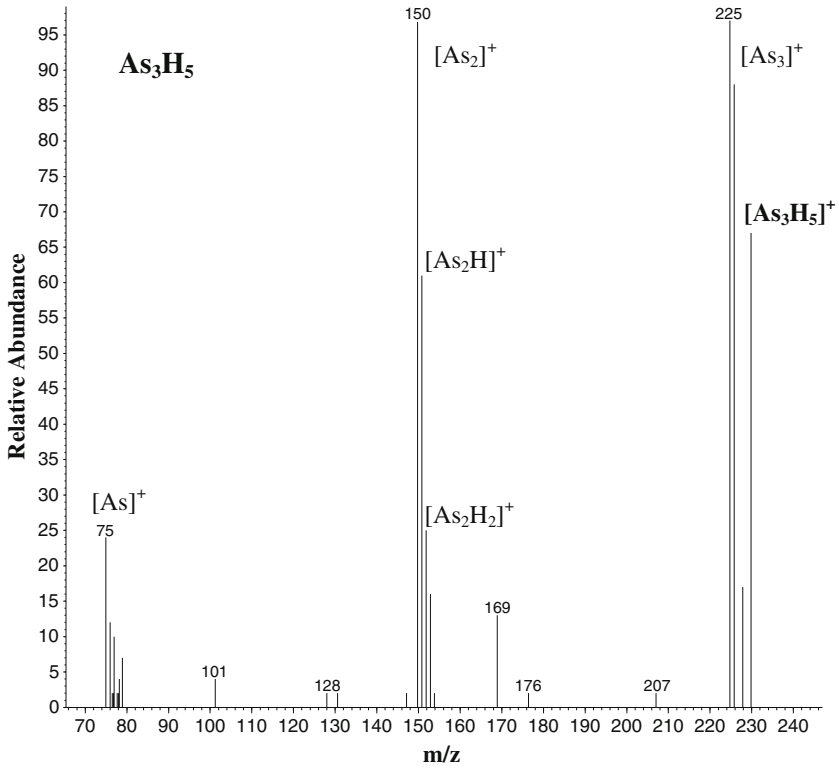

Fig. 5 EI mass spectrum of As_3H_5. Molecular ion at m/z=230 Da $[As_3H_5]^+$. Fragment ions: m/z 225 $[As_3]^+$; m/z 152 $[As_2H_2]^+$; m/z 151 $[As_2H]^+$; m/z 150 $[As_2]^+$; m/z 75 $[As]^+$

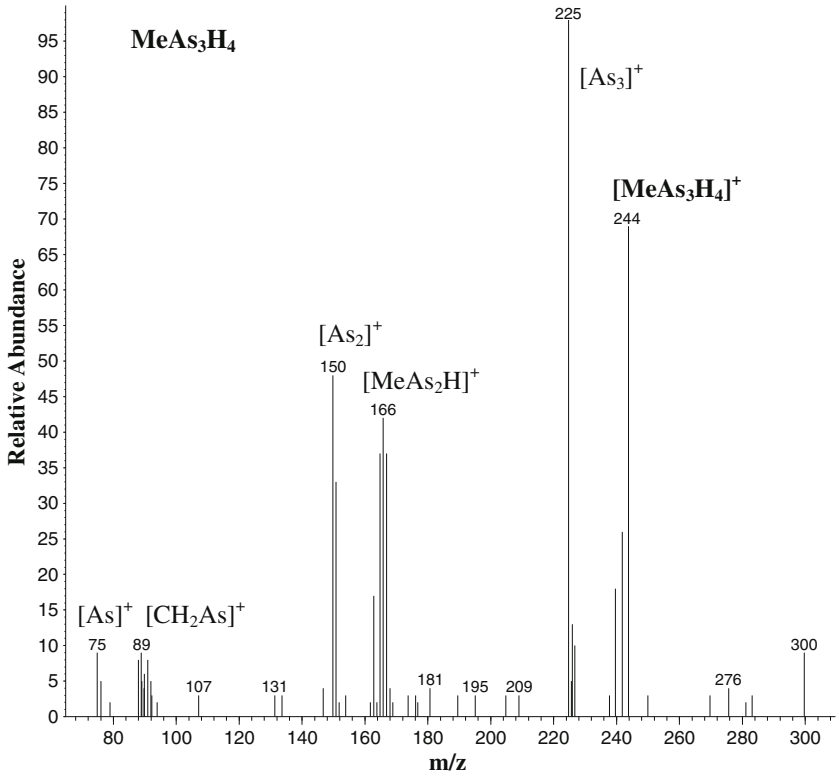

Fig. 6 EI mass spectrum of $MeAs_3H_4$. Molecular ion at m/z=244 Da $[MeAs_3H_4]^+$. Fragment ions: m/z 225 $[As_3]^+$; m/z 166 $[MeAs_2H]^+$; m/z 150 $[As_2]^+$; m/z 89 $[CH_2As]^+$; m/z 75 $[As]^+$

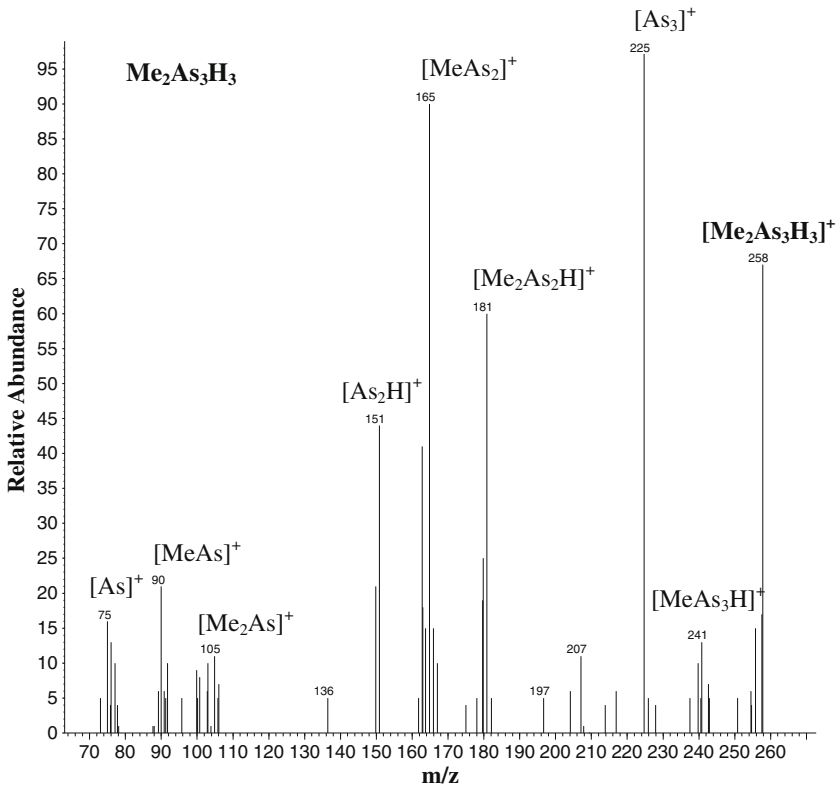

Fig. 7 EI mass spectrum of $Me_2As_3H_3$. Molecular ion at m/z=258 Da $[Me_2As_3H_3]^+$. Fragment ions: m/z 241 $[MeAs_3H]^+$; m/z 225 $[As_3]^+$; m/z 181 $[Me_2As_2H]^+$; m/z 165 $[MeAs_2]^+$; m/z 151 $[As_2H]^+$; m/z 105 $[Me_2As]^+$; m/z 90 $[MeAs]^+$; m/z 75 $[As]^+$

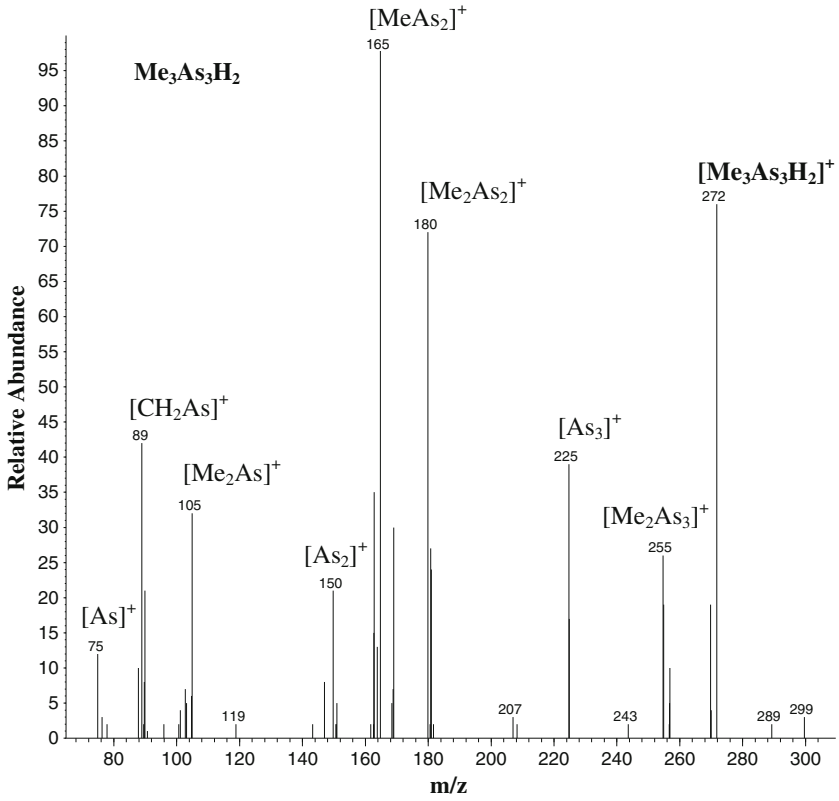

Fig. 8 EI mass spectrum of $Me_3As_3H_2$. Molecular ion at m/z=272 Da $[Me_3As_3H_2]^+$. Fragment ions: m/z 255 $[Me_2As_3]^+$; m/z 225 $[As_3]^+$; m/z 180 $[Me_2As_2]^+$; m/z 165 $[MeAs_2]^+$; m/z 150 $[As_2]^+$; m/z 105 $[Me_2As]^+$; m/z 89 $[CH_2As]^+$; m/z 75 $[As]^+$

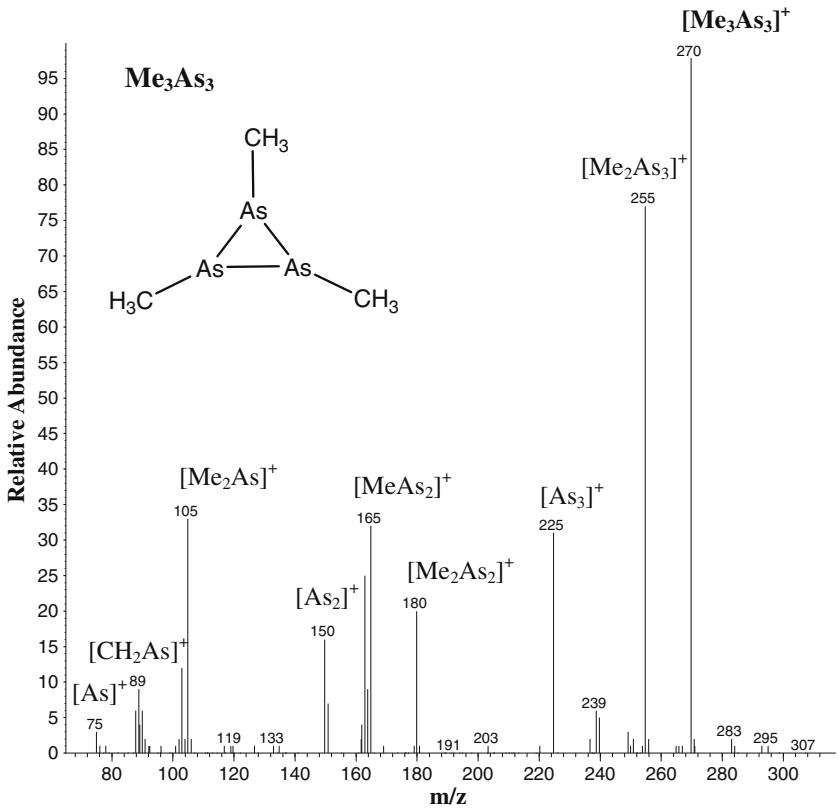

Fig. 9 EI mass spectrum of Me_3As_3. Molecular ion at *m/z*= 270 Da $[Me_3As_3]^+$. Fragment ions: *m/z* 255 $[Me_2As_3]^+$; *m/z* 225 $[As_3]^+$; *m/z* 180 $[Me_2As_2]^+$; *m/z* 165 $[MeAs_2]^+$; *m/z* 150 $[As_2]^+$; *m/z* 105 $[Me_2As]^+$; *m/z* 89 $[CH_2As]^+$; *m/z* 75 $[As]^+$

This is due to the replacement of the –OH groups by the methyl groups. The simultaneous presence of the reaction intermediates and the final hydrides leads to the formation of diarsanes via condensation reactions:

$$\mathbf{Me_2AsOH} + \mathbf{Me_2AsH} \rightleftarrows \mathbf{Me_2As{-}AsMe_2} + H_2O \quad (5)$$

$$MeAsH(OH) + \mathbf{MeAsH_2} \rightleftarrows \mathbf{MeHAs{-}AsHMe} + H_2O \quad (6)$$

$$AsH_2(OH) + \mathbf{AsH_3} \rightleftarrows \mathbf{H_2As{-}AsH_2} + H_2O \quad (7)$$

The bidirectional reaction 5 is also supported by Rheingold et al. [25] who reported that tetramethyl diarsane was formed in a reaction of Me_2AsH with Me_2AsX (X=Cl, Br, I, or CN) in benzene:

$$Me_2AsX + Me_2AsH \rightleftarrows Me_2As{-}AsMe_2 + HX \quad (8)$$

When aqueous As(III), $MeAsO(OH)_2$, or $Me_2AsO(OH)$, alone or in combination with each other, are treated with $NaBH_4$, all (six) possible structural isomers of diarsanes were detected in the headspace, i.e., $H_2As{-}AsH_2$, $MeHAs{-}AsH_2$, $Me_2As{-}AsH_2$, $MeHAs{-}AsHMe$, $Me_2As{-}AsHMe$, and $Me_2As{-}AsMe_2$, including the oxidation product ($Me_2As{-}As(O)Me_2$) of the latter and some triarsane species (Table 4). This clearly indicates that a condensation cascade took place among all possible intermediates which are

Table 3 Volatile arsenic compounds detected during $Me_2AsO(OH)$ reaction with metallic Zn powder

Conditions[a]	Time (min)	Volatile arsenic species[b]						
		AsH_3	$MeAsH_2$	Me_2AsH	Me_3As	Me_2AsOH	Me_2AsCl	As_2Me_4
1 M HCl	2	–	3.7	100	13.4	2.4	0.6	7.3
	25	3.9	3.5	100	38.5	0.1	–	0.4
0.1 M HCl	2	–	1.0	100	0.64	0.1	–	0.6
	25	12.5	5.4	76	100	–	–	0.3
	65	11.4	5.2	51	100	–	–	–

[a] $Me_2AsO(OH)$ (1.1 μmol) added into 1 mL sample solution reacted by 150 μmol zinc

[b] Relative signals are the integrated area of the TIC peaks. Relative signals <0.1 are not reported

Table 4 Volatile diarsanes and triarsanes detected in the headspace of reaction vials

As substrate	Arsanes[a]	t_R (min)[a]	Diarsanes	t_R (min)[b]	Triarsanes	t_R (min)[b]	Mass spectra
As(III)	AsH_3	1.35	$H_2As–AsH_2$	2.64	$H_2As–AsH–AsH_2$	9.08	Fig. 5
$MeAsO(OH)_2$	$MeAsH_2$	1.43	$MeHAs–AsH_2$	4.45	$Me_3As_3H_2$	11.60 (broad)	Fig. 8
			MeHAs–AsHMe	6.60	Me_3As_3	12.15	Fig. 9
			$Me_2As–AsHMe$	7.30			
$Me_2AsO(OH)$	Me_2AsH	1.65	$Me_2As–AsHMe$	7.30			
	Me_3As	1.84	Me_4As_2O	7.81			
			Me_4As-$AsMe_2$	8.06			
$MeAsO(OH)_2$ and As(III)	AsH_3	1.35	$H_2As–AsH_2$	2.64	$MeAs_3H_4$	9.40	Fig. 6
	Me_2AsH	1.65	$MeHAs–AsH_2$	4.45	$Me_2As_3H_3$	10.60	Fig. 7
			$Me_2As–AsH$	5.35			
			MeHAs–AsHMe	6.60			
$MeAsO(OH)_2$ and $Me_2AsO(OH)$	AsH_3	1.35	$Me_2As–AsH_2$	5.35	Me_3As_3	12.15	Fig. 9
	Me_2AsH	1.65	$Me_2As–AsHMe$	6.60			
	Me_3As	1.84	$Me_2As–AsMe_2$	8.06			

In all proofs, an acid solution (0.1 MHCl) containing the aforementioned As compounds (10 mM As content) was reduced by 0.2 M$NaBH_4$ in 0.1 MNaOH. A final pH 3–4 was measured

[a] The retention times of some detected mono-arsanes are given for comparison with the retention times of diarsanes and triarsanes. Other detected monoarsanes are reported in Table 2

[b] Retention times obtained with DB-5 column. See "Instrumentation" for details

formed in the reaction pathways of different arsenic substrates, including the final hydrides. The interaction between the proposed reaction intermediates is also confirmed in experiments where As(III) was reduced in the presence of Sb(III). In this case, the formation of the dimer $H_2As–SbH_2$ was observed (Fig. 10). The stibodiarsane could be formed only by the reaction of AsH_3 with SbH_2OH or AsH_2OH with SbH_3.

The formation of diarsanes and triarsanes also provides an explanation for the formation of precipitates in the case

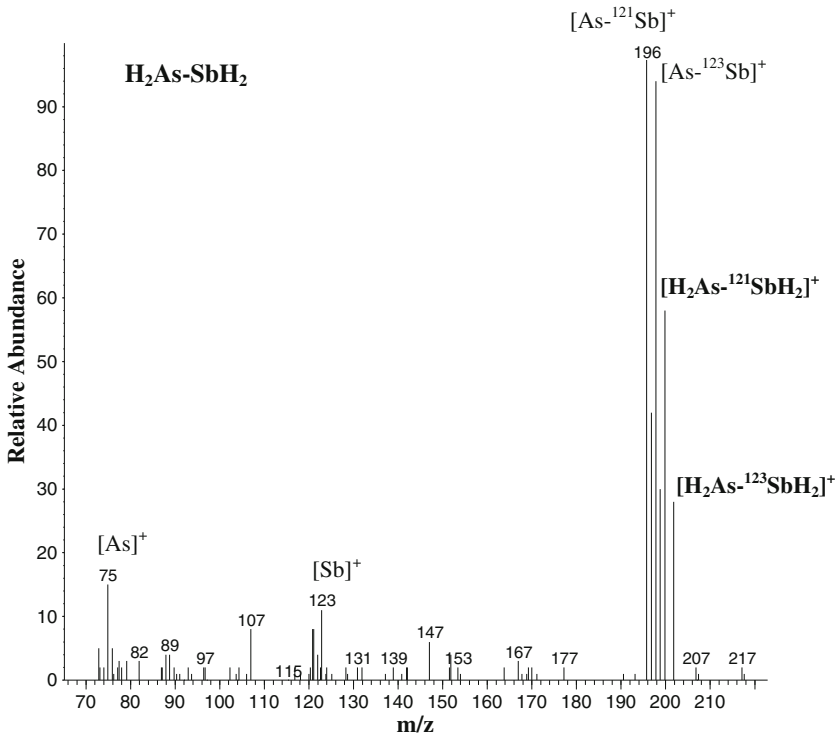

Fig. 10 EI mass spectrum of $H_2As–SbH_2$. Molecular ion at *m/z*=202 Da $[H_2{}^{75}As–{}^{123}SbH_2]^+$ and 200 Da $[H_2{}^{75}As–{}^{121}SbH_2]^+$. Fragment ions: *m/z* 198 $[{}^{75}As–{}^{123}Sb]^+$ and *m/z* 196 $[{}^{75}As–{}^{121}Sb]^+$

of As(III), As(V), and $MeAsO(OH)_2$. When mono-arsenic species contain either only one –H or –OH moiety, the condensation cascade terminates with the formation of a dimer (see reactions 5–7). Triarsanes, on the other hand, can be formed by condensation reactions of the following type:

$$H–(AsX)_2–OH + H–(AsX_2) \rightarrow \quad (9)$$

$$H–(AsX)_2–AsX_2 + H_2O \qquad (X = Me, H)$$

In cases when the reaction intermediates contain arsenic bound to hydride and the hydroxo groups (H–AsX–OH, X=Me, H, or OH), the condensation reaction may proceed to the formation of linear or branched polymers,

$$2nH–(AsX)–OH \rightarrow H–(XAs–AsX)_n–OH + 2(n-1)H_2O \quad (10)$$

or cyclic As species,

$$nH–(AsX)–OH \rightarrow (AsX)_n + n\ H_2O, \quad (11)$$

which remain in the solid phase.

The reaction schemes presented above are in agreement with observations reported elsewhere. Under conditions typically employed in analytical protocols for trace analysis, the main reaction products are the simple volatile arsanes (reactions 1–4). Approaching conditions for synthesis reactions, however, the occurrence of condensation reactions becomes more pronounced, which leads to the formation of non-volatile arsenic species that remain in the reaction solution in either soluble or insoluble form. For example, reddish solid arsenic hydrides, arising from the chemical reduction of inorganic As(III) in aqueous solution, are reported by Jolly et al. [26]. In the case of $MeAsO(OH)_2$, its reduction with H_3PO_2 resulted in the formation of linear or cyclic methyl polyarsanes [27, 28]. Under similar conditions, the reduction of $Me_2AsO(OH)$ with H_3PO_2 yields the water-soluble $Me_2As–AsMe_2$ [27]. The fully methylated diarsane cannot react further with other arsenic intermediates from reaction 1 and therefore is the terminus of the condensation cascade.

Formation of trimethylarsane

The observation that trimethylarsane, and not dimethylarsane, is the main volatile product of reduction of $Me_2AsO(OH)$ under non-analytical reaction conditions is puzzling. It appears, from the results reported in Table 2, that the formation of Me_3As coincides with the disappearence of Me_2AsH. This indicates that Me_3As is formed by the interaction of Me_2AsH with an arsenic intermediate capable of acting as a methylation agent. The presence of such species was confirmed in the reaction of $Me_2AsO(OH)$ and $NaBH_4$ in the presence of Sb(III). The formation of $MeSbH_2$ was confirmed. The formation of Me_3As during the reduction of $Me_2AsO(OH)$ by $NaBH_4$ is likely due to the known intermediate $Me_2As–AsMe_2$. Tetramethyl diarsane is also able to form Me_2AsH from $MeAsH_2$ [29]. As described above, the formation of diarsanes is supressed when the $NaBH_4$ reduction is performed in the presence of thiols. When this is conducted with the $Me_2AsO(OH)$/$NaBH_4$ reaction, Me_3As is not formed (Table 2).

Methyl transfer reactions take place also in the case of elevated concentrations of $MeAsO(OH)_2$, as is evident from the results reported in Table 1 (formation of AsH_3 and Me_2AsH) and in Table 4 (the formation of $MeHAs–AsH_2$ and $MeHAs–AsMe_2$ cannot be explained only by condensation reactions). The effects produced by methyl transfer reactions during the reaction of $MeAsO(OH)_2$ with $NaBH_4$/HCl are much less pronounced than those observed for $Me_2AsO(OH)$, and the main volatile product is still the expected $MeAsH_2$ (>92%).

Conclusions

The mechanism for the reaction of arsenates—$As(OH)_3$, $AsO(OH)_3$, $MeAsO(OH)_2$, $Me_2AsO(OH)$—with aqueous tetrahydroborate(III) has been proposed. It applies to a wide range of reaction conditions employed both in trace analysis and synthesis. Under analytical conditions, the action of $NaBH_4$ on the arsenic substrate promotes their conversion to the corresponding volatile hydrides AsH_3, $MeAsH_2$, and Me_2AsH. This process is the consequence of the direct stepwise hydrogen transfer from tetrahydroborate (III) to arsenic. The formation of volatile hydrides passes through arseno-intermediates wherein the –OH groups are sequentially replaced by hydrogen atoms. Under non-analytical (synthesis) conditions, reduction by $NaBH_4$ competes with two other processes: condensation between As–H and HO–As and the transfer of methyl group. The first effect arises from the condensation of intermediates and causes the formation of As–As bonds. Consequently, volatile diarsanes and triarsanes are formed along with a reddish precipitate of polymeric arsanes. The transfer of a methyl group between the reaction products and intermediates is peculiar to the reduction of $Me_2AsO(OH)$ with $NaBH_4$. Here, the identification of Me_3As as the main volatile reduction product is evidence that transfer of a methyl group has occurred. The likely alkylating agent seems to be the condensation cascade product, As_2Me_4, which has been detected in the headspace of the reaction medium.

The detected cross-reactions among intermediates belonging to different reaction pathways of the different arsenic compounds and arsenic and antimony compounds make the proposed reaction model also interesting for the

interpretation and the comprehension of interference mechanisms in CGVS.

References

1. Sturgeon RE, Mester Z (2002) Appl Spectrosc 56:202A–213A
2. Dědina J, Tsalev DL (1995) Hydride generation atomic absorption spectroscopy. Wiley, Chichester
3. D'Ulivo A, Loreti V, Onor M, Pitzalis E, Zamboni R (2003) Anal Chem 75:2591–2600
4. D'Ulivo A (2010) Spectrochim Acta Part B 65:360–375
5. D'Ulivo A, Dědina J, Mester Z, Sturgeon RE, Wang Q, Welz B (2011) Pure Appl Chem 83:1283–1340
6. D'Ulivo A, Mester Z, Sturgeon RE (2005) Spectrochim Acta Part B 60:423–438
7. D'Ulivo A, Mester Z, Meija J, Sturgeon RE (2007) Anal Chem 79:3008–3015
8. D'Ulivo A (2004) Spectrochim Acta Part B 59:793–825
9. D'Ulivo A, Baiocchi C, Pitzalis E, Onor M, Zamboni R (2004) Spectrochim Acta Part B 59:471–486
10. Petrick K, Krivan V (1987) Fresenius Z Anal Chem 327:338–342
11. D'Ulivo A, Marcucci K, Bramanti E, Lampugnani L, Zamboni R (2000) Spectrochim Acta, Part B 55:1325–1336
12. D'Ulivo A, Battistini SST, Pitzalis E, Zamboni R, Mester Z, Sturgeon RE (2007) Anal Bional Chem 388:783–791
13. Köster J, Diaz-Bone RA, Planer-Friederich B, Rothweiler B, Hirner H (2003) J Mol Structure 661–662:347–346
14. Meija J, Mester Z, D'Ulivo A (2007) J Am Soc Mass Spectrom 18:337–345
15. Pitzalis E, Ajala D, Onor M, Zamboni R, D'Ulivo A (2007) Anal Chem 79:6324–6333
16. Meija J, Mester Z, D'Ulivo A (2006) J Am Soc Mass Spectrom 17:1028–1036
17. D'Ulivo A, Mester Z, Meija J, Sturgeon RE (2006) Spectrochim Acta Part B 61:778–787
18. Pergantis SA, Winnik W, Eimar WR, Cullen WR (1997) Talanta 44:1941–1947
19. Raab A, Meherag AA, Jaspars M, Genney DR, Feldmann J (2004) J Anal At Spectrom 19:183–190
20. Rey NA, Howarth OW, Pereira-Maia ECJ (2004) Inorg Biochem 98:1151–1159
21. Scott N, Hatlelid KM, MacKenzie NE, Carter DE (1993) Chem Res Toxicol 6:102–106
22. Spuches AM, Kruszyma HG, Rich AM, Wilcox DE (2005) Inorg Chem 44:2964–2972
23. Le X-C, Cullen WR, Reimer KJ (1994) Anal Chim Acta 285:277–285
24. Tsalev DL, Sperling M, Welz B (2000) Talanta 51:1059–1068
25. Rheingold AL, Pleau EJ, Ferrar WT (1977) Inorg Chim Acta 22:215–218
26. Jolly WL, Anderson LB, Beltrami RT (1957) J Am Chem Soc 79:2443–2447
27. Knoll F, Marsmann HC, Van Wazer JR (1969) J Am Chem Soc 91:4986–4989
28. Waser J, Schoemaker V (1945) J Am Chem Soc 67:2014–2018
29. Gupta VK, Krannich LK, Watkins L (1987) Inorg Chim Acta 132:163–164

Annex IV

Pagliano, E. (ca); Meija, J.; Sturgeon R.E.; Mester, Z.; D'Ulivo, A.

Negative chemical ionization GC/MS determination of nitrite and nitrate in seawater using exact matching double spike isotope dilution and derivatization with triethyloxonium tetrafluoroborate

Anal. Chem. **2012**, *84*, 2592-2596

Copyright 2012 American Chemical Society

analytical chemistry

Technical Note

pubs.acs.org/ac

Negative Chemical Ionization GC/MS Determination of Nitrite and Nitrate in Seawater Using Exact Matching Double Spike Isotope Dilution and Derivatization with Triethyloxonium Tetrafluoroborate

Enea Pagliano,*[,†,‡] Juris Meija,[‡] Ralph E. Sturgeon,[‡] Zoltan Mester,[‡] and Alessandro D'Ulivo[§]

[†]Scuola Normale Superiore, Piazza dei Cavalieri, 7, 56126, Pisa, Italy

[‡]National Research Council of Canada, 1200 Montreal Road, Ottawa, ON K1A 0R6, Canada

[§]CNR, Consiglio Nazionale delle Ricerche, Istituto di Chimica dei Composti Organometallici, Via G. Moruzzi, 1, 56124 Pisa, Italy

ABSTRACT: The alkylation of nitrite and nitrate by triethyloxonium tetrafluoroborate allows determination of their ethyl esters by headspace gas chromatography/mass spectrometry (GC/MS). In the present study, significant improvement in analytical performance is achieved using negative chemical ionization providing detection limits of 150 ng/L for NO_2^- and 600 ng/L for NO_3^-, an order of magnitude better than those achieved using electron impact ionization. The derivatization procedure was optimized and alkaline conditions adopted to minimize conversion of nitrite to nitrate (determined to be 0.07% at 100 mg/L NO_2^-) and to avoid the exchange of oxygen between the analytes and the solvent (water). Quantitation entails use of isotopically enriched standards ($N^{18}O_2^-$ and $^{15}NO_3^-$), which also permits monitoring of potential conversion from nitrite to nitrate during the analysis (double spike isotope dilution).

The determination of nitrite and nitrate in samples of different origin is a challenge to analytical chemistry, and it is important from environmental and biological perspectives.[1] Moorcroft et al.[1] reviewed strategies for detection of these analytes, discussing advantages and limitations of the various methodologies. Jobgen et al.[2] focused their analysis on the determination of nitrite and nitrate in biological samples using high-pressure liquid chromatography (HPLC), whereas Helmke et al.[3] discussed the application of gas chromatography/mass spectrometry (GC/MS). In general, methods which entail the use of molecular spectroscopy or electrochemical detection have limited sensitivity and selectivity and suffer from matrix effects. Furthermore, there are more methods for the direct detection of nitrite than nitrate, and in many analytical protocols the determination of nitrate is achieved following a critical reduction to nitrite, usually by cadmium.[4] Nitrite and nitrate are nonvolatile anions, and their determination by GC/MS can be achieved by derivatization in order to generate volatile species, for example, nitration of aromatic compounds has been used for this purpose.[3] This approach, however, does not work for nitrite and requires the use of strong acid conditions which may be critical if any nitrite is present because of its possible conversion to nitrate.[5,6] Another technique used with GC/MS entails alkylation with pentafluorobenzyl bromide (F_5BzBr)[7] to convert nitrite and nitrate to $F_5Bz–NO_2$ and $F_5Bz–ONO_2$, respectively. The pentafluorobenzyl derivatives are suitable for negative chemical ionization (CI−) GC/MS, but they are not employed for static headspace analysis at room temperature due to their low volatility. Despite the availability of low detection limits (sub-fmol, absolute) and the possibility of simultaneous determination of both analytes, the derivatization method requires organic solvents (acetone and toluene) and the subsequent injection of the organic extract which may contain sample matrix and the unreacted F_5BzBr. The use of reverse phase liquid chromatography coupled with electrospray ionization mass spectrometry has recently been used for the determination of nitrite and nitrate in water with detection limits of 1 and 12 μg N L^{-1} for nitrate and nitrite, respectively.[8]

Alkylation of anions with triethyloxonium tetrafluoroborate has been proposed only recently[9,10] despite the well-established chemistry of $Et_3O^+[BF_4^-]$.[11,12] From a practical point of view, the use of triethyloxonium offers several advantages which make this analytical technique unique: (i) alkylation can be performed in an aqueous medium; and (ii) alkylation entails the chemical vapor generation of simple inorganic anions (Cl^-, Br^-, I^-, CN^-, SCN^-, S^{2-}, NO_3^-, NO_2^-) to their volatile derivatives, potentially permitting headspace and solid phase microextraction (SPME) sampling with GC/MS detection. In general, the application of chemical vapor generation is always advantageous because it is a separation technique which eliminates the introduction of sample matrix to the instrument, thereby minimizing contamination of the device and reducing background levels.[13]

Received: November 11, 2011
Accepted: February 9, 2012
Published: February 9, 2012

ACS Publications © 2012 American Chemical Society

An isotope dilution method based on alkylation by triethyloxonium for simultaneous determination of nitrite and nitrate by electron ionization (EI) GC/MS has recently been discussed by the authors.[10] The drawbacks of the previous procedure are related to poor detection limits and the potential conversion of nitrite to nitrate during the analysis due to acid hydrolysis of the reactant. Here, we propose an improved method which eliminates the above-mentioned drawbacks: pretreatment of the sample with ammonium hydroxide maintains an alkaline pH during alkylation, avoiding the problem of conversion of nitrite to nitrate, and CI− provides enhanced detection limits for both analytes.

EXPERIMENTAL SECTION

Reagents and Materials. Isotopically labeled nitrate ($K^{15}NO_3$, $x(^{15}N)$ = 0.99 mol/mol; $KN^{18}O_3$, $x(^{18}O)$ = 0.75(5) mol/mol) were obtained from Cambridge Isotope Laboratories (Cambridge MA). Aqueous solutions of these salts were prepared by dissolution in ultrapure water. Triethyloxonium tetrafluoroborate, $Et_3O^+[BF_4^-]$, (Fluka; w > 0.97 g/g) alkylating solution was prepared by dissolving x g of the solid salt in 1.5x g of ultrapure water. Since aqueous triethyloxonium salts undergo hydrolysis, the solution was prepared prior to sample derivatization. $Et_3O^+[BF_4^-]$ must be handled in a fume hood, prolonged contact with moist air should be avoided, and unused reagent should be kept in a freezer.

Standard solutions of nitrite and nitrate were prepared by dissolution/dilution of $NaNO_2$ (Aldrich; w = 0.999 99 g/g) and Nitrate Anion Standard Solution (SRM 3185, NIST) with ultrapure water. All solutions were stored at 4 °C temperature. A NH_4OH solution (Tamapure AA-100; $w(NH_3)$ = 0.2 g/g) was employed.

Preparation of $KN^{18}O_2$. The ^{18}O-labeled nitrite was prepared from a 15 mM aqueous solution of potassium (^{18}O)nitrate. To reduce nitrate to nitrite, a copper−cadmium reductor column was used through which 2 mL of nitrate solution were passed using a peristaltic pump. The effluent was collected in a vial and stored overnight in the presence of 0.5 g of Cu−Cd grains. After separation of the metal, the solution was diluted to 150 mL with NaOH (pH = 10) and used for isotope dilution experiments (150−200 μM $KN^{18}O_2$, $x(^{18}O)$ = 0.75(5) mol/mol in aqueous NaOH at pH = 10). The completeness of the nitrite/nitrate conversion was verified by GC/MS using the method described herein.

GC/MS Methods. After derivatization to the corresponding ethyl ester, nitrite and nitrate were separated and detected by GC/MS using a Hewlett-Packard 6890 gas chromatograph equipped with a Hewlett-Packard 5973 mass detector. The operating conditions are summarized in Table 1. A manual injection of 250 μL of sample vial headspace taken with a gastight syringe was performed for subsequent quantitation by CI−. Selected ion monitoring (SIM) mode was employed: m/z = 45, 47, 63, and 65 Da for Et−ONO and m/z = 46, 47, 48, and 50 Da for Et−ONO_2 (100 ms dwell time used for each ion).

Sample Preparation. A 2 mL volume of sample was introduced without any pretreatment into a 4 mL vial and spiked with 200 μL of (^{18}O)nitrite and 50 μL of 864 μM (^{15}N)nitrate. The amount of spike was chosen to provide an exact (1:1) match to the concentration of these analytes in a MOOS-2 sample for signals m/z = 45, 47 (nitrite) and m/z = 46, 47 (nitrate). After addition of 50 μL of NH_4OH solution ($w(NH_3)$ = 0.2 g/g), the sample was derivatized by adding 100 μL of triethyloxonium tetrafluoroborate solution. The vial was then sealed with a screw cap PTFE/silicone septum and kept in the dark at room temperature for at least 30 min. Headspace analysis was then performed by GC/MS.

Table 1. GC/MS Operating Conditions

Gas Chromatography		
column	model	J&W 122-1364 DB-624
	length	60 m
	mode	constant flow (1 mL He/min)
inlet	mode	pulsed split
	temperature	120 °C
	split ratio	8:1
	pulsed pressure	172 kPa (25.0 psi) for 0.5 min
oven	isotherm	30 °C for 10 min
	ramp	20 °C/min to 140 °C
	isotherm	140 °C for 1.5 min
	run time	17 min

Mass Spectrometry	CI+	CI−
reaction gas	CH_4	CH_4
transfer line temperature	250 °C	250 °C
emission current	237.3 μA	49.4 μA
electron energy	151.5 eV	114.4 eV
ion source temperature	250 °C	150 °C
quadrupole temperature	150 °C	106 °C
EMV	1388 V	2000 V

RESULTS AND DISCUSSION

Chemical Ionization Mass Spectra. Triethyloxonium tetrafluoroborate can convert nitrite and nitrate to their ethyl esters through an O-alkylation of both analytes. The characterization and the EI mass spectra of these derivatives have been discussed earlier.[10] Both Et−ONO and Et−ONO_2 undergo chemical ionization by methane in positive (CI+) and negative (CI−) mode. In CI+ mass spectra, the molecular ion appears as the most intense for both analytes. However, because of poor sensitivity, the CI− mode was employed.

CI− mass spectra of nitrite and nitrate derivatives are reported in Figure 1. Ethyl nitrite (Figure 1a) shows ions $CH_2{=}CHO^-$ (m/z = 43 Da), $CH_3{-}CH_2O^-$ (m/z = 45 Da), and $CH_3{-}CH_2O^-{\cdot}H_2O$ (m/z = 63 Da). The latter is due to the formation of a H_2O-adduct with the $CH_3{-}CH_2O^-$ (during the experiment, the recommended cartridge for moisture retention in the reagent gas was not used). The mass spectrum of ethyl (^{18}O)nitrite is reported in Figure 1c, and the notable shifts from m/z 43 to 45 and from 45 to 47 are the consequence of the oxygen-18 substitution. Since the CI− mass spectrum of ethyl nitrite does not show any nitrogen-containing fragments, nitrogen labeling is not suitable for nitrite. Ethyl nitrate (Figure 1b) shows ions NO_2^- (m/z = 46 Da) and $CH_2{=}CHO^-$ (m/z = 43 Da). The ^{15}N-labeled compound (Figure 1d) exhibits $^{15}NO_2^-$ (m/z = 47 Da) as the most abundant fragment. For isotope dilution quantitation purposes, the signal ratios 45/47 and 46/47 were used for nitrite and nitrate, respectively.

Double Spike Isotope Dilution and Analyte Interconversion. Despite the numerous methods proposed for the simultaneous determination of nitrite and nitrate, the possibility of their interconversion is seldom considered.[14,15] As discussed previously,[10] during the derivatization with triethyloxonium, no conversion of nitrate to nitrite occurs even at a high nitrate concentration; however, oxidation of nitrite occurs (<10%). In this work, attention has been given to minimize the conversion

dx.doi.org/10.1021/ac2030128 | Anal. Chem. 2012, 84, 2592−2596

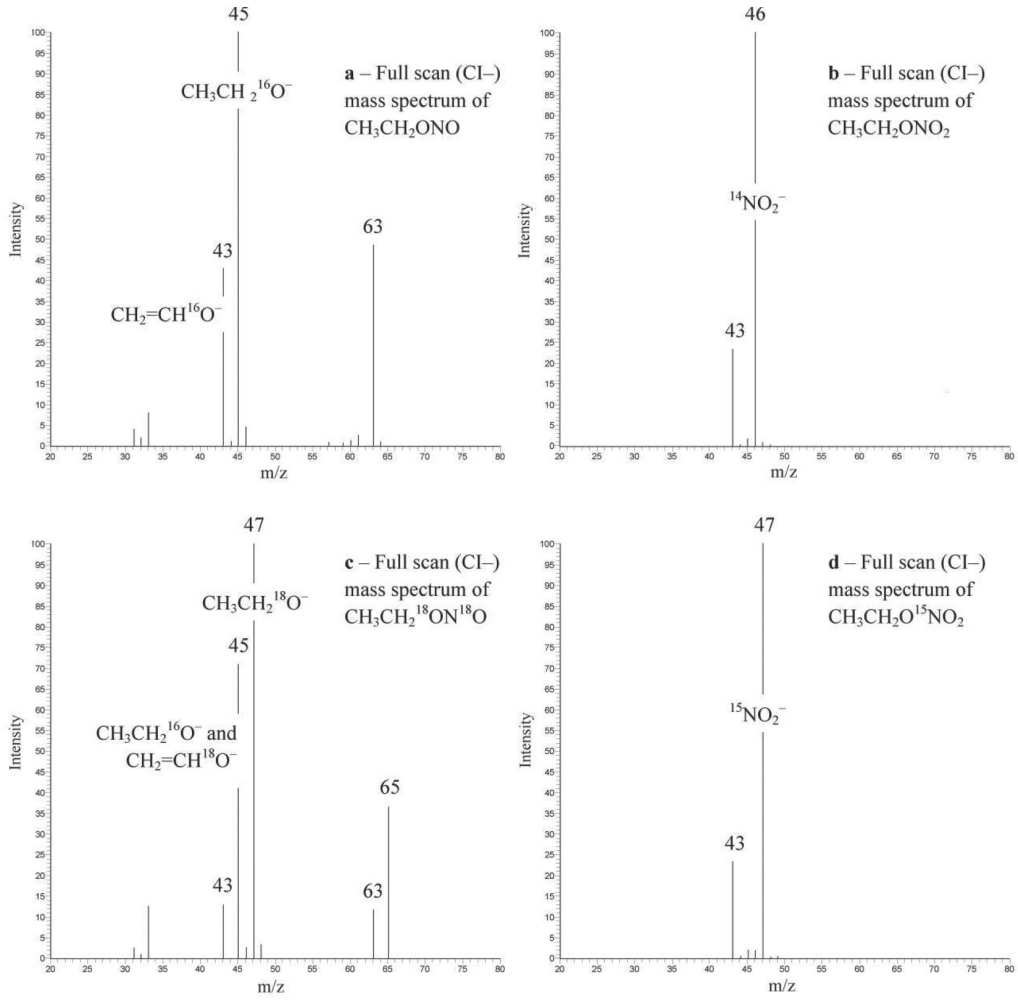

Figure 1. Negative chemical ionization mass spectra (a) ethyl nitrite: $CH_2{=}CH^{16}O^-$ (m/z = 43 Da), $CH_3{-}CH_2{}^{16}O^-$ (m/z = 45 Da), and $CH_3{-}CH_2{}^{16}O^-{\cdot}H_2O$ (m/z = 63 Da). (b) Ethyl nitrate: $CH_2{=}CH^{16}O^-$ (m/z = 43 Da), $^{14}NO_2^-$ (m/z = 46 Da). (c) Ethyl (^{18}O)nitrite: $CH_2{=}CH^{16}O^-$ (m/z = 43 Da), $CH_3{-}CH_2{}^{16}O^-$ and $CH_2{=}CH^{18}O^-$ (m/z = 45 Da), $CH_3{-}CH_2{}^{18}O^-$ (m/z = 47 Da), $CH_3{-}CH_2{}^{16}O^-{\cdot}H_2O$ (m/z = 63 Da), and $CH_3{-}CH_2{}^{18}O^-{\cdot}H_2O$ (m/z = 65 Da). (d) Ethyl (^{15}N)nitrate: $CH_3{=}CH_2{}^{16}O^-$ (m/z = 43 Da) and $^{15}NO_2^-$ (m/z = 47 Da).

of nitrite to nitrate. This conversion is likely a consequence of the acid hydrolysis of the alkylating agent which promotes the formation of nitrous acid from the nitrite ion. The reaction of the nitrous acid with dissolved oxygen results in the production of nitrate.[5,6] In order to avoid this effect, alkylation was conducted in an alkaline medium (pH = 10) promoted by the pretreatment of the samples with NH_4OH solution. In this alkaline environment, significant oxidation of nitrite only occurred at high concentrations of nitrite. At 100 mg/L of nitrite, only 0.07% of the nitrite ions converted to nitrate and no conversion was detected below this mass fraction.

Despite these improvements, constant monitoring of potential interconversion is necessary to ensure a valid analytical procedure. This could be achieved by the use of double spiking isotope dilution.[16,17] In this case, by spiking the sample with (^{18}O)nitrite and (^{15}N)nitrate, it is possible to correct for the conversion from nitrite to nitrate by monitoring signals at m/z 48 and 50 in the mass spectrum of the ethyl nitrate. Conversion of $N^{18}O_2^-$ into nitrate (with O_2) yields $N^{18}O_2{}^{16}O^-$, whose CI− spectrum features ions $N^{18}O_2^-$ (m/z = 50) and $N^{18}O^{16}O^-$ (m/z = 48).

Oxygen Scrambling. When an isotopically enriched standard is used for quantitation, it is crucial that any scrambling which can alter the isotope pattern of the enriched spike be avoided. From evidence reported by Klein et al.[18] for nitrate and from the experimental results obtained herein, oxygen exchange/scrambling between nitrite, nitrate, and water may occur. However, no oxygen scrambling occurs in alkaline or neutral conditions for either nitrite or nitrate. Hence, the working pH was chosen to be in the alkaline region (pH = 10) to enable the use of (^{18}O)nitrite for isotope dilution analysis. At pH = 10, the mass spectrum arising from the (^{18}O)nitrite was constant during the time of the analysis.

Analysis of MOOS-2 CRM. Figure 2 shows the CI− GC/MS chromatogram obtained for the analysis of nitrite and nitrate in seawater (MOOS-2 CRM). An exact-matching isotope dilution technique was utilized.[19] Results for 14 independent measurements of MOOS-2 are reported in Table 2 and achieved by the use of the following equation:

$$c_A = c_A^0 \frac{R_2 - R_N}{R_2 - R_E} \frac{R_1 - R_E}{R_1 - R_N} \quad (1)$$

dx.doi.org/10.1021/ac2030128 | Anal. Chem. 2012, 84, 2592−2596

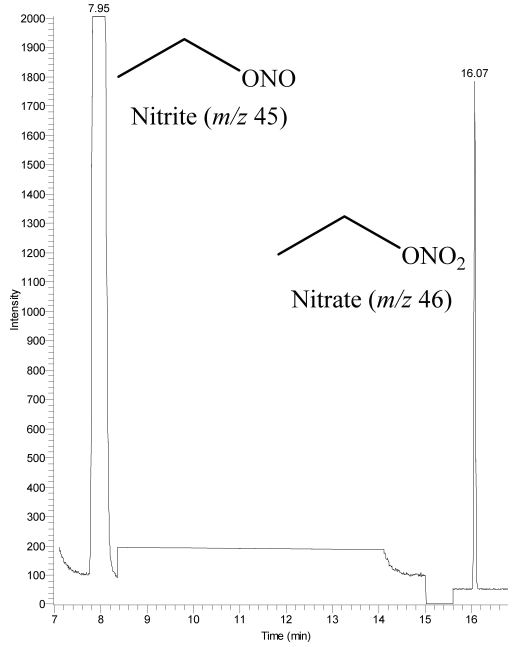

Figure 2. HS CI− GC/MS chromatogram (SIM mode) of MOOS-2 CRM with $c(NO_2^-)$ = 3.4 μM and $c(NO_3^-)$ = 22 μM. Nitrite ion in the form of CH_3CH_2−ONO elutes at 7.95 min (m/z = 45 Da); and nitrate ion in the form of CH_3CH_2−ONO_2 elutes at 16.07 min (m/z = 46 Da).

where c_A is the concentration of the analyte in the sample, c_A^0 is the concentration of the reference analyte (primary standard); R_1 and R_2 are the isotope amount ratios (m/z 45/47 for nitrite and 46/47 for nitrate) arising from the spiked blend of the sample (MOOS-2) and of the spiked blend of the reference, respectively; R_N and R_E are the isotope amount ratios for the sample and the enriched spike, respectively. The isotope patterns of the analyte and the primary standard are identical. Note that there is no need for mass bias correction since all four isotope amount ratios R_1, R_2, R_E, and R_N in eq 1 can be substituted with the corresponding measured isotope ratios r_1, r_2, r_E, and r_N. The above equation is equivalent to that reported in 1994 by Henrion.[19] Formally, the concentration of the analyte is written as a function of the concentration of a primary standard (eq 1) and measured isotope amount ratios. In order to minimize the instrumental measurement biases, both the sample and the reference were spiked with the same amount of enriched analyte in order to obtain matching amount ratios $R_1 = R_2 = 1$. To realize this, the concentration of the primary standard has to be the same as that of the analyte in the sample. When $R_1 = R_2 = 1$, eq 1 reduces to $c_A = c_A^0$, which permits significant reduction in the systematic errors arising from measurements. In addition, prior knowledge of the isotope patterns of the spike and analyte is not necessary.[19] From a practical point of view, an initial estimate of the analyte concentration in the sample can be obtained by use of an external calibration method. Subsequently, a primary standard solution is prepared at the same concentration as the analyte in the sample. Table 2 summarizes results for the measurements on MOOS-2 obtained by exact matching. For each measurement, the values of r_1 and r_2 and the concentration of the reference c_A^0 are presented. The concentration of nitrite and nitrate found, $c(NO_2^-)$ = 3.37 ± 0.08 μM and $c(NO_3^-)$ = 22.0 ± 0.2 μM, are in good agreement with the certified property values, $c(NO_2^-)$ = 3.31 ± 0.18 μM and $c(NO_2^-) + c(NO_3^-)$ = 24.9 ± 1.0 μM, and exhibit good precision for both nitrite and nitrate. Instrumental detection limits obtained from the standard solutions of the analytes in water are 150 ng/L for nitrite and 600 ng/L for nitrate. The estimation of the detection limits is based on the signal-to-noise ratio calculated from the standard deviation of the baseline (i.e., detection limit is the concentration which produce a signal-to-noise ratio of 3).

Table 2. Exact Matching Isotope Dilution Determination of Nitrite and Nitrate in MOOS-2[a]

nitrite				nitrate			
r_1	r_2	c_A^0/μM	$c_{A,\ MOOS\text{-}2}$/μM	r_1	r_2	c_A^0/μM	$c_{A,\ MOOS\text{-}2}$/μM
0.9356			3.31	1.030			22.1
0.9543			3.48	1.028			22.1
0.9325	0.9371	3.32	3.28	1.035	1.007	21.6	22.3
0.9477			3.42	1.025			22.0
0.9255			3.22	1.022			22.0
1.086			3.48	1.003			21.7
1.073			3.38	1.022			22.1
1.068	1.064	3.32	3.35	1.029	0.9993	21.6	22.3
1.086			3.48	1.017			22.0
1.066			3.34	1.016			22.0
0.9565			3.41	1.021			21.9
0.9415	0.9596	3.43	3.29	1.021	1.027	22.0	21.9
0.9450			3.32	1.025			22.0
0.9606			3.44	1.028			22.0
		mean	3.37			mean	22.0
		u	0.08			u	0.2
		u_r	2.5%			u_r	0.7%

[a]Certified property values: $c(NO_2^-)$ = 3.31 ± 0.18 μM and $c(NO_2^-) + c(NO_3^-)$ = 24.9 ± 1.0 μM.

dx.doi.org/10.1021/ac2030128 | Anal. Chem. 2012, 84, 2592−2596

Standard solutions of 10 μg/L NO_2^- and 50 μg/L NO_3^- produce signal-to-noise ratios of 211 and 327, respectively.

With the present procedure, only 250 μL of headspace was used for analysis (vs 2 mL of headspace available). In order to further enhance the limits of detection, a purge-and-trap procedure operating above ambient temperature should prove beneficial.

CONCLUSIONS

GC/MS analytical methodology for the determination of nitrite and nitrate by their derivatization to corresponding ethyl esters[10] has been improved in terms of sensitivity and accuracy. Pretreatment of the sample with ammonium hydroxide to ensure alkaline conditions during the alkylation is crucial to avoid conversion of nitrite to nitrate, and negative chemical ionization allows detection limits to be improved by at least 1 order of magnitude. The vapor generation methodology proposed here is based on exact matching isotope dilution and is suitable for measurement with high precision and accuracy. This method achieves a transparent traceability and is promising for application to samples of varying origin.

AUTHOR INFORMATION

Corresponding Author

*E-mail: e.pagliano@sns.it or e.pagliano@libero.it.

Notes

The authors declare no competing financial interest.

REFERENCES

(1) Moorcroft, M. J.; Davis, J.; Compton, R. G. *Talanta* **2001**, *54*, 785−803.
(2) Jobgen, W. S.; Jobgen, S. C.; Li, H.; Meininger, C. J.; Wu, G. *J. Chromatogr., B* **2007**, *851*, 71−82.
(3) Helmke, S. M.; Duncan, M. W. *J. Chromatogr., B* **2007**, *851*, 83−92.
(4) Nydahl, F. *Talanta* **1976**, *23*, 349−357.
(5) Dhar, N. R.; Tandon, S. P.; Biswas, N. N.; Bhateacharya, A. K. *Nature* **1934**, *133*, 213−214.
(6) Mudgal, P. K.; Bansal, S. P.; Gupta, K. S. *Atmos. Environ.* **2007**, *41*, 4097−4105.
(7) Tsikas, D. *Anal. Chem.* **2000**, *72*, 4064−4072.
(8) Li, Y.; Whitaker, J. S.; McCarty, C. L. *J. Chromatogr., A* **2011**, *1218*, 476−483.
(9) D'Ulivo, A.; Pagliano, E.; Onor, M.; Pitzalis, E.; Zamboni, R. *Anal. Chem.* **2009**, *81*, 6399−6406.
(10) Pagliano, E.; Onor, M.; Pitzalis, E.; Mester, Z.; Sturgeon, R. E.; D'Ulivo, A. *Talanta* **2011**, *85*, 2511−2516.
(11) Granik, V. G.; Pyatin, B. M.; Glushkov, R. G. *Russ. Chem. Rev.* **1971**, *40*, 747−759.
(12) Olah, G. A.; Laali, K. K.; Wang, Q.; Surya Prakash, G. K. *Onium Ions*; Wiley: New York, 1998.
(13) Sturgeon, R. E.; Guo, X.; Mester, Z. *Anal. Bioanal. Chem.* **2005**, *382*, 881−883.
(14) Daiber, A.; Bachschmid, M.; Kavaklí, C.; Frein, D.; Wendt, M.; Ullrich, V.; Munzel, T. *Nitric Oxide* **2003**, *9*, 44−52.
(15) Tsikas, D.; Frölich, J. C. *Nitric Oxide* **2004**, *11*, 209−213.
(16) Meija, J.; Mester, Z. *Anal. Chim. Acta* **2008**, *607*, 115−125.
(17) Hintelman, H.; Evans, R. D. *Fresenius J. Anal. Chem.* **1997**, *358*, 378−385.
(18) Klein, R.; Friedel, R. A. *J. Am. Chem. Soc.* **1950**, *72*, 3810−3811.
(19) Henrion, A. *Fresenius J. Anal. Chem.* **1994**, *350*, 657−658.

Annex V

Pagliano, E. (ca); D'Ulivo, A.; Mester, Z.; Sturgeon, R.E.; Meija, J.

The binomial distribution of hydrogen and deuterium in arsanes, diarsanes, and triarsanes generated from As(III)/$[BH_nD_{4-n}]^-$ and the effect of trace amounts of Rh(III) ions

J. Am. Soc. Mass Spectrom. **2012,** *25*, 2178–2186

Copyright 2012 Her Majesty the Queen in Right of Canada

© Her Majesty the Queen in Right of Canada, 2012

J. Am. Soc. Mass Spectrom. (2012)
DOI: 10.1007/s13361-012-0489-5

RESEARCH ARTICLE

The Binomial Distribution of Hydrogen and Deuterium in Arsanes, Diarsanes, and Triarsanes Generated from As(III)/$[BH_nD_{4-n}]^-$ and the Effect of Trace Amounts of Rh(III) Ions

Enea Pagliano,[1,3] Alessandro D'Ulivo,[2] Zoltán Mester,[3] Ralph E. Sturgeon,[3] Juris Meija[3]

[1]Scuola Normale Superiore, Piazza dei Cavalieri, 7, 56126 Pisa, Italy
[2]CNR, Consiglio Nazionale delle Ricerche, Istituto di Chimica dei Composti Organometallici, Via G. Moruzzi, 1, 56124 Pisa, Italy
[3]National Research Council Canada, 1200 Montreal Road, Ottawa, ON K1A 0R6, Canada

Abstract

Recent studies of the formation of arsane in the borohydride/arsenate reaction demonstrate the occurrence of condensation cascades whereby small quantities of di- and triarsanes are formed. In this study, the isotopic composition of these di- and triarsanes was examined using deuterium labelled borohydrides. A statistical model was employed to construct the mass spectra of all diarsane and triarsane isotopologues ($As_2H_nD_{4-n}$ and $As_3H_nD_{5-n}$) from the mass spectra of isotopically pure compounds (As_2H_4, As_2D_4, As_3H_5, and As_3D_5). Subsequent deconvolution of the experimental mixed spectra shows that incorporation of hydrogen closely follows the binomial distribution, in accord with arsane formation. The H/D distribution in arsane, diarsane, and triarsane isotopologues is binomial in the absence of any interference. However, this is significantly altered by the presence of some transition metals; presented here, for the first time, are the effects of Rh(III). The presence of Rh(III) in the As(III)/$[BD_4]^-$ system entails the incorporation of hydrogen into the arsanes arising from the solvent, altering the expected binomial H/D distribution.

Key words: Hydride generation, Statistical modeling, Arsane, diarsane and triarsane, Mechanistic interference

Introduction

Generation of volatile compounds is regarded as one of the most robust analytical tools for determination (and speciation) of trace and ultra-trace levels of numerous elements [1, 2]. The main advantage of this technique lies with the possibility of separating the analyte from its matrix in the form of a vapor, thus allowing for better sensitivity, detection power, and less interference [2]. Chemical vapor generation using $NaBH_4$ is a common practice in analytical chemistry and it finds routine application for the determination of many elements [3]. Furthermore, other boranes, such as $NaBEt_4$, and more recently, triethyloxonium tetrafluoroborate, have been successfully applied for speciation of organometallic compounds [4] and vapor generation of anionic substrates such as Br^-, NO_3^-, and NO_2^- [5, 6]. Despite widespread analytical application of hydride generation, attention to mechanistic aspects of this derivatization reaction has only recently arisen [7–10].

Reaction of inorganic As(III) with $NaBH_4$ occurs via a concerted multistep process wherein all hydrogen atoms in AsH_3 arise from different $[BH_4]^-$ molecules [11]. This mechanism, however, is strongly altered in the presence of noble metals such as Au(III), Pd(II), and Pt(II)—their action on hydride generation cannot be completely explained as

Correspondence to: Enea Pagliano; *e-mail:* e.pagliano@sns.it and e.pagliano@libero.it

Received: 30 May 2012
Revised: 30 August 2012
Accepted: 30 August 2012

causing a decrease in the amount of hydride generated *(yield interference)* [12]; they play an active role in the transfer of hydrogen from $[BH_4]^-$ to the arsenic *(mechanistic interference)* [13]. Furthermore, another source of complexity in the formation of arsane arises due to condensation reactions that occur at high substrate concentration; the formation of polyarsanes, such as diarsane (As_2H_4) and triarsane (As_3H_5), is due to a reaction of the form [14]:

$$R_1R_2 - As - OH + H - As - R_3R_4 \rightarrow R_1R_2 - As - As - R_3R_4 + H_2O.$$

Herein, we investigate the formation of these polyarsanes generated under non-analytical conditions in the absence and presence of Rh(III) ions. In particular, this work illustrates how complex mass spectra can be deconstructed and interpreted with the aid of simple mathematical models based on molecular symmetry considerations [15, 16] so as to infer valuable information about the mechanisms of arsane condensation.

Experimental

Reagents and Materials

Sodium tetrahydroborate pellets (Alfa Aesar, Ward Hill, MA, USA) and sodium tetradeuteroborate (Cambridge Isotope Laboratories, Andover, MA, USA; $x(D)=0.99$) were employed to prepare stock solutions of 0.2 M $NaBH_4$ and 0.2 M $NaBD_4$ in 0.1 M NaOH. In order to vary the deuterium mole fraction in the reducing agent, different mixtures of the above solutions were also prepared. Arsane generation was performed in septum-sealed vials using inorganic As(III) from Oak Ridge National Laboratory (Oak Ridge, TN, USA). Rhodium (III) (1000 mg/L in 10 % HCl) was purchased from SCP Science (Baie D'Urfé, Québec, Canada) and used for the interference experiments. All other reagents were analytical grade.

GC/MS Method

A Hewlett-Packard gas chromatograph (Wilmington, DE) equipped with a Hewlett-Packard 5973 mass spectrometer was operated in splitless mode and fitted with a DB-5 capillary column (30 m×0.25 mm i.d. × 5 µm). The GC was operated under the following conditions: injector temperature: 160 °C; oven: isothermal at 35 °C for 4 min, 15 °C/min up to 200 °C; transfer line program: initial temperature 150 °C, 30 °C/min up to 250 °C; He gas flow of 1.2 mL/min was chosen. MS detector was working in positive EI at 70 eV (full-scan mode). The pressure of the source was 2 mPa.

Generation of Arsane and Polyarsanes

For generating arsane and polyarsanes, the following non-analytical procedure was adopted: 1 mL 800 mg/L As(III) in 1 M HCl was transferred to a screw capped vial (4 mL; Pierce Chemical Co., Rockford, IL, USA) fitted with a PTFE/silicone septum. The vial was closed and the headspace flushed with nitrogen. Hydride generation was subsequently performed by injecting 0.2 mL of 0.2 M $[BH_4]^-/[BD_4]^-$ through the septum. GC/MS analysis was achieved by sampling a 0.5 mL volume of the vial headspace.

Interference of Rhodium(III) on Arsane Generation

To test the mechanistic interference of Rh(III) on arsane generation, the following procedure was adopted: 2 mL of 1 mg/L As(III) in 1 M HCl+20 µL 1000 mg/L Rh(III) in 10 % HCl were placed into a 4 mL vial. After flushing the headspace with nitrogen, 0.2 mL of 0.2 M $[BD_4]^-$ in 0.1 M NaOH was injected into the solution using a plastic syringe fitted with a stainless steel needle to pierce the septum. A 0.4 mL volume of vial headspace was taken for analysis by GC/MS and the mass spectrum of the generated arsanes was monitored. The same procedure, omitting the spike of the interfering metal, was followed for reference purposes. Four independent replicates of this experiment were performed in order to assess the difference between the mass spectrum of the arsanes generated in the presence and absence of Rh(III).

Health and Safety Considerations

Due to the toxicity of the gaseous arsanes generated, all experiments should be conducted in a fume hood, and extreme care should be taken to avoid any exposure to these substances.

Results and Discussion

Mass spectra of arsenic hydride isotopologues show significant overlap (e.g., AsD^+ and AsH_2^+, etc.). Moreover, it is not feasible to synthesize pure partially deuterated isotopologues or separate them by conventional gas chromatography. Nevertheless, the determination of the mole fraction of each isotopologue in a mixture can be achieved mathematically by applying a statistical mass balance model [15, 16]. Using this method, it was possible to delineate the mechanism of formation of diarsane and triarsane in the As(III)/$[BH_4]^-$ system and to discover a strong perturbation to the mechanism of arsane generation due to the presence of Rh(III).

Statistical Model for the Mass Spectra of $As_2H_nD_{4-n}$ and $As_3H_nD_{5-n}$

Statistical reconstruction of partially deuterated hydride has been reported previously for deuterated homologues of diborane [17], methane [18], ethane [19], water, selane

[15], arsane, stibane, bismuthane, stannane, and germane [16]. Here, a model proposed by Meija et al. [16] was used for this purpose. For the application of this model to diarsane ($H_2As{-}AsH_2$) and triarsane ($H_2As{-}AsH{-}AsH_2$) it was assumed that the arsenic backbone (As−As; As−As−As) behaves as a virtual super-atom; in this way it is possible to consider diarsane and triarsane as tetra- and penta-hydrides (EH_4 and EH_5). A statistical mass balance method bases the reconstruction of EH_nD_m mass spectra on experimental EH_{n+m} and ED_{n+m} mass spectra. All possible EH_nD_m fragmentation pathways can be written as combinations of events, such as loss of H ($k_{H,i}$), loss of D ($k_{D,i}$), loss of HD ($k_{HD,i}$), loss of H_2 ($k_{H2,i}$), and loss of D_2 ($k_{D2,i}$). For each reaction, a probability coefficient k is assigned (see Figure 1).

The abundance of a particular molecular ion/fragment ion with composition EH_nD_m can be written as follows:

$$I(EH_nD_m) = \left[1 - \sum f_{-}(EH_nD_m)\right] \cdot f_{+}(EH_nD_m) \cdot \quad (1)$$

where $\Sigma f_{-}(EH_nD_m)$ is the sum of all events comprising the fragmentation of EH_nD_m:

$$\sum f_{-} = f_{-H} + f_{-D} + f_{-HD} + f_{-H_2} + f_{-D_2} \quad (2)$$

$$\sum f_{-} = \frac{{}_nC_1}{{}_{n+m}C_1} k_{H,i} + \frac{{}_mC_1}{{}_{n+m}C_1} k_{D,i} + \frac{{}_nC_1 \cdot {}_mC_1}{{}_{n+m}C_2} k_{HD,i} + \frac{{}_nC_2}{{}_{n+m}C_2} k_{H2,i} + \frac{{}_mC_2}{{}_{n+m}C_2} k_{D2,i} \quad (3)$$

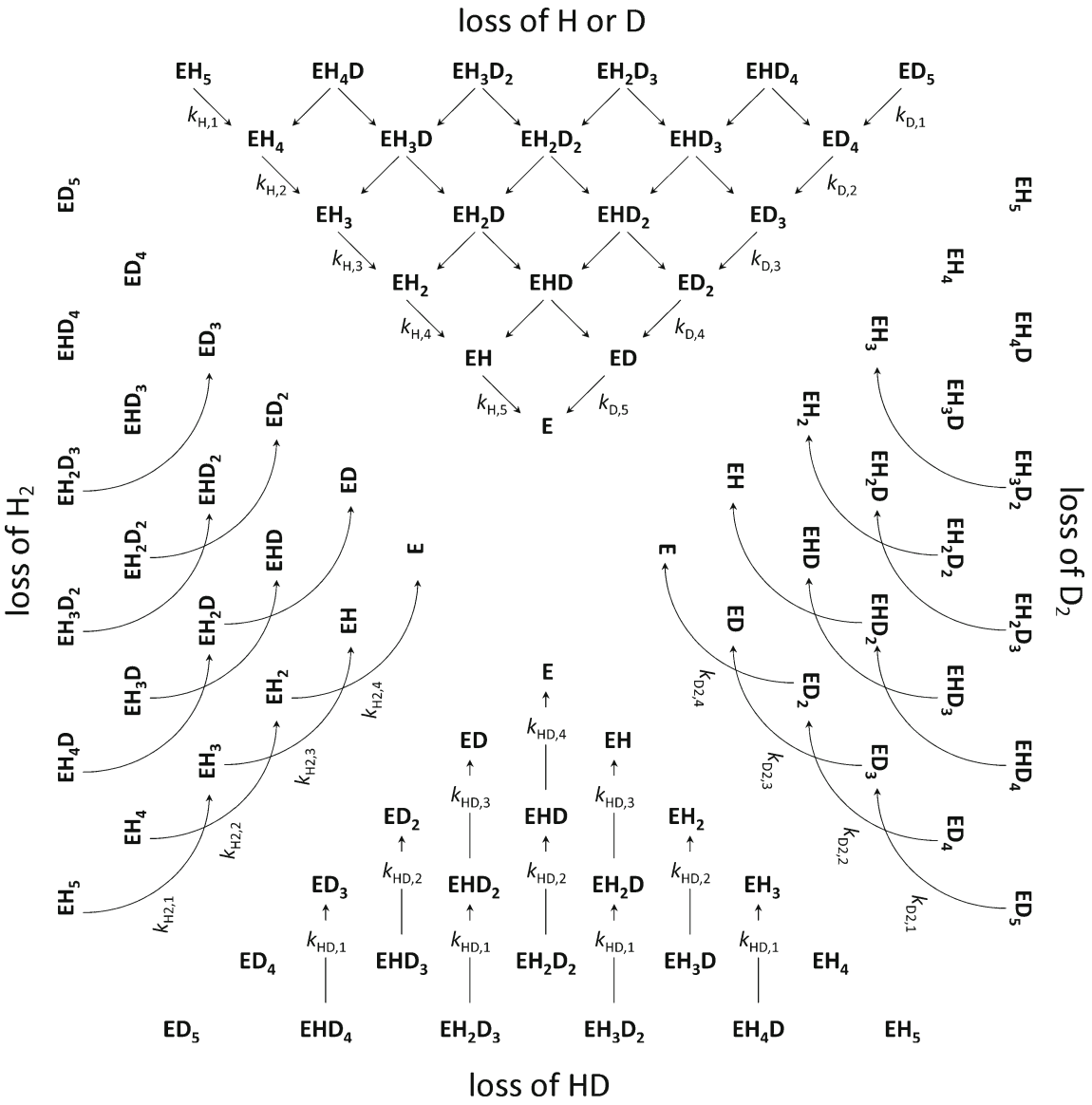

Figure 1. Deconstruction of the EH_nD_{5-n} mass spectrum. The symbol "E" represents the atom or group of atoms which constitute the backbone of the hydride. In this case E = As_3 and the diagram provides an atlas of all fragmentation pathways for the statistical model for $As_3H_nD_{5-n}$: loss of H or D (top); loss of HD (bottom); loss of H_2 (left); and loss of D_2 (right)

and $f_+(EH_nD_m)$ is the sum of all events comprising the formation of EH_nD_m from other ions. For the molecular ion $f_+=1$ by definition, whereas for the fragment ions with formula EH_nD_m the following can be written:

$$\begin{aligned} f_+(EH_nD_m) = {} & f_{-H}(EH_{n+1}D_m)\cdot f_+(EH_{n+1}D_m)+ \\ & f_{-D}(EH_nD_{m+1})\cdot f_+(EH_nD_{m+1})+ \\ & f_{-HD}(EH_{n+1}D_{m+1})\cdot f_+(EH_{n+1}D_{m+1})+ \\ & f_{-H_2}(EH_{n+2}D_m)\cdot f_+(EH_{n+2}D_m)+ \\ & f_{-D_2}(EH_nD_{m+2})\cdot f_+(EH_nD_{m+2}). \end{aligned} \quad (4)$$

Therefore, $f_+(EH_nD_m)$ is obtained from all precursor fragments, $EH_{n+\alpha}D_{m+\beta}$. Using the above recursive equations, it is possible to express the observed abundance of each fragment ion in terms of the probability coefficients k_i. Figure 1 shows the pictorial representation of all of these events for compounds EH_nD_m with $n+m\leq 5$. The numerical values for coefficients k_i are obtained from the mass spectra of the EH_{n+m} and ED_{n+m} compounds. As an example, from the mass spectrum of EH_{n+m}, one can write the following:

$$\begin{aligned} I(EH_{n+m}) &= 1-k_{H,1}-k_{H2,1}, \\ I(EH_{n+m-1}) &= \left(1-k_{H,2}-k_{H2,2}\right)\cdot\left[k_{H,1}\cdot f_+(EH_{n+m})\right], \\ \text{where } f_+(EH_{n+m}) &= 1, \\ I(EH_{n+m-2}) &= \left(1-k_{H,3}-k_{H2,3}\right)\cdot \\ &\quad \left[k_{H,2}\cdot f_+(EH_{n+m-1})+k_{H2,1}\cdot f_+(EH_{n+m})\right], \\ \text{where } f_+(EH_{n+m-1}) &= k_{H,1}\cdot f_+(EH_{n+m}), \\ &\vdots \\ I(E) &= f_+(E). \end{aligned} \quad (5)$$

From Equation (5) it is possible to obtain coefficients k_{Hi} as a function of the observed ion intensities I_i. Unfortunately, considering also the equations arising from ED_{n+m} (for the coefficients k_{Di}), this is always an undetermined system of $2(n+m)$ equations in $2(2n+2m-1)$ unknown variables. However, one can assign all the possible combinations in $k_i \in [0; 1]$ to an arbitrary set of $2(n + m - 1)$ values for k_i, and then calculate the remaining reaction probabilities from Equation (5). To estimate the probability of HD elimination, the following formula is used [16]:

$$k_{HD,i} = \frac{k_{H2,i}+k_{D2,i}}{2} \quad (6)$$

The choice of the arithmetic mean to estimate the loss of HD is conventional, and no difference in the results is observed if the geometric mean is utilized instead. In addition, all sets of k_i with negative values were discarded in order to obtain physically meaningful results. All sets that satisfy the above condition are then used to reconstruct the mass spectra of the isotopologues. Mass spectra obtained from the various sets of k present no substantial differences and the average results of the constructed mass spectra of $As_2H_nD_{4-n}$ and $As_3H_nD_{5-n}$ isotopologues are given in Tables 1 and 2. As a consequence of the statistical model, the individual k-set values do not reflect any physical properties of the fragmentation. Rather, they represent a mathematical fit consistent with the input data. However, it is possible to select only k-sets which satisfy certain physical properties of the system. For example, one can discard sets with k_H and k_D values differing by more than 50 %. This condition is in agreement with the isotopic effect observed in the mass spectra of AsH_3 and AsD_3 and has previously been used for arsanes [16]. The data reported in Tables 1 and 2 were calculated by omitting this condition, which does not alter the resulting mass spectra of di- and triarsanes. However, larger uncertainties are obtained (corresponding to the "worst-case scenario").

Although the statistical model suffers limitations when applied to small molecules (it fails to predict the mass spectrum of HOD with great accuracy [15]), it has proven to be effective for heavier molecules such as selane [15], arsane, stibane, bismuthane, stannane, and germane [16].

In practice it is difficult to obtain a mass spectrum of pure ED_{n+m} from $NaBD_4$ in D_2O and NaOD or DCl. The omnipresence of H_2O in the ambient air inevitably leads

Table 1. Reconstructed mass spectra of $As_2H_nD_{4-n}$ isotopologues

(m/z)/Da	As_2H_4[a]	As_2H_3D[b]	$As_2H_2D_2$[b]	As_2HD_3[b]	As_2D_4[a]
150	0.478±0.003	0.449±0.022	0.431±0.029	0.423±0.023	0.425±0.003
151	0.146±0.002	0.109±0.025	0.072±0.029	0.036±0.020	0.000
152	0.158±0.002	0.121±0.037	0.101±0.037	0.100±0.027	0.120±0.003
153	0.003±0.001	0.096±0.022	0.125±0.018	0.094±0.018	0.000
154	0.215±0.003	0.003±0.001	0.039±0.015	0.106±0.026	0.208±0.002
155	0.000	0.222±0.003	0.003±0.002	0.003±0.001	0.000
156	0.000	0.000	0.229±0.003	0.002±0.001	0.004±0.001
157	0.000	0.000	0.000	0.236±0.004	0.000
158	0.000	0.000	0.000	0.000	0.243±0.004

[a]Experimental mass spectrum. Each experimental set of data represents the mean of three independent determinations. Uncertainties represent the standard deviation of replicate measurements.
[b]Statistical model. Each set of data represents the mean of 5×10^7 simulations. Uncertainties represent the standard deviation of replicate measurements.

Table 2. Reconstructed mass spectra of $As_3H_nD_{5-n}$ isotopologues

(m/z)/Da	As_3H_5[a]	As_3H_4D[b]	$As_3H_3D_2$[b]	$As_3H_2D_3$[b]	As_3HD_4[b]	As_3D_5[a]
225	0.360±0.008	0.333±0.017	0.310±0.025	0.288±0.024	0.269±0.016	0.250±0.006
226	0.327±0.009	0.250±0.024	0.183±0.029	0.120±0.025	0.060±0.015	0.000
227	0.002±0.002	0.078±0.019	0.144±0.027	0.206±0.028	0.267±0.021	0.330±0.014
228	0.062±0.004	0.028±0.009	0.011±0.005	0.004±0.002	0.002±0.001	0.000
229	0.000±0.000	0.043±0.008	0.040±0.008	0.022±0.008	0.007±0.003	0.009±0.003
230	0.250±0.003	0.002±0.001	0.022±0.008	0.040±0.008	0.037±0.006	0.000
231	0.000	0.269±0.005	0.003±0.001	0.009±0.004	0.027±0.009	0.061±0.009
232	0.000	0.000	0.288±0.006	0.003±0.001	0.003±0.001	0.000
233	0.000	0.000	0.000	0.307±0.008	0.002±0.001	0.005±0.001
234	0.000	0.000	0.000	0.000	0.326±0.011	0.000
235	0.000	0.000	0.000	0.000	0.000	0.345±0.015

[a]Experimental mass spectrum. Each experimental set of data represents the mean of three independent determinations. Uncertainties represent the standard deviation of replicate measurements.
[b]Statistical model. Each set of data represents the mean of 8×10^7 simulations. Uncertainties represent the standard deviation of replicate measurements.

to a mixture of ED_{n+m} with traces of EHD_{n+m-1}. For example, a typical mass spectrum of As_2D_4 is

$$\begin{pmatrix} m/z \\ I \end{pmatrix} = \begin{pmatrix} 150 & 151 & 152 & 153 & 154 & 155 & 156 & 157 & 158 \\ 0.425 & \mathbf{0.002} & 0.119 & \mathbf{0.008} & 0.200 & \mathbf{0.000} & 0.004 & \mathbf{0.020} & 0.223 \end{pmatrix},$$

where the presence of signals at odd nominal mass values is indicative of the presence of protium-containing isotopologues. In the first iteration of the calculations, the spectrum of As_2D_4 is taken by simply ignoring the odd-mass signals. Then, the spectrum of As_2HD_3 is obtained using the statistical model. At this point it is feasible to subtract the obtained spectrum of As_2HD_3 from the experimental spectrum of "crude" As_2D_4 (shown above). This calculation loop is repeated until all odd-mass signals vanish. After three iterations this procedure converged to the following mass spectrum of "pure" As_2D_4:

$$\begin{pmatrix} m/z \\ I \end{pmatrix} = \begin{pmatrix} 150 & 151 & 152 & 153 & 154 & 155 & 156 & 157 & 158 \\ 0.425 & \mathbf{0.000} & 0.120 & \mathbf{0.000} & 0.208 & \mathbf{0.000} & 0.004 & \mathbf{0.000} & 0.243 \end{pmatrix},$$

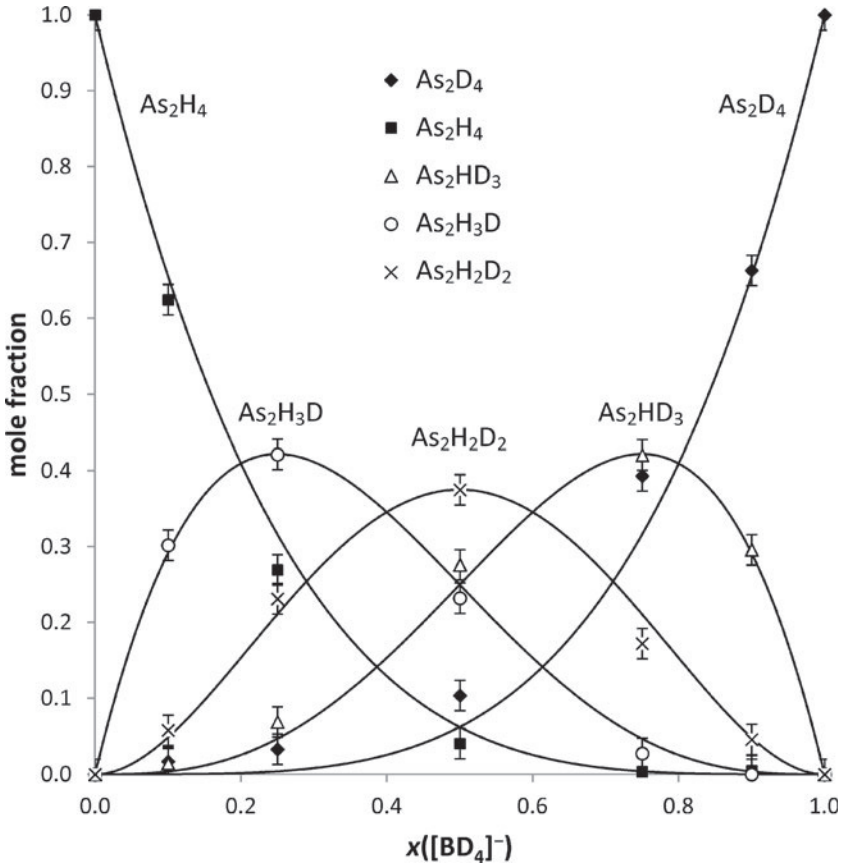

Figure 2. Mole fraction of diarsane isotopologues, $x(As_2H_nD_{4-n})$, generated using mixtures of $NaBH_4$ and $NaBD_4$. The continuous lines portray the theoretical trend based on a multistep direct hydrogen transfer from tetrahydroborate to the As-substrate

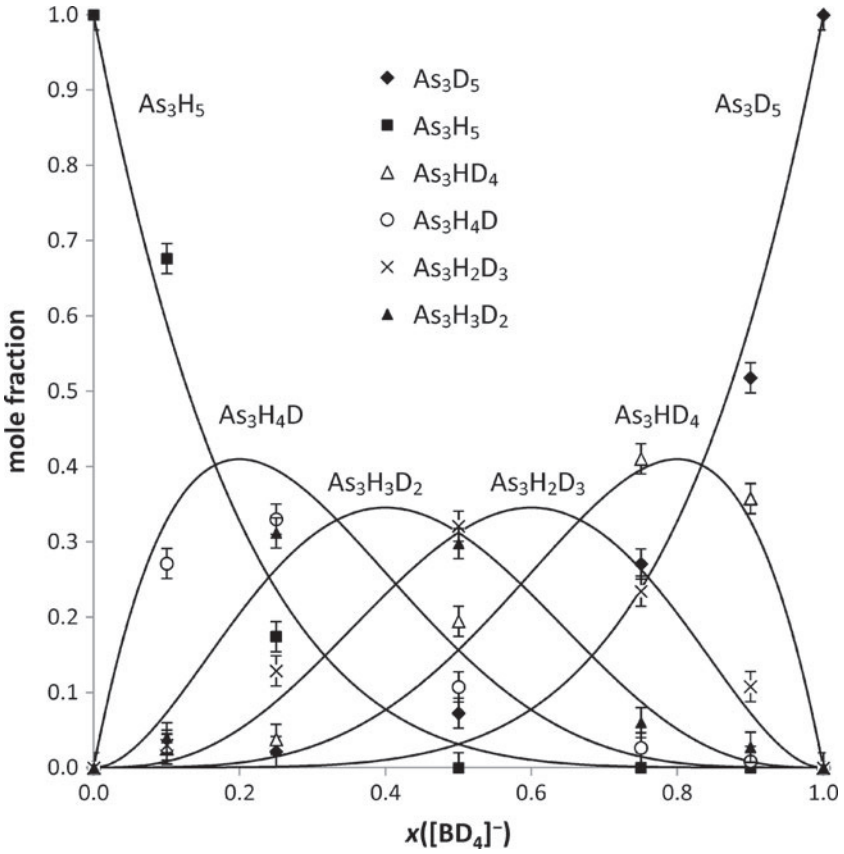

Figure 3. Mole fraction of triarsane isotopologues, $x(As_3H_nD_{5-n})$, generated using mixtures of $NaBH_4$ and $NaBD_4$. The continuous lines portray the theoretical trend based on a concerted multistep hydrogen transfer from tetrahydroborate to the As-substrate

The mass spectra of all isotopologues of diarsane and triarsane are shown in Tables 1 and 2. Contributions of $As_2H_2D_2$ and As_2H_3D are omitted in this iteration procedure due to the extremely low levels of these isotopologues in the "crude" As_2D_4.

Application

The statistical model allows the calculation of the mass spectra of the isotopologues, as presented in Tables 1 and 2. The model has been validated by comparing generated results to the weighted two-band target entropy minimization model [15, 16] which produced consistent mass spectra of isotopologues of arsane, stibane, and selane.

From the reconstructed spectra in Tables 1 and 2, it is possible to determine the quantity of the various isotopologues from their mixtures. This is achieved using the relationship:

$$Y = FA, \tag{7}$$

where Y is the mass spectrum (vector) of the mixture of isotopologues, F is the matrix reporting the mass spectra of the pure isotopologues (Tables 1 and 2) and A is the vector reporting the mole fraction of each component in the mixture. In this work, Equation (7) was solved for A with a least squares method using the LINEST function in Microsoft *Excel*. Moreover, agreement between the gravimetric mole fraction of deuterium in the reducing agent ($NaBH_4$+$NaBD_4$) and the net mole fraction of deuterium in the generated isotopologue mixtures as calculated from the statistical model (R^2>0.98) is obtained.

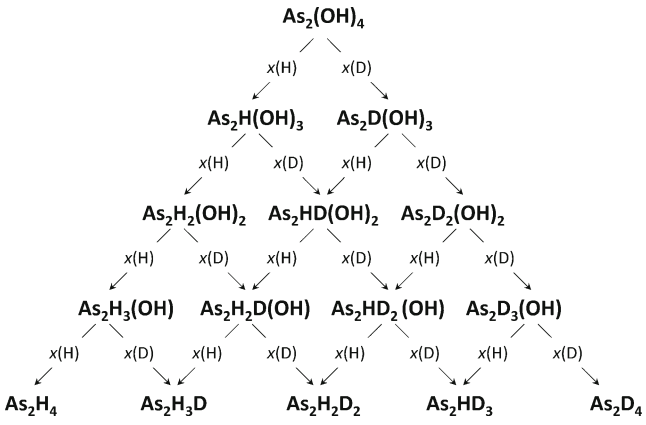

Figure 4. Pascal triangle used to predict the isotopic composition of diarsane generated using various mixtures of $NaBH_4$ and $NaBD_4$

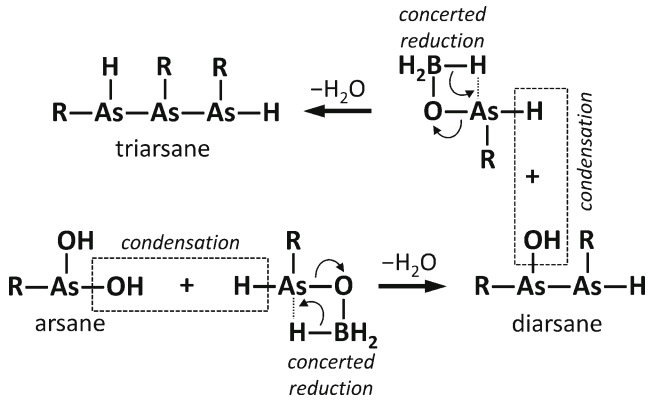

Scheme **1.** Formation of di- and triarsanes in a concerted reduction and condensation cascade (R = H or OH).

Mechanism of Formation of Polyarsanes

Reduction of arsenates and methylarsenates with boranes is a concerted multistep reaction wherein all −OH groups from the As-substrate are replaced by −H groups originating from different borane molecules [11]:

$$\mathrm{As(OH)_3} + 3[\mathrm{BX_3H}]^- \rightarrow \mathrm{AsH_3} + 3[\mathrm{BX_3OH}]^- (\mathrm{X = H, OH}).$$

The incorporation of hydrogen into the final hydride can be monitored using tetrahydroborate enriched in deuterium *via* plots of the mole fraction of each isotopologue generated versus the mole fraction of deuterium in the tetrahydroborate reductant [8]. The stoichiometry of the above reaction is respected only when arsenic compounds are present at trace levels in an excess of boranes (i.e., under analytical conditions). When the concentration of arsenic rises above the millimolar level, however, a complex set of side reactions takes place [14] with formation of condensation products:

$$\mathrm{X_2As - OH + H - AsX_2 \rightarrow X_2As - AsX_2 + H_2O},$$

$$\mathrm{X_2As - OH + H - AsX - AsX_2 \rightarrow X_2As - AsX - AsX_2 + H_2O},$$

$$\mathrm{X_2As - AsX_2, X_2As - AsX - AsX_2 + [BH_4]^- \rightarrow As_2H_4, As_3H_5 (X = H, OH)}.$$

In this work, we have investigated for the first time the mechanism of incorporation of hydrogen into the di- and triarsanes arising from these condensation cascades. Experimental conditions are chosen to avoid any unwanted H/D exchange with the solvent (H_2O) [20].The mole fraction of deuterium in the $NaBH_4$ and $NaBD_4$ mixtures was obtained

Table 3. Composite mass spectra of arsanes generated in the reaction of As(III) with $[BD_4]^-$ in the presence and absence of Rh(III) ions (**A**) and the corresponding isotopologue distribution (**B**)

A		B		
Reaction: As(III) + $[BD_4]^-$ + Rh(III) ⟶ AsH_nD_{3-n}				
(*m*/*z*)/Da	Intensity[a]	Isotopologue	Experimental	Binomial[b]
75	0.146±0.004	AsH_3	0.133±0.046	0.013
76	0.092±0.013	AsH_2D	0.058±0.013	0.127
77	0.342±0.012	$AsHD_2$	0.175±0.057	0.413
78	0.062±0.014	AsD_3	0.629±0.048	0.448
79	0.082±0.003			
80	0.060±0.019			
81	0.216±0.016	*x*(D)	0.765±0.035	0.765
Reaction: As(III) + $[BD_4]^-$ ⟶ AsH_nD_{3-n}				
(*m*/*z*)/Da	Intensity[a]	Isotopologue	Experimental	Binomial[b]
75	0.149±0.002	AsH_3	0.000±0.006	0.000
76	0.003±0.003	AsH_2D	0.021±0.006	0.005
77	0.411±0.005	$AsHD_2$	0.145±0.011	0.111
78	0.011±0.006	AsD_3	0.856±0.018	0.885
79	0.089±0.004			
80	0.047±0.005			
81	0.289±0.006	*x*(D)	0.960±0.010	0.960

[a]Each set of experimental data reflects the mean of four independent determinations. Uncertainties represent the standard deviation of replicate measurements.
[b]The experimental isotopologue distribution is compared with the calculated binomial distribution corresponding to the same level of deuterium incorporation, *x*(D).

gravimetrically and the mass spectra of the resultant di- and triarsanes were deconvoluted to obtain the mole fraction of each isotopologue. Results are shown in Figures 2 and 3. It is evident that the incorporation of protium and deuterium in di- and triarsanes closely follows the binomial distribution, i.e.,

$$x_{As_2H_nD_{4-n}} = \frac{4!}{n!(4-n)!} \cdot x_D^{4-n} \cdot (1-x_D)^n \quad (8)$$

$$x_{As_3H_nD_{5-n}} = \frac{5!}{n!(5-n)!} \cdot x_D^{5-n} \cdot (1-x_D)^n \quad (9)$$

as illustrated by the continuous line in Figures 2 and 3. The binomial distribution originates from the multistep hydrogen transfer, as outlined for diarsane in Figure 4. The trends observed in the composition of diarsane and triarsane follow the hypothesis of a concerted multistep formation of arsane in a fashion already demonstrated for AsH_3 [11], and they further validate the proposed condensation cascade mechanism [14]. Therefore, the formation of di- and triarsanes can be described as a combination of two independent events: *condensation* of two hydroxoarsanes and their *reduction* by borohydrides via the concerted transfer of hydrogen to the arsenic substrate, as summarized in Scheme 1.

Mechanistic Interference from Rhodium(III)

The interaction between transition elements and tetrahydroborate is of great importance in chemistry, not just in analytical chemistry. Tetrahydroborate is of interest due to its capability to store hydrogen and its hydrolysis is catalyzed by noble and transition elements [21, 22]. Reaction of transition elements with tetrahydroborate is also employed in the synthesis of nanoparticles [23, 24] and to generate volatile derivatives suitable for analytical purposes [10]. Noteworthy is also the possibility of using transition elements, such as Co(II), Ni(II) [25], and Rh(III) [26], to modify the reducing power of the tetrahydroborate. For example, $[BH_4]^-$ cannot reduce nitriles, amides, and olefins, but it can do so in combination with transition element halides [27, 28]. Recent observations of the effects of Au(III), Pd(II), and Pt(II) on generation of arsane [13] confirm a peculiar chemistry in this system, and in this study we report a similar behaviour with Rh (III). The first macroscopic observation regarding the interference of Rh(III) within the As(III)/$[BD_4]^-$ system is the increased incorporation of hydrogen from the solvent into the arsanes. Indeed, when As(III) is derivatized to arsane by $[BD_4]^-$ in aqueous media, AsD_3 is the major isotopologue formed, 86 %, while trace (<1 %) AsH_3 is observed. The presence of rhodium alters this composition to 63 % AsD_3 and 13 % AsH_3.

Although this phenomenon could be interpreted as an H/D exchange of the arsane catalyzed by the presence of rhodium, it would be inconsistent with the observation that the injection of preformed AsD_3 into a vial containing Rh (III)/$[BD_4]^-$ does not alter the integrity of AsD_3. This evidence suggests that this H/D exchange occurs during the generation of arsane.

Therefore, the presence of Rh(III) causes a strong perturbation to the mechanism of hydrogen transfer from tetrahydroborate to arsenic, creating a "loss" in the typical binomial character (Table 3), *i.e.*, the amount of AsH_3 (among the other isotopologues) increases significantly in the presence of Rh(III). A possible interpretation of the results shown in Table 3 can be achieved by considering the reductive process as the sum of two competing events: the reduction by $[BD_4]^-$ which is binomial, and the reduction by a hydride-borane-Rh intermediate, present in the early stages of the reaction, and able to exchange hydrogen with the solvent. The postulation of the formation of a "new" reducing agent, with differing reductive power with respect to $[BD_4]^-$, is also supported by observations reported in the organic chemistry literature, as noted earlier.

It was not possible to study how the mechanistic interference of rhodium ions propagates from arsane to di- and triarsane generated *via* the condensation cascades under non-analytical conditions. This was due to the fact that the large concentration of As(III) necessary to produce polyarsanes creates prohibitive conditions for Rh(III), leading to significant precipitation and significant reduction in the yield of the volatile arsanes.

References

1. Dědina, J., Tsalev, D.L.: Hydride generation atomic absorption spectroscopy. Wiley, Chichester (1995)
2. Sturgeon, R.E., Guo, X., Mester, Z.: Chemical vapor generation: are further advances yet possible? *Anal. Bioanal. Chem.* **382**, 881–883 (2005)
3. Luna, A.S., Sturgeon, R.E., de Campos, R.C.: Chemical vapor generation: atomic absorption by Ag, Au, Cu, and Zn following reduction of aquo ions with sodium tetrahydroborate(III). *Anal. Chem.* **72**, 3523–3531 (2000)
4. Rapsomanikis, S.: Derivatization by ethylation with sodium tetraethylborate for the speciation of metals and organometallics in environmental samples. A review. *Analyst* **119**, 1429–1439 (1994)
5. D'Ulivo, A., Pagliano, E., Onor, M., Pitzalis, E., Zamboni, R.: Vapor generation of inorganic anionic species after aqueous phase alkylation with trialkyloxonium tetrafluoroborates. *Anal. Chem.* **81**, 6399–6406 (2009)
6. Pagliano, E., Meija, J., Sturgeon, R.E., Mester, Z., D'Ulivo, A.: Negative chemical ionization GC/MS determination of nitrite and nitrate in seawater using exact matching double spike isotope dilution and derivatization with triethyloxonium tetrafluoroborate. *Anal. Chem.* **84**, 2592–2596 (2012)
7. D'Ulivo, A.: Chemical vapor generation by tetrahydroborate(III) and other borane complexes in aqueous media: a critical discussion of fundamental processes and mechanisms involved in reagent decomposition and hydride formation. *Spectrochim. Acta Part B* **59**, 793–825 (2004)
8. D'Ulivo, A.: Mechanism of generation of volatile species by aqueous boranes: towards the clarification of most controversial aspects. *Spectrochim. Acta Part B* **65**, 360–375 (2010)
9. D'Ulivo, A., Dědina, J., Mester, Z., Sturgeon, R.E., Wang, Q., Welz, B.: Mechanisms of chemical generation of volatile hydrides for trace element determination. *Pure Appl. Chem.* **83**, 1283–1340 (2011)

10. Feng, Y.-L., Sturgeon, R.E., Lam, J.W., D'Ulivo, A.: Insights into the mechanism of chemical vapor generation of transition and noble metals. *J. Anal. At. Spectrom.* **20**, 255–265 (2005)
11. D'Ulivo, A., Mester, Z., Sturgeon, R.E.: The mechanism of formation of volatile hydrides by tetrahydroborate(III) derivatization: a mass spectrometric study performed with deuterium labeled reagents. *Spectrochim. Acta Part B* **60**, 423–438 (2005)
12. Bax, D., Agterdenbos, J., Worrell, E., Beneken Kolmer, J.: The mechanism of transition metal interference in hydride generation atomic absorption spectrometry. *Spectrochim. Acta Part B* **43**, 1349–1354 (1988)
13. Pagliano, E., Onor, M., Meija, J., Mester, Z., Sturgeon, R.E., D'Ulivo, A.: Mechanism of hydrogen transfer in arsane generation by aqueous tetrahydridoborate: interference effects of Au^{III} and other noble metals. *Spectrochim. Acta Part B* **66**, 740–747 (2011)
14. D'Ulivo, A., Meija, J., Mester, Z., Pagliano, E., Sturgeon, R.E.: Condensation cascades and methylgroup transfer reactions during the formation of arsane, methyl- and dimethylarsane by aqueous borohydride and (methyl) arsenates. *Anal. Bioanal. Chem.* **402**, 921–933 (2012)
15. Meija, J., Mester, Z., D'Ulivo, A.: Mass spectrometric separation and quantitation of overlapping isotopologues. H_2O/HOD/D_2O and H_2Se/HDSe/D_2Se mixtures. *J. Am. Soc. Mass Spectrom.* **17**, 1028–1036 (2006)
16. Meija, J., Mester, Z., D'Ulivo, A.: Mass spectrometric separation and quantitation of overlapping isotopologues. Deuterium containing hydrides of As, Sb, Bi, Sn, and Ge. *J. Am. Soc. Mass Spectrom.* **18**, 337–345 (2007)
17. Ditter, J.F., Klusmann, E.B., Perrine, J.C., Shapiro, I.: Mass spectra of deuterated diboranes. *J. Phys. Chem.* **64**, 1682–1685 (1960)
18. Schoofs, B., Martens, J.A., Jacobs, P.A., Schoonheydt, R.A.: Kinetic of hydrogen-deuterium exchange reactions of methane and deuterated acid FAU- and MFI-type zeolites. *J. Catal.* **183**, 355–367 (1999)
19. Amenomiya, Y., Pottie, R.F.: Mass spectra of some deuterated ethanes. II. An empirical method of calculation of the spectra. *Can. J. Chem.* **46**, 1741–1746 (1968)
20. D'Ulivo, A., Mester, Z., Meija, J., Sturgeon, R.E.: Gas chromatography–mass spectrometry study of hydrogen–deuterium exchange reactions of volatile hydrides of As, Sb, Bi, Ge and Sn in aqueous media. *Spectrochim. Acta Part B* **61**, 778–787 (2006)
21. Muir, S.S., Yao, X.: Progress in sodium borohydride as a hydrogen storage material: development of hydrolysis catalysts and reaction systems. *Int. J. Hydrogen Energy* **36**, 5983–5997 (2011)
22. Guella, G., Zanchetta, C., Patton, B., Miotello, A.: New insights on the mechanism of palladium-catalyzed hydrolysis of sodium borohydride from ^{11}B NMR measurements. *J. Phys. Chem. B* **110**, 17024–17033 (2006)
23. Dragieva, I.D., Stoynov, Z.B., Klabunde, K.J.: Synthesis of nanoparticles by borohydride reduction and their applications. *Scripta Mater.* **44**, 2187–2191 (2001)
24. Van Hyning, D.L., Zukoski, C.F.: Formation mechanisms and aggregation behavior of borohydride reduced silver particles. *Lagmuir* **14**, 7034–7046 (1998)
25. Satoh, T., Suzuki, S., Suzuki, Y., Miyaji, Y., Imai, Z.: Reduction of organic compounds with sodium borohydride-transition metal salt systems: reduction of organic nitrile, nitro and amide compounds to primary amines. *Tetrahedron Lett.* **10**, 4555–4558 (1969)
26. Nishiki, M., Miyataka, H., Niino, Y., Mitsuo, N., Satoh, T.: Facile hydrogenation of aromatic nuclei with sodium borohydride-rhodium chloride in hydroxylic solvents. *Tetrahedron Lett.* **23**, 193–196 (1982)
27. Heinzman, S.W., Ganem, B.: Mechanism of sodium borohydride-cobaltous chloride reductions. *J. Am. Chem. Soc.* **104**, 6801–6802 (1982)
28. Osby, J.O., Heinzman, S.W., Ganem, B.: Studies on the mechanism of transition-metal-assisted sodium borohydride and lithium aluminum hydride reductions. *J. Am. Chem. Soc.* **108**, 67–72 (1986)

Annex VI

Pagliano, E (ca); Meija, J.; Ding, J.; Sturgeon, R.E.; D'Ulivo, A.; Mester, Z.

Novel ethyl-derivatization approach for the determination of fluoride by headspace gas chromatography/mass spectrometry

Anal. Chem. **2012,** DOI: 10.1021/ac302303r

Copyright 2012 American Chemical Society

analytical chemistry

Article

pubs.acs.org/ac

Novel Ethyl-Derivatization Approach for the Determination of Fluoride by Headspace Gas Chromatography/Mass Spectrometry

Enea Pagliano,*[,†,‡] Juris Meija,[†] Jianfu Ding,[†] Ralph E. Sturgeon,[†] Alessandro D'Ulivo,[§] and Zoltán Mester[†]

[†]National Research Council of Canada, 1200 Montreal Road, Ottawa, ON K1A 0R6, Canada

[‡]Scuola Normale Superiore, Piazza dei Cavalieri, 7, 56126, Pisa, Italy

[§]CNR, Consiglio Nazionale delle Ricerche, Istituto di Chimica dei Composti Organometallici, Via G. Moruzzi, 1, 56124 Pisa, Italy

ABSTRACT: We report a novel derivatization chemistry for determination of fluoride based on the batch reaction of fluoride ions with triethyloxonium tetrachloroferrate(III) in a closed vessel to yield fluoroethane. Gaseous fluoroethane was readily separated from the matrix, sampled from the headspace, and determined by gas chromatography/mass spectrometry. The method was validated using rainwater certified reference material (IRMM CA408) and subsequently applied to the determination of fluoride in various matrixes, including tap water, seawater, and urine. An instrumental limit of detection of 3.2 μg/L with a linear range up to 50 mg/L was achieved. The proposed derivatization is a one-step reaction, requires no organic solvents, and is safe, as the derivatizing agent is nonvolatile. Determination of fluoride is affected by common fluoride-complexing agents, such as Al(III) and Fe(III). The effect of large amounts of these interferences was studied, and the adverse effect of these ions was eliminated by use of the method of standard additions.

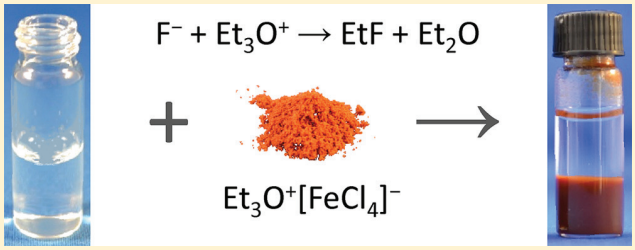

A large number of municipalities in North America supplement their drinking water with fluoride as it prevents tooth decay owing to its cariostatic activity. Ensuing debates over the efficacy of fluoridation notwithstanding, accurate monitoring of fluoride is of importance in countries where water fluoridation is practiced.[1−4] Because of the toxic effects of fluoride at higher concentrations, a guideline value of 1.5 mg/L is recommended by the World Health Organization as a level at which dental fluorosis should be minimal.[5] Considering also that elevated levels of fluoride occur in natural waters over an extensive geographical belt, reaching well above 10 mg/L in some regions of Kenya[6] and India,[7] the monitoring of fluoride in water and food products is important from a toxicological point-of-view.

Fluorine, like boron, does not enter into chemical reactions that are selective enough to permit its direct determination in the presence of concomitant elements.[8,9] Consequently, no direct or specific spectrophotometry or fluorescence methods are available for its quantitation.[10−13] A significant advance in the determination of fluoride was development of the fluoride ion-selective electrode in 1966.[14] Owing to its simplicity, this has effectively become the method of choice for field and laboratory settings, providing a detection limit of ∼20 μg/L.[15] However, ion-selective electrodes respond to the activity of fluoride ions, not to their concentration, and are affected by the presence of hydroxide ions.[14]

Modern instrumental methods can address the problem of measurement specificity. Fluorine can be determined by inductively coupled plasma mass spectrometry (ICPMS), although poor sensitivity is reported (negative ion mode has been attempted yielding a detection limit of 110 μg/L[16]). Molecular absorption from ions such as GaF has been exploited for the determination of fluoride using high-resolution continuum source atomic absorption spectrometry with reported detection limits close to 1 μg/L.[17,18] Similar figures of merit are reported for electrospray MS.[19,20]

Derivatization of fluoride ions has traditionally been performed using silicon-based chemistry in order to convert F^- to Me_3SiF[21,22] or Ph_3SiF.[23] The resulting volatile fluorosilanes can be determined by gas chromatography following either liquid extraction with organic solvents or solid-phase microextraction from the headspace, achieving a detection limit of 6 μg/L in the latter case with Me_3SiF.[21] However the Si−F bond in these derivatives is not stable in aqueous solutions, especially at high pH. Consequently, Kage et al.[24] proposed carbon-based alkylation of fluoride with pentafluorobenzylbromide (F_5BzBr), yielding volatile F_5BzF which can be determined by gas chromatography/mass spectrometry (GC/MS). Although stability of the resultant derivative is achieved, the method is limited by a poor detection limit (0.5 mg/L). Carbon-based derivatization of fluoride can also be achieved using tertiary oxonium salts. Despite their common use as alkylation agents in organic chemistry,[25,26] oxonium salts have only recently been introduced to the field of

Received: August 10, 2012
Accepted: December 10, 2012

 © XXXX American Chemical Society dx.doi.org/10.1021/ac302303r | *Anal. Chem.* XXXX, XXX, XXX−XXX

analytical chemistry.[27−29] The commercially available triethyloxonium tetrafluoroborate permits otherwise difficult alkylation reactions to be undertaken in aqueous media; in addition, $Et_3O^+[BF_4]^-$ has been successfully applied for the derivatization of inorganic anions,[27] including chloride, bromide, iodide, cyanide, thiocyanate, sulfide, nitrite, and nitrate.[28,29] Generation of volatile derivatives allows for the separation of the analyte from the matrix, thereby minimizing spectral interferences and reducing background levels in the separation and detection phase of the analysis.[30] However, $Et_3O^+[BF_4]^-$ is not suitable for determination of fluoride because tetrafluoroborate slowly hydrolyzes, releasing fluoride ions. To overcome this drawback, the method proposed here employs triethyloxonium tetrachloroferrate(III) to convert fluoride to stable fluoroethane which can be subjected to analysis by GC/MS.

EXPERIMENTAL SECTION

Reagents and Materials. Standard solutions of fluoride were prepared by dissolution of sodium fluoride (Baker; w = 0.999 g/g) in deionized water generated with a Milli-Q system. Anhydrous diethyl ether (Sigma-Aldrich), anhydrous iron(III) chloride (Sigma-Aldrich, $w \geq 0.98$ g/g), and 2-(chloromethyl)-oxirane (Fluka, w = 0.99 g/g; also known as (±)-epichlorohydrin) were used for the synthesis of triethyloxonium tetrachloroferrate(III). Triethyloxonium tetrafluoroborate (Fluka, $w > 0.97$ g/g) and triethyloxonium hexachloroantimonate(VI) (Aldrich, $w > 0.97$ g/g) were also sourced. An aqueous solution of ammonia (Tamapure AA-100; $w(NH_3)$ = 0.2 g/g) was used for adjustment of the pH of the sample. Rainwater, certified for fluoride content, was obtained from the Institute for Reference Materials and Measurements (CA408; Geel, Belgium). All other reagents were of analytical grade. Samples of different origin were also selected for testing: seawater (MOOS-2 certified reference material; NRC Canada), City of Ottawa drinking water, and urine from a healthy volunteer.

Safety Considerations. Despite widespread use of alkylation and silylation reactions for gas chromatography, the health risks of handling potentially toxic and volatile compounds, such as diazomethane, chloroformates, or trimethylsilyl chloride, must be carefully considered.[31] Triethyloxonium tetrachloroferrate(III) is a strong ethylating agent and must be handled in a fume-hood with appropriate personal protective equipment. However, in comparison to other reagents used for derivatization, its potential toxicity is reduced because it is a nonvolatile crystalline salt which undergoes complete hydrolysis within 3 h.[32] $Et_3O^+[FeCl_4]^-$ is hygroscopic, but considerably less so than tetrafluoroborate, and it should be stored in a freezer. In order to avoid excessive exposure to ambient moisture, the bottle containing the reagent should be allowed to reach room temperature before opening and use of contents.

Triethyloxonium Tetrachloroferrate(III). Triethyloxonium tetrachloroferrate(III) was synthesized according to the procedure of Meerwein et al:[33]

$$2Et_2O{\cdot}FeCl_3 + C_2H_3(O)CH_2Cl \rightarrow Et_3O^+[FeCl_4]^- + FeCl_2[(OCH(CH_2Cl)CH_2OEt]$$

For this purpose, 0.2 mol (32.4 g) of anhydrous $FeCl_3$ was dissolved in 150 mL of dry diethyl ether. The headspace above the resultant solution was evacuated and purged with argon three times using a Schlenk line while keeping argon flowing during the reaction. During magnetic stirring, 0.1 mol (9.25 g) of 2-(chloromethyl)oxirane was added dropwise using a syringe. The addition of 2-(chloromethyl)oxirane was controlled to keep the ether under constant boiling. After this addition, the resultant mixture was further stirred for 5 min and then cooled to 0 °C using an ice/water bath and held at this temperature for 2 h with gentle magnetic stirring. The brown crystalline product was filtered on a Büchner funnel and subsequently washed twice with dry ether. A 23.2 g mass of $Et_3O^+[FeCl_4]^-$ was obtained (77% yield), enough to perform all the experiments described herein.

Although the triethyloxonium tetrachloroferrate(III) is soluble in water, it slowly undergoes hydrolysis. Aqueous solutions of this salt should therefore be prepared shortly before use. In this work, the $Et_3O^+[FeCl_4]^-$ solutions were prepared by dissolving 0.4 g of $Et_3O^+[FeCl_4]^-$ in 16 mL of Milli-Q water.

Sample Preparation. A 2 mL volume of aqueous sample was introduced without pretreatment into five different vials, four of which were spiked with 0.2 mL of different fluoride standard solutions whereas 0.2 mL of Milli-Q water was added to the remaining vial. Quantitation of fluoride was based on the method of standard additions, and the concentration of the standard was chosen so to obtain a maximum 4-fold increase in the analytical signal compared to the nonspiked sample. The samples were spiked with a 50 μL volume of ammonia solution ($w(NH_3)$ = 0.2 g/g) and then with a 1 mL volume of the $Et_3O^+[FeCl_4]^-$ solution prepared as described above. After the addition of all reagents, the vials were quickly sealed with a screw-cap containing a PTFE/silicone septum and kept at room temperature for 3 h before sampling the headspace with a gastight syringe. Triethyloxonium converts F^- into fluoroethane which is gaseous at ambient temperature (t_{vap} = −37 °C). Therefore, in order to avoid analyte loss, it is important that unpunctured septa be used for sealing.

GC/MS Analysis. A Hewlett-Packard 6890 gas chromatograph equipped with a Hewlett-Packard 5973 mass selective detector and fitted with a 60 m DB-624 column (6% cyanopropyl-phenyl 94% dimethyl polysiloxane) was operated at a constant flow of 0.9 mL He/min. Pulsed split (5:1) injection mode was chosen, with a pulsed pressure of 172 kPa for 1 min. The inlet temperature was set to 100 °C. After the first isotherm at 30 °C (held for 7 min), the oven was heated at 20 °C/min to 200 °C. The transfer line temperature was 230 °C. The generated fluoroethane was manually sampled with a gastight syringe from the vial headspace and a 250 μL volume injected into the GC/MS. Fluoroethane eluted at 5 min under the 30 °C isotherm. In addition, chromatographic performance was improved with use of a narrow inlet liner (internal diameter of 0.75 mm) designed for solid phase microextraction (SPME).

The mass spectrometer was operated in electron impact mode (70 eV) using standard settings (ion source temperature 250 °C; quadrupole temperature 150 °C). The intensity of the fluoroethane molecular ion shown in Figure 1 is low (10% of the base peak); the most abundant fluorine-containing ions are $CH_2CH_2{-}F^+$ (m/z = 47 Da) and $CH_2{-}F^+$ (m/z = 33 Da). Therefore, quantitation of fluoroethane was done by selected ion monitoring (SIM) using the area of the peak extracted at m/z = 47 Da. The fragment ion at m/z = 33 Da was monitored for quality control purposes. Both were acquired using a 100 ms dwell time.

dx.doi.org/10.1021/ac302303r | Anal. Chem. XXXX, XXX, XXX−XXX

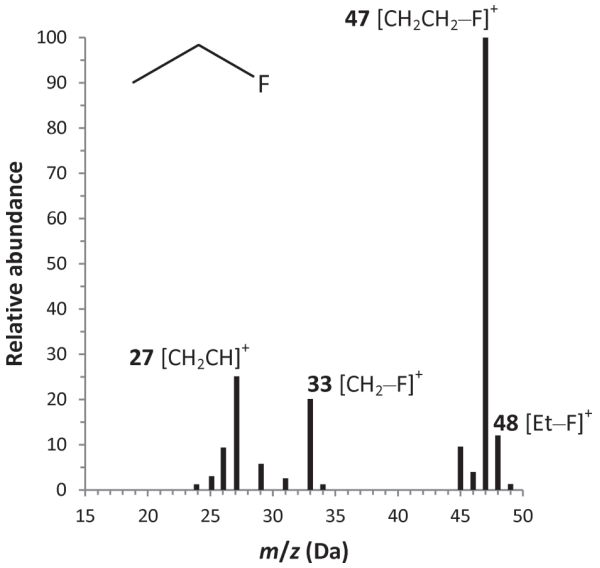

Figure 1. Electron impact mass spectrum of fluoroethane.

RESULTS AND DISCUSSION

Derivatization. The use of triethyloxonium salts as derivatizing reagents is a recent introduction to the field of analytical chemistry.[27−29] Unlike triethyloxonium tetrachloroferrate(III), which was selected for determination of fluoride in this work, the two commercially available oxonium salts, $Et_3O^+[BF_4]^-$ and $Et_3O^+[SbCl_6]^-$, are unsuitable analytical reagents for conversion of fluoride to fluoroethane,

$$Et_3O^+(aq) + F^-(aq) \rightarrow EtF(g) + Et_2O$$

because $Et_3O^+[BF_4]^-$ releases fluoride ions during hydrolysis of the tetrafluoroborate,[34] whereas $Et_3O^+[SbCl_6]^-$ is not water-soluble. Ethylation of fluoride with $Et_3O^+[FeCl_4]^-$ was performed in an alkaline medium (pH = 10) because an acidic environment releases Fe(III) from the salt which then binds to the fluoride ions. Additionally, the alkalinity of the sample causes precipitation of a number of endogenous metal ions, resulting in the removal of potential interferences in the determination of fluoride. Moreover, alkaline conditions prevent the conversion of fluoride to gaseous HF, a significant advantage compared to an acidic silylation method, wherein this may occur. The ethylation reaction stops after hydrolysis of Et_3O^+ is complete. Granik et al.[25] reported that complete hydrolysis of Et_3O^+ occurs in 80 min. From our previous research[27] and from similar experiments repeated here for $Et_3O^+[FeCl_4]^-$, we found that complete hydrolysis and equilibration of the headspace is complete in 3 h. After this time, the headspace can be sampled for analysis by GC/MS. Fluoroethane is a stable compound and was detected in the headspace up to 3 days after the derivatization. The chemical yield for derivatization, achieved using the experimental conditions described herein, was determined to be 8%. For this purpose, four fluoride standard solutions were prepared and subjected to the ethylation procedure. The headspace was then purged with nitrogen to eliminate the fluoroethane, and the remaining solutions were analyzed for the residual content of fluoride.

The purpose of this work was to demonstrate the performance of $Et_3O^+[FeCl_4]^-$ for derivatization of fluoride. However, one must be mindful that, much like $Et_3O^+[BF_4]^-$, triethyloxonium tetrachloroferrate is also able to ethylate other inorganic anions.[27]

Figures of Merit and Applications. The determination of fluoride was undertaken in various liquid matrixes using a standard additions calibration approach whereby the fluoroethane peak (m/z = 47 Da signal) was integrated and linearly regressed against the mass of fluoride added. Headspace sampling and injection into the GC/MS was manually performed; no internal standards were used to correct for variations that may occur during these operations. This method was validated using IRMM CA408 rainwater certified reference material, yielding good agreement with the certified property value, as summarized in Table 1. Other matrixes were also examined, including City of Ottawa drinking water, seawater reference material (NRC MOOS-2), and urine from a healthy volunteer. Results are based on the mean values of three independent measurements derived from four point (in addition to the unspiked sample) standard additions curves, and the uncertainties were evaluated according to the ISO/GUM guidelines. For each measurement, the relation between the mass of fluoride added and the integrated signal was always linear and characterized by a coefficient of determination R^2 > 0.99. The mass concentration of fluoride determined in City of Ottawa drinking water, $\gamma(F^-)$ = 0.72 ± 0.06 mg/L, is in agreement with the target level of 0.70 mg/L recommended by Health Canada and adopted by the City of Ottawa.[35]

Table 1. Determination of Fluoride in IRMM CA408 Rainwater Certified Reference Material[a]

run	γ (F^-)/(mg/L)[b]
1	0.186 ± 0.034
2	0.196 ± 0.020
3	0.195 ± 0.017
4	0.199 ± 0.011
mean	0.194 ± 0.012
u_r	6.5%

[a]Certified property value: $\gamma(F^-)$ = 0.194 ± 0.008 mg/L. [b]Uncertainty of each standard additions experiment was evaluated according to ISO/GUM guidelines. All uncertainties are reported here as expanded uncertainties with coverage factor k = 1.

The results for the other two samples were as follows: $\gamma(F^-)$ = 0.59 ± 0.07 mg/L in urine and $\gamma(F^-)$ = 1.39 ± 0.09 mg/L in north Atlantic water (MOOS-2). The fluoride content in MOOS-2 is also in good agreement with ion selective electrode measurements of ocean water of similar salinity.[36]

All samples yield three phases after derivatization with $Et_3O^+[FeCl_4]^-$: (1) a precipitate which contains $Fe(OH)_3$ and part of the matrix, (2) a homogeneous aqueous phase, and (3) an upper gas phase (headspace) from which the fluoroethane is sampled. Derivatization allows separation of the analyte from the sample into the headspace and enables the realization of extremely clean chromatograms. Figure 2 shows the results from a urine sample; even with such a complex matrix, there are no interferences coeluting with the analytical peak. The instrumental limit of detection obtained by processing calibration solutions is $\gamma(F^-)_{DL}$ = 3.2 μg/L with a linear range up to 50 mg/L. The estimation of $\gamma(F^-)_{DL}$ is based on the signal-to-noise ratio calculated from the standard deviation of the baseline in proximity to the analyte peak (i.e., detection limit is the concentration which produces a signal-to-noise-ratio

dx.doi.org/10.1021/ac302303r | Anal. Chem. XXXX, XXX, XXX−XXX

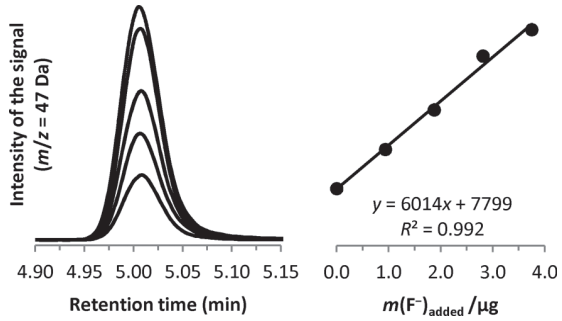

Figure 2. Analytical peaks for fluoroethane (at m/z = 47 Da) and the resulting standard additions calibration plot derived from a sample of incrementally spiked urine.

of 3). Standard solutions of $\gamma(F^-)$ = 123 μg/L and 531 μg/L give signal-to-noise ratios of 115 and 492, respectively.

Interferences. Fluoride forms strong complexes with many metal cations, such as Al(III), and Fe(III). These interferences are common to any method of determination of fluoride. Therefore, the method of standard additions should be used to overcome such matrix effects.[36] Interferences arising from the complexation of fluoride reduce the analytical signal and deteriorate the performance of analytical methods. Therefore, the effect of the presence of large amounts of various metal cations on the analytical response was evaluated. Table 2

Table 2. Interference Effect Arising from the Presence of 10 mM Metal Ion in a Standard Solution of 0.05 mM Fluoride

interference	S/S_0[a]
none	1.00 ± 0.07
Al(III)	0.11 ± 0.09
Fe(III)	0.62 ± 0.07
Ca(II)	0.83 ± 0.03
Mg(II)	0.32 ± 0.02
Zn(II)	0.97 ± 0.06
Cu(II)	1.01 ± 0.06

[a] S/S_0 is the ratio between the analytical signal from fluoride in the presence of interference (S) to that generated without interference (S_0). Three independent measurements were performed.

summarizes the interference arising from the presence of 10 mM (240–650 mg/L) levels of several cations added to standard solutions containing 0.05 mM fluoride. The 200-fold excess of these potential interferences over the analyte was chosen in order to show the robustness of the proposed method in coping with the interference of metal cations. Signal suppression is observed in the presence of Mg(II), Ca(II), Fe(III), and Al(III). The latter exhibits the most severe suppression and contributes to a 10-fold decrease in the analytical signal. Negligible effects were evident with Zn(II) and Cu(II). The alkaline condition induced by pretreatment of the sample with ammonia results in precipitation of many metal cations as hydroxides, thus significantly reducing their ability to complex fluoride.

CONCLUSIONS

Triethyloxonium tetrachloroferrate(III) was successfully employed for derivatization of fluoride ion in aqueous solutions to produce stable volatile fluoroethane, which is amenable to analysis by GC/MS. Although it is a lower throughput approach compared to ion selective electrode methods, this novel ethylation chemistry coupled with GC/MS provides better selectivity and specificity. With respect to other GC/MS approaches, this method offers a comparable or better detection limit, and it is considerably safer to use than silylation or alkylation with F_5BzBr because $Et_3O^+[FeCl_4]^-$ is a water-soluble salt which undergoes complete hydrolysis in a few hours. Additionally, it is not a volatile liquid such as Me_3SiCl, and the oxonium alkylation proceeds in aqueous media at room temperature which adds to the speed and convenience of the method. Further improvement to the analytical figures of merit appears possible by employing an internal standard. Bromide and iodide ions should serve as ideal internal standards since they undergo the same derivatization chemistry as fluoride.

AUTHOR INFORMATION

Corresponding Author

*E-mail: e.pagliano@sns.it, enea.pagliano@nrc.ca.

Notes

The authors declare no competing financial interest.

REFERENCES

(1) Verkerk, R. H. J. *Toxicology* **2010**, *278*, 27–38.
(2) Harrison, P. T. C. *J. Fluorine Chem.* **2005**, *126*, 1448–1456.
(3) Levy, S. M. *J. Public Health Dent.* **1999**, *59*, 211–223.
(4) Ekstrand, J. *J. Nutr.* **1989**, *119*, 1856–1860.
(5) WHO. *Guidelines for Drinking-Water Quality. Vol. 2. Health Criteria and Other Supporting Information.*; World Health Organization: Geneva, Switzerland, 1984.
(6) Wambu, E. W.; Muthakia, G. K. *Fluoride* **2011**, *44*, 37–41.
(7) Meenakshi; Maheshwari, R. C. *J. Hazard. Mater.* **2006**, *137*, 456–463.
(8) Fuwa, K. *Stud. Environ. Sci.* **1985**, *27*, 3–14.
(9) Lundell, G. E. F.; Hoffman, J. I. *Outlines of Methods of Chemical Analysis*; Wiley: New York, 1948.
(10) Williams, W. J. In *Handbook of Anion Determination*; Butterworth: London, 1979; pp 335–373.
(11) Zhu, C.-Q.; Chen, J.-L.; Zheng, H.; Wu, Y.-Q.; Xu, J.-G. *Anal. Chim. Acta* **2005**, *539*, 311–316.
(12) Bayón, M. M.; Rodríguez Garcia, A.; García Alonso, J. I.; Sanz-Medel, A. *Analyst* **1999**, *124*, 27–31.
(13) Garrido, M.; Lista, A. G.; Palomeque, M.; Fernández Band, B. S. *Talanta* **2002**, *58*, 849–853.
(14) Frant, M. S.; Ross, J. W., Jr. *Science* **1966**, *154*, 1553–1555.
(15) Campbell, A. D. *Pure Appl. Chem.* **1987**, *59*, 695–702.
(16) Fulford, J. E.; Quan, E. S. K. *Appl. Spectrosc.* **1988**, *42*, 425–428.
(17) Gleisner, H.; Welz, B.; Einax, J. W. *Spectrochim. Acta, Part B* **2010**, *65*, 864–869.
(18) Heitmann, U.; Becker-Ross, H.; Florek, S.; Huang, M. D.; Okruss, M. *J. Anal. At. Spectrom.* **2006**, *21*, 1314–1320.
(19) Barnett, D. A.; Horlick, G. *J. Anal. At. Spectrom.* **1997**, *12*, 497–501.
(20) Hotta, H.; Kurihara, S.; Johno, K.; Kitazume, M.; Sato, K.; Tsunoda, K.-I. *Anal. Sci.* **2011**, *27*, 953–956.
(21) Wejnerowska, G.; Karczmarek, A.; Gaca, J. *J. Chromatogr., A* **2007**, *1150*, 173–177.
(22) Tashkov, W.; Benchev, I.; Rizov, N.; Kolarska, A. *Chromatographia* **1990**, *29*, 544–546.
(23) Musijowski, J.; Szostek, B.; Koc, M.; Trojanowicz, M. *J. Sep. Sci.* **2010**, *33*, 2636–2644.
(24) Kage, S.; Kudo, K.; Nishida, N.; Ikeda, H.; Yoshioka, N.; Ikeda, N. *Forensic Toxicol.* **2008**, *26*, 23–26.
(25) Granik, V. G.; Pyatin, B. M.; Glushkov, R. G. *Russ. Chem. Rev.* **1971**, *40*, 747–759.
(26) Olah, G. A.; Laali, K. K.; Wang, Q.; Surya Prakash, G. K. *Onium Ions*; Wiley: New York, 1998.

(27) D'Ulivo, A.; Pagliano, E.; Onor, M.; Pitzalis, E.; Zamboni, R. *Anal. Chem.* **2009**, *81*, 6399−6406.
(28) Pagliano, E.; Onor, M.; Pitzalis, E.; Mester, Z.; Sturgeon, R. E.; D'Ulivo, A. *Talanta* **2011**, *85*, 2511−2516.
(29) Pagliano, E.; Meija, J.; Sturgeon, R. E.; Mester, Z.; D'Ulivo, A. *Anal. Chem.* **2012**, *84*, 2592−2596.
(30) Sturgeon, R. E.; Guo, X.; Mester, Z. *Anal. Bioanal. Chem.* **2005**, *382*, 881−883.
(31) Wells, R. J. *J. Chromatogr., A* **1999**, *843*, 1−18.
(32) Raber, D. J.; Gariano, P., Jr.; Brod, A. O.; Gariano, A.; Guida, W. C.; Guida, A. R.; Herbst, M. D. *J. Org. Chem.* **1979**, *44*, 1149−1154.
(33) Meerwein, H.; Battenberg, E.; Gold, H.; Pfeil, E.; Willfang, G. *J. Prakt. Chem.* **1939**, *154*, 83−156.
(34) Morales, R.; West, P. W. *Anal. Chim. Acta* **1966**, *35*, 526−529.
(35) Health Canada. *Guidelines for Canadian Drinking Water Quality: Guideline Technical Document - Fluoride*; Health Canada: Ottawa, Ontario, 2010.
(36) Rix, C. J.; Bond, A. M.; Smith, J. D. *Anal. Chem.* **1976**, *48*, 1236−1239.